DISSERTATION

USING POSITIVE ALLOSTERIC MODULATORS TO DETERMINE MECHANISMS OF GLUR2 DESENSITIZATION AND DEACTIVATION

Submitted by

Autumn M. Weeks

Department of Biomedical Sciences

In partial fulfillment of the requirements

for the degree of Doctor of Philosophy

Colorado State University

Fort Collins, Colorado

Summer 2006

COLORADO STATE UNIVERSITY

July 5, 2006

WE HEREBY RECOMMEND THAT THE DISSERTATION PREPARED UNDER OUR SUPERVISION BY AUTUMN MARIE WEEKS ENTITILED: USING POSITIVE ALLOSTERIC MODULATORS TO DETERMINE MECHANISMS OF GLUR2 DESENSITIZATION AND DEACTIVATION BE ACCEPTED AS FULFILLING IN PART REQUIREMENTS FOR THE DEGREE OF DOCTOR OF PHILOSOPHY.

Committee on Graduate Work

Advisor

Department Head

ABSTRACT OF DISSERTATION

USING POSITIVE ALLOSTERIC MODULATORS TO DETERMINE MECHANISMS OF GLUR2 DESENSITIZATION AND DEACTIVATION

Recent crystallographic and functional analyses of AMPA receptors have identified a common binding pocket for two classes of positive allosteric AMPA receptor modulators, cyclothiazide (CTZ) and AMPAkine CX614. Based on differences in modulator binding and function, those experiments have provided a working model consisting of two distinct pathways for channel desensitization and deactivation where rearrangement of the ligand binding core at the interdimer interface is responsible for receptor desensitization, and cleft opening of the ligand binding core is responsible for deactivation. This study focuses on comparing structural and functional data for GluR2 flip and flop in the presence of four AMPA receptor modulators: CTZ, CX614, LY506091, and LY2152080. Additionally we have tested the effects of point mutations at the three subdomains implicated in receptor deactivation (Hinge 1 and Hinge 2) and desensitization (flip/flop) and modulation. We have also used computer simulations to model the effects of slowing cleft-opening, entry into

desensitization and channel closure rate on macroscopic deactivation and desensitization kinetics. Together, these data test and refine the current model of AMPA receptor gating and modulation that has been based on static snapshots of crystal structures. These findings lend support to the idea that deactivation and desensitization (as well as the modulation of each) are, in fact, inextricably coupled, likely with only one mechanism for closing the receptor gate.

Autumn M. Weeks
Department of Biomedical Sciences
Colorado State University
Fort Collins, CO 80523
Summer 2006

ACKNOWLEDGEMENTS

This work was carried out with the supervision and funding (NIH R01) of Dr. Kathryn Partin, without whose patience, guidance, encouragement, and candy jar, none of this would have been possible. I would also like to thank the rest of the Partin lab, for useful discussions, shoulders to cry on when experiments and writing were not going well, and much of the molecular biology that I did not want to do. Thanks, John for obsessing over figures so I didn't have to (even though I still did). Thanks Matt for helping me to take my ideas more seriously and think for myself more, and Bridget for helping me to stop and breathe more—the perfect balance in the lab. I warmly thank all my co-authors and committee members (past and present), and the Dudek lab—Jessica, Heidi, and Shilpa, together we kept each other mostly sane from the very beginning. And last (but definitely not least), I would like to thank my family—thanks for keeping things in perspective and promising you would still love me if I "just got my Master's". To my super-human husband, Tim, thanks for keeping me (and the dogs) alive and giving me all your support and encouragement. Thank you, you are all amazing!

Autumn M. Weeks

Department of Biomedical Sciences

Colorado State University

Fort Collins, CO 80523

Summer 2006

TABLE OF CONTENTS

LIST OF TABLES

LIST OF FIGURES

CHAPTER 1: DISSERTATION INTRODUCTION

1.1 AMPA Receptor Structure and Function

Glutamate is the main excitatory neurotransmitter in the central nervous system; thus, the binding of glutamate to its receptors regulates a wide variety of processes including developmental synaptic plasticity and learning and memory. There are three types of ion-permeable glutamate receptors: N-methyl-D-aspartate (NMDA), kainate, and AMPA. At synapses, kainate and AMPA receptors mediate the initial rapid peak of excitatory postsynaptic potentials (EPSPs). By initiating the EPSP, AMPA receptors serve as the "trigger" for the cellular basis of learning and memory, Long Term Potentiation (LTP). Upon activation, AMPA receptors pass sufficient Na^{2+} into the cell to relieve the NMDA receptor's Mg^{2+} block. Activation of NMDA receptors, in turn, allows Ca^{2+} to enter the cell and initiates the CaMKII-dependent insertion of AMPA receptors into the postsynaptic membrane, strengthening synapses in an activity-dependent manner (Malinow and Malenka 2002).

AMPA receptors can be composed of four distinct subunits, GluR1-4 (A-D). Various permutations of AMPA receptor subunits form heteromeric tetramers in vivo (Bettler and Mulle 1995; Rosenmund, Stern-Bach et al. 1998; Mansour, Nagarajan et al. 2001). Two other mechanisms for AMPA receptor variation exist:

the flip/flop splice variants (the alternatively spliced 38 amino acid region between the M3 and M4 domains of each AMPA receptor subunit) and post-transcriptional receptor editing (e.g. the Q/R site mediating calcium permeability) (Koike, Tsukada et al. 2000). The diversity of receptor structure corresponds to different cell types and brain regions in normal states(Dingledine, Borges et al. 1999). Changes in receptor subunit composition can occur in certain pathological conditions. For example, following an ischemic insult, AMPA receptors lacking the GluR2 subunit are upregulated. Increasing Ca^{2+}-permeable AMPA receptor expression is thought to contribute to ischemia-induced synaptic remodeling and cell death (Sommer, Keinänen et al. 1990; Lomeli, Mosbacher et al. 1994; Ying, Weishaupt et al. 1997; Dingledine, Borges et al. 1999; Liu, Liao et al. 2006). Thus, mechanisms behind these subunit switches and subunit function are important targets for therapeutic drug design.

Much of what we know about AMPA receptor organization, stochiometry and function comes from structural analysis of the channel. The entire AMPA receptor has not been crystallized, but the membrane helices of AMPA receptors share considerable structural homology (although inverted) with those of K^+ channels while the AMPA receptor ligand binding domain is related to bacterial amino acid binding proteins (e.g., leucine-isoleucine-valine binding proteins, LIVBP)(Stern-Bach, Bettler et al. 1994). Many predictions of how AMPA receptors are organized come from studies of these two separate structures which together are also an exemplary model of protein evolution (Oswald 2004).

The modular nature of AMPA receptors has also allowed for the crystallization of the isolated extracellular GluR2 flop ligand binding core and has provided an excellent model of how glutamate binding can provide the energy required to bring about a conformational change that subsequently opens the ion channel. Based on crystallographic studies, AMPA receptors open proportionally in response to the degree of closure or stability of the closed-cleft conformation of each subunit's ligand binding core around agonist (Jin, Banke et al. 2003; Robert and Howe 2003; Robert, Armstrong et al. 2005). Although models of the basic mechanisms of receptor opening and desensitization have been established with these crystal studies, little is known about the mechanisms by which channel closing or deactivation occur or the receptor's ability to fine-tune this gating process (how the ligand binding core "talks" to the activation gate). Additionally, recent studies have shown that mutating residues outside the ligand binding core can also have similar effects on desensitization (Ramanoudjame, Du et al. 2006). Interpretation of crystal structure data proposes that the interface between each subunit for domains 1 and 2 is important for desensitization, while the interface at the hinges of each subunit is important for deactivation, predicted from modulator binding. However, crystals of nondesensitizing mutant receptor, $L_{483}Y$ have been shown to form bonds across the dimer interface, stabilizing the dimer and blocking desensitization much like the action of CTZ, but L483Y has a more profound effect on deactivation than CTZ (and it is not located at the hinges) (Stern-Bach, Russo et al. 1998; Sun, Olson et al. 2002; Sun, Olson et al. 2002). Additionally, studies isolating the ligand binding core may lose valuable

information about the channel, for example, how the ligand binding core moves when tethered to the membrane and N-terminal domain or mechanisms closer to or within the membrane-spanning region that may regulate the channel gate or ligand binding core dimer dissociation. As a case in point, other mutations such as the Lurcher mutation (A622T) and a mutation at the S2-M3 linker (R628E), outside the crystallized portion of the ligand binding core, affect gating properties of the channel (Wollmuth, Kuner et al. 2000; Klein and Howe 2004), stressing the need for more information derived from studies using the intact AMPA receptor.

1.2 AMPA Receptor Modulation

Modulators of AMPA receptors can have inhibitory (negative) or enhancing (positive) effects on AMPA receptors. Positive allosteric modulators of AMPA receptors have been used to study AMPA receptor gating. They work by enhancing normal AMPA receptor activity and thereby enhancing cognitive function(Staubli, Rogers et al. 1994). Upon opening, AMPA receptors can deactivate, simply the reverse of activation, where ligand may unbind and the process can start over. Alternatively, the channel may become desensitized, a high-affinity state in which conformational changes permit ligand to remain bound, but the channel cannot open and must recover from desensitization before it can be activated again (Figure 1.1). Benzothiadiazides, such as cyclothiazide (CTZ), and pyrrolidinones, such as the AMPAkine CX614, have been shown to increase AMPA receptor activity by increasing the probability that the receptor channel is open (Partin, Patneau et al. 1994; Suppiramaniam, Bahr

et al. 2001). CTZ (EC50 73 μM) and CX614 (EC50 ~ 0.17 mM) maintain this open channel configuration by slowing primarily desensitization or deactivation, respectively (Nagarajan, Quast et al. 2001). CTZ predominantly modulates desensitization by blocking entry into the desensitized state as seen in studies using homomeric GluR1 flip receptor (Partin, Fleck et al. 1996). CX614, on the other hand, has a more profound effect on deactivation (particularly in the flop AMPA receptor variant) by slowing the rate of exit from the open state (Arai, Kessler et al. 2000). Crystal structure studies have shown that the AMPA receptor ligand binding core tetramer is composed of a dimer of dimers with a site for modulators to bind separate from the agonist binding site. Two molecules of CTZ bind to each dimer at the interface between the two subunits and stabilize the bonds of each of the two dimers that make up the receptor tetramer. Dissociation of these dimers corresponds to desensitization of the channel. Recent experiments provide evidence that CTZ blocks desensitization by blocking this dimer dissociation (Sun, Olson et al. 2002; Horning and Mayer 2004). The crystal structure of the GluR2 ligand binding core bound with CX614 shows that like CTZ, the AMPAkine binds between the two dimers, but unlike CTZ, it makes different contacts, binding primarily between the hinges of each subunit and is thought to trap Domain 2 up after domain closure around agonist (Jin, Clark et al. 2005). By slowing rates of channel closure, CTZ and CX614 essentially maintain the AMPA receptor in its open configuration (Figure 1.2). CTZ and CX614 modulate AMPA receptor gating either from or to the agonist-

bound, non-desensitized state, thereby linking modulation with gating and agonist binding in distinct ways.

Kinetics of AMPA receptor gating and modulation are governed by the alternatively spliced "flip/flop" region. Receptors possessing the flop splice variant gate more rapidly than those with the flip form. This observation has not been reconciled with crystal structure data because the closest structure available that resembles a flip receptor is a flop ligand binding core with a single point mutation ($N_{754}S$) previously shown to confer flip-like sensitivity to cyclothiazide on flop receptors (Partin, Bowie et al. 1995; Sun, Olson et al. 2002). However, recent studies have shown that this residue may not be the only important difference between the two isoforms. Other residues in the flip/flop domain also seem to play an important role in isoform differences in gating, particularly in the response of receptors to different allosteric modulators, many of these residues do not lie within the crystallized ligand binding core (Quirk and Nisenbaum 2003).

1.3 Aims of this research

Functional studies exploiting these different mechanisms of AMPA modulators have improved the understanding of AMPA receptor gating and how it is coupled to binding of agonist, but there are still problems with defining AMPA receptor gating states using drugs that have overlapping actions. To tease apart these properties at the molecular level, we must identify the different binding sites of the two drugs. Residues uniquely hydrogen-bonded to each modulator have a

high probability of being responsible for the individual effects of each drug: governing deactivation or desensitization. Once the molecular determinants of GluR2 gating and modulation are established, more selective and efficient cognition-enhancing drugs can be developed. This work has provided the necessary step to learning these molecular determinants.

1.4 Clinical Significance of AMPA receptor research

Although AMPA receptor activation and upregulation are important for LTP, excessive activation of excitatory synapses can be harmful. After a stroke, affected neurons undergo excitoxicity followed by apoptosis, which may then lead to cognitive impairment. It is believed that a switch in glutamate receptor subunit composition occurs after an ischemic event that leads to down-regulation of AMPA-type glutamate receptors that contain the GluR2 subunit. Because GluR2-comprised receptors are largely impermeable to Ca^{2+} influx, increasing the ratio of other subunits in AMPA receptors that pass Ca^{2+} can increase the net Ca^{2+} influx into the cell and initiate cell death pathways (Pollard, Heron et al. 1993; Heurteaux, Lauritzen et al. 1994; Pellegrini-Giampietro, Gorter et al. 1997; Opitz, Grooms et al. 2000; Tanaka, Grooms et al. 2000). This phenomenon is referred to as the "GluR2 hypothesis". Recent therapies target the GluR2 down-regulation process, aiming to protect the cells that may otherwise be programmed to die (Colbourne, Grooms et al. 2003). This approach is promising but requires that treatment be administered immediately following an ischemic attack. For patients that are currently living with the effects of stroke or those

that do not receive rapid enough treatment, alternative therapies must be developed. Another way to preserve neurons after ischemia may be to target the remaining GluR2-containing receptors, selectively enhancing their contribution to the glutamate-mediated current and thereby buffering the activity of receptors that pass Ca^{2+}. However, current therapies that treat cognitive disorders rely on the potentiation of other AMPA receptors that are permeable to Ca^{2+} as well as GluR2. Although the GluR2 hypothesis predicts that these drugs would have deleterious effects by increasing global excitotoxicity, no harmful side effects in humans have cancelled any of AMPAkine clinical trials to date, but aniracetam, the parent drug of AMPAkines which is on the market in Europe has been shown to reverse the effects of anticonvulsants (De Sarro, Siniscalchi et al. 2000; Black 2005). Lower potency, and less efficacious AMPAkines are now being pursued, for example, CX516 has shown improvements in memory tasks in humans, but even at high does, these improvements are limited (Lynch, Granger et al. 1997). Higher-potency drugs that can be specifically targeted to subunit and isoform types may be more beneficial in the treatment of distinct disease states. Because AMPAkines show great promise for clinical use, more research on the molecular mechanisms of their effects is needed to understand AMPA receptor gating and modulation, and design more specific therapies in the future.

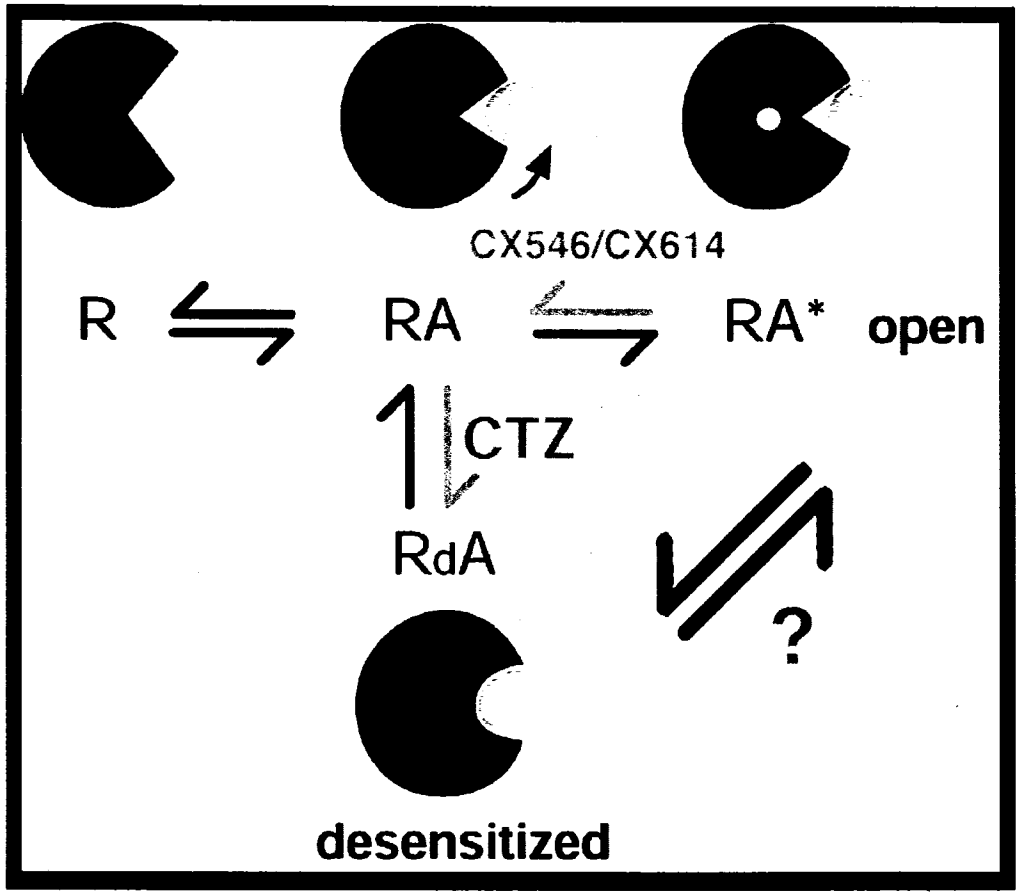

Figure 1.1 Diagram showing agonist (A) binding to receptor (R) causing an agonist-induced stabilization (arrow) of the closed "clamshell" (RA). This conformation permits the pore to open (RA*), or the channel to desensitize (RdA) to a very stable, closed-pore conformation. The proposed actions of CX (CX546 and CX614) and CTZ are shown, where gray arrows mark a decrease in equilibrium. It is unclear whether or not desensitization can occur directly from the open state.

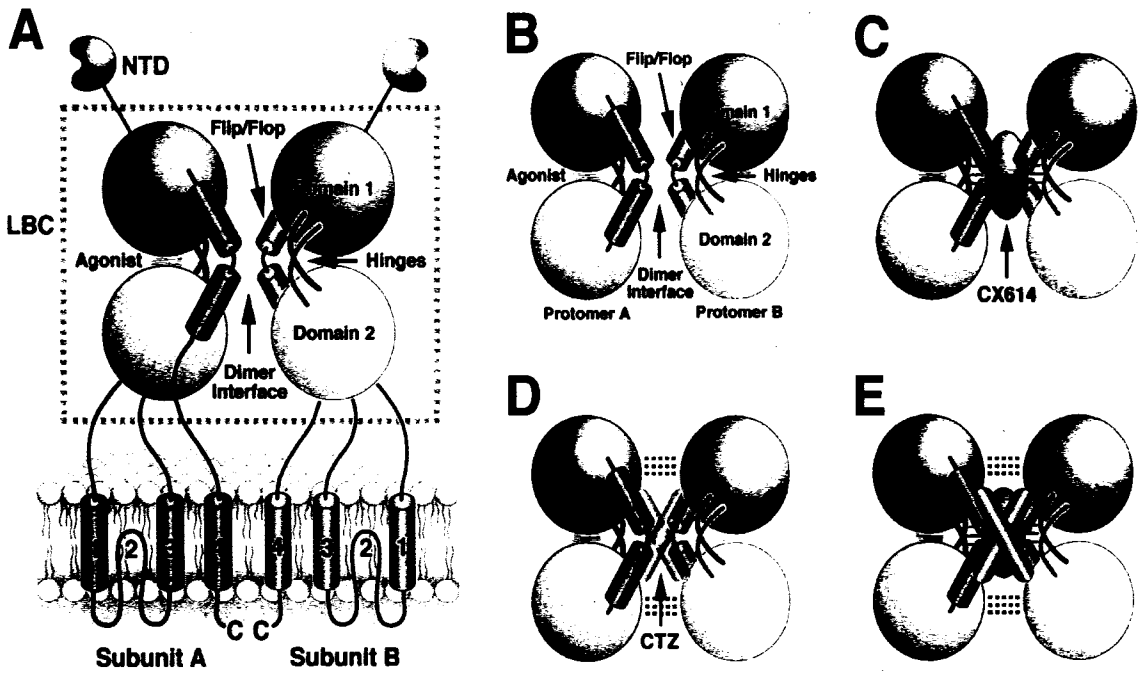

Figure 1.2. Structure of GluR2. (A) Cross-section of a GluR2 tetramer, showing domains, flip/flop region, hinge region, and ligand binding core (LBC) in relation to N-terminus and membrane. (B) Cartoon of LBC domains (from crystal structure) (C) LBC bound with CX614 (purple elipse), black lines indicate "independent" model interaction with hinges. (D) LBC bound with CTZ, cyan dashes indicate "independent" model interaction with Domains 1 & 2 across the dimer interface. (E) Overlay of CX614 and CTZ crystal structures, suggesting possible overlapping contacts in addition to independent contacts (black and dashed cyan lines).

CHAPTER 2: CONTRIBUTIONS TO RECENT PUBLICATIONS

2.1 Introduction

Although I will focus on my own personal work in Chapter3, this chapter describes other projects in the Partin lab to which I have contributed. My role in most of these projects has been to provide technical assistance with electrophysiology and molecular biology, as well as in the writing, editing and proofing of the resultant manuscripts. Below I have included the title and abstract of each resulting manuscript with a brief description of my roles in the research. Full copies of each paper can be found in APPENDIX 1.

2.2 Identification of a site in GluR1 and GluR2 that is important for modulation of deactivation and desensitization (J. Duncan Leever, Suzanne Clark, Autumn M. Weeks, and Kathryn M. Partin, Molecular Pharmacology, 2003)

2.2.1 Abstract

The alpha-amino-3-hydroxy-5-methyl-4-isoxazolepropionic acid subtype of ionotropic glutamate receptors consists of rapidly gating ion channels. Positive modulation of channel gating may slow gating kinetics through at least two

distinct mechanisms, evidenced by the predominant slowing of either the rate of receptor desensitization or the rate of offset after agonist withdrawal (deactivation). This study compares the actions of two positive allosteric modulators [cyclothiazide, which modulates desensitization, and 1-(1,4-benzodioxan-6-ylcarbonyl)piperidine (CX546), which modulates deactivation] in a mutant shown previously to impede modulation by cyclothiazide. These experiments test the hypothesis that the point mutation, GluR1 (S493T), would also cause a loss of modulation by CX546. Wild-type GluR1 through -4 receptors were modulated by CX546, as assayed by the potentiation of steady-state currents in the *Xenopus laevis* oocyte expression system. CX546 potentiated steady-state currents of both splice isoforms of GluR1. Modulation by CX546 was completely abolished in GluR1(S493T) and its homolog, GluR2(S497T), although this mutation did not affect apparent agonist affinity in the absence of CX546. Thus, the GluR1(S493T) mutation has a similar impairment of modulation by either cyclothiazide or CX546, indicating that some residues at the subunit interface of glutamate receptors play an important role in channel deactivation and desensitization.

2.2.2 Discussion

I did not contribute to the design of these experiments, but I helped Duncan gather data for the oocyte studies while I learned how to use the two-electrode voltage clamp rig and harvest and prepare oocytes. In addition, I contributed to this work by editing and proofreading the various drafts. The results of this paper

stress the importance of a single residue in modulation by both CX546 (analog of CX614) and CTZ, providing evidence that the processes (and modulation of) of deactivation and desensitization may be linked.

2.3 Mechanism of Positive Allosteric Modulators Acting on AMPA receptors (Rongsheng Jin, Suzanne Clark, Autumn M. Weeks, Joshua T. Dudman, Eric Gouaux, and Kathryn M. Partin, Journal of Neuroscience, 2005)

2.3.1 Abstract

Ligand-gated ion channels involved in the modulation of synaptic strength are the AMPA, kainate, and NMDA glutamate receptors. Small molecules that potentiate AMPA receptor currents relieve cognitive deficits caused by neurodegenerative diseases such as Alzheimer's disease and show promise in the treatment of depression. Previously, there has been limited understanding of the molecular mechanism of action for AMPA receptor potentiators. Here we present cocrystal structures of the glutamate receptor GluR2 S1S2 ligand-binding domain in complex with aniracetam [1-(4-methoxybenzoyl)-2-pyrrolidinone] or CX614 (pyrrolidino-1,3-oxazino benzo-1,4-dioxan-10-one), two AMPA receptor potentiators that preferentially slow AMPA receptor deactivation. Both potentiators bind within the dimer interface of the nondesensitized receptor at a common site located on the twofold axis of molecular symmetry. Importantly, the potentiator binding site is adjacent to the "hinge" in the ligand-binding core "clamshell" that undergoes conformational rearrangement after glutamate

binding. Using rapid solution exchange, patch-clamp electrophysiology experiments, we show that point mutations of residues that interact with potentiators in the cocrystal disrupt potentiator function. We suggest that the potentiators slow deactivation by stabilizing the clamshell in its closed-cleft, glutamate-bound conformation.

2.3.2 Discussion

I assisted Suzanne with construction of some mutants and recording of electrophysiological data, mainly screening several hinge mutants in *Xenopus* oocytes using two-electrode voltage clamp (TEVC, see section 2.1.2). The screening was essential to this work, as it allowed the lab to focus in on critical mutants to be carried onto the patch rig for further kinetic studies. I also contributed to the editing and proofreading of this manuscript. The results of this paper helped to define the current model of AMPA receptor gating and modulation, focusing on channel deactivation and modulation of deactivation by AMPAkine CX614. These studies implicated the hinges of the ligand binding core, where CX614 prevents the opening of the ligand binding cleft for each subunit and thereby slows receptor deactivaiton.

2.4 Kynurenic acid has a dual action on AMPA receptor responses (Christina Prescott, Autumn M. Weeks, Kevin J. Staley, and Kathryn M. Partin, Neuroscience Letters, 2006)

2.4.1 Abstract

Glutamate is the predominant excitatory neurotransmitter in the central nervous system. The receptors that bind glutamate, including N-methyl-d-aspartate (NMDA) and alpha-amino-3-hydroxy-5-methyl-4-isoxazole propionic acid (AMPA) receptor subtypes, are strongly implicated in higher cognitive processes, especially learning and memory. Loss of glutamate receptor function impairs the ability to acquire and retain information in some patients subsequent to stroke or brain injury, and positive allosteric modulators of glutamate receptors can restore learning and memory in some of these patients. Here we demonstrate that kynurenic acid (KYNA), an endogenous tryptophan metabolite, acts upon heterologous AMPA receptors via two distinct mechanisms. Low (nanomolar to micromolar) concentrations of KYNA facilitate AMPA receptor responses, whereas high (millimolar) concentrations of KYNA competitively antagonize glutamate receptors. Low concentrations of KYNA appear to increase current responses through allosteric modulation of desensitization of AMPA receptors. These findings suggest the possibility that low concentrations of endogenous KYNA acting at AMPA receptors may be a positive modulator of excitatory synaptic transmission.

2.4.2 Discussion

For this manuscript, I harvested and prepared the oocytes and taught Christina how to use TEVC to test the dual effect of KYNA on AMPA receptors. I repeated some of the same experiments with outside-out patches of HEK293 cells

expressing AMPA receptors, but this data was not significantly different from wt. I also helped proofread the manuscript. Although in high doses KYNA acts as an antagonist, in very low concentrations, a potentiation effect can be seen. These studies argue for the possibility of an endogenous positive modulator of AMPA receptors.

2.5 Different domains of the AMPA receptor direct stargazin-mediated trafficking and stargazin-mediated modulation of kinetics (Matthew A. Bedoukian, Autumn M. Weeks, and Kathryn M. Partin, Journal of Biological Chemistry, 2006)

2.5.1 Abstract

Stargazin is an accessory protein of AMPA receptors that enhances surface expression and also affects the biophysical properties of the receptor. AMPA receptor domains necessary for either of these two processes have not yet been identified. Here, we used confocal imaging and electrophysiology of heterologously expressed, fluorophore-tagged GluR1, GluR2 and stargazin to study surface expression and desensitization kinetics. Stargazin-mediated trafficking was sensitive to the nature of the AMPA receptor cytoplasmic domain. The insertion of YFP after residue 15 of the truncated cytoplasmic tail of GluR1i perturbed stargazin-mediated trafficking of the receptor but not its modulation of desensitization kinetics. This construct also failed to permit fluorescence resonance energy transfer (FRET) with stargazin in the ER, whereas FRET between fluorophore-tagged stargazin and non-truncated AMPA receptors

demonstrated a specific interaction between these proteins, both in the ER and the plasma membrane. Rather than encoding a specific binding site, the fluorophore-tagged C-terminus may restrict access to one or more endoplasmic reticulum (ER) retention sites. Although perturbations of the C-terminus impeded stargazin-mediated trafficking to the plasma membrane, their effects on the biophysical properties of AMPA receptors (i.e., modulation of desensitization) remained intact. These data provide strong evidence that the AMPA receptor domains required for stargazin-modulation of gating and trafficking are separable.

2.5.2 Discussion

For this manuscript, I tested the functionality of Matt's AMPA receptor constructs using outside-out patch clamp electrophysiology on HEK293 cells. In particular, I contributed to the design and execution of critical experiments relating the graded electrophysiological effects of stargazin on desensitization to the graded fluorescence morphology. In addition, I assisted in the editing and proofreading of several drafts. The results of this paper lend further support to the importance of the auxiliary subunit, stargazin in AMPA receptor expression and function and help to define the interactions between AMPA receptors and stargazin responsible for stargazin's dual functions.

2.6 Chapter 2 Summary

Although my contributions to these manuscripts have been as second or third author, their impact on the design and rationale for my project analyzing AMPA receptor structure, function, and modulation have been critical, especially the Leever et al. paper and the Jin et al. paper, which directly shaped my hypothesis about the structural determinants of AMPA receptor modulation, deactivation and desensitization which will be addressed in Chapter 3. Together, these papers underscore the importance of using functional, electrophysiological data in conjunction with structural or optical data and how, without real-time physiological relevance, interpretations of "snapshot" data are greatly limited.

CHAPTER 3: STRUCTURAL AND FUNCTIONAL ANALYSIS OF TWO NOVEL POSITIVE ALLOSTERIC MODULATORS REVEALS MECHANISMS OF GLUR2 DESENSITIZATION AND DEACTIVATION

3.1 Abstract

Recent crystallographic and functional analyses of AMPA receptors have identified a common binding pocket for two classes of positive allosteric AMPA receptor modulators. From those studies, a working model of channel desensitization and deactivation has been established. Here we present structural and functional data on two new positive allosteric modulators of AMPA receptors, LY506091 and LY2152080. These compounds have some structural similarities to CTZ and CX614, and they bind at the dimer interface within the solvent accessible pocket. Rapid perfusion of outside-out patches of HEK293 cells expressing homomeric GluR2 receptors reveals that, as predicted, LY506091 and LY2152080 block desensitization (like CTZ) and slow deactivation (like CX614). However, these compounds have unique properties that distinguish them from other known positive allosteric modulators. LY506091 is less isoform-selective than CTZ at blocking desensitization, and LY2152080 is more selective

for the flip isoform at blocking desensitization, but unlike CTZ robustly slows deactivation. In addition to characterizing these compounds on wild-type GluR2 flip and flop receptors, we have mutated several residues within the modulator binding pocket from three subdomains of the ligand binding core previously implicated in modulator efficacy and discrete states of channel deactivation and desensitization: Hinge 1 ($S_{497}A$, $S_{497}T$), Hinge 2 ($S_{729}A$, $G_{731}A$) and Flip/Flop ($K_{763}Q$). Subsequent analysis of four positive modulators refines the current model of AMPA receptor modulation and challenges assumptions about domains subserving channel deactivation and desensitization, supporting the idea that deactivation and desensitization (as well as the modulation of each) are, in fact, inextricably coupled, and the AMPA receptor domains governing these processes are not separable.

3.2 Introduction

AMPA receptors are essential components contributing to the initial rapid peak of excitatory postsynaptic potentials (EPSPs) and are critical for the strengthening and weakening of synapses that underlies the cellular basis of learning and memory. Positive allosteric modulators of AMPA receptors are used to treat cognitive impairment and act by enhancing normal AMPA receptor activity (Staubli, Rogers et al. 1994), prolonging macroscopic open-channel time by slowing or preventing channel closure (Partin, Patneau et al. 1994; Suppiramaniam, Bahr et al. 2001). The AMPA receptor-mediated synaptic response may be terminated by two different, agonist-dependent mechanisms.

When the exposure to glutamate is brief, AMPA receptors will close and ligand may unbind sequentially, leaving receptors in the activatable state. Alternatively, after closing the channel may desensitize in response to prolonged exposure to glutamate. In this case, receptors occupy a high-affinity state in which conformational changes uncouple ligand binding from channel opening, permitting ligand to remain bound, but the channel must rearrange and recover before it can be activated again.

Two classes of cognition-enhancing drugs, the benzothiadiazides, (e.g., cyclothiazide, CTZ), and the pyrrolidinones (e.g., AMPAkine CX614) maintain open channel configuration by slowing primarily desensitization or deactivation, respectively (Nagarajan, Quast et al. 2001). CTZ predominantly modulates desensitization by preventing rearrangement at the dimer interface, thereby blocking entry into the desensitized state with little effect on deactivation (Partin, Fleck et al. 1996). CX614, on the other hand, slows desensitization with a more profound effect on deactivation by slowing the rate of exit from the open state (Arai, Kessler et al. 2000; Arai, Xia et al. 2002). Structural and functional studies exploiting the different mechanisms of AMPA modulators have improved the understanding of AMPA receptor gating and how it is coupled to binding of agonist, but although the rates of deactivation and desensitization can be isolated and determined experimentally, the structural relationship between these two processes is unclear. It is not known whether each process proceeds independently or whether they must converge into one final common, structurally

indistinct pathway. Three subdomains of the ligand-binding core have been implicated in receptor deactivation and desensitization. Desensitization is governed by interactions across the dimer interface, as well as by the flip/flop region, the alternatively spliced helices that also contact the interface. In contrast, the hinge domain, two beta strands that connect the upper lobe (Domain 1) to the lower lobe (Domain 2), have been implicated in stabilization of the closed cleft conformation, thereby governing the rate of deactivation. Here we test predictions of the current model of AMPA receptor gating and modulation using two novel positive allosteric modulators and point mutations at the common modulator-binding pocket.

3.3 Methods and Materials

Molecular Biology. Plasmids encoding cDNAs for the flip (i) and flop (o) variants of rat wild-type GluR2 were gifts of Dr. Peter Seeburg (University of Heidelberg, Germany). WT GluR2 DNA was made with the pore mutant GluR2 $R_{607}Q$ (QuikChange II XL Site-Directed Mutagenesis Kit, Stratagene; La Jolla, CA). The receptors made from this mutant conduct robust current and have an inwardly rectifying current-voltage relationship.

HEK293 Cell Culture. Human embryonic kidney 293 fibroblasts (HEK 293 cells; ATCC CRL 1573 from American Type Culture Collection, Rockville, MD) were cultured as described previously. Cells were cultured in DMEM supplemented with 10% fetal bovine serum (Gemini Bio-Products, Inc, Calabasas, CA), penicillin/streptomycin (100 units/ml each) and 1% GlutaMax-1

(both from Gibco, Grand Island, NY). Cells were transiently transfected using FuGene 6 reagent (Roche Diagnostic Corp., Indianapolis, IN) with GluR2 (flip or flop) cDNA and enhanced yellow fluorescent protein (EYFP) cDNA (1 and 0.2 μg/ 35 mm dish, respectively).

HEK293 Electrophysiology. During recordings, cells were perfused continuously with extracellular bath solution containing (in mM): 20 sucrose, 145 NaCl, 5.4 KCl, 5 HEPES, 1 $MgCl_2$, 1.8 $CaCl_2 \cdot 2H_2O$ and 0.01 mg/ml phenol red, pH 7.3. Currents were recorded 24-72 hours after transfection as described previously. Outside-out membrane patches from transfected HEK 293 cells were voltage-clamped at a holding potential of -60 mV using an Axopatch 200B amplifier (Axon Instruments, Foster City, CA). Synapse software (version 3.6d) (Synergy Research, Inc., Silver Springs, MD) was used for piezoelectric protocols, data acquisition, flow-pipe protocols, and trace analysis. Responses were filtered at 5 kHz, digitized at 10-500 μsec/point, and stored on a Power Macintosh computer using an ITC-16 interface (InstruTech, Port Washington, NY). Electrodes of of 2-5 MΩ were filled with (in mM): 135 CsCl, 10 CsF, 10 HEPES, 5 Cs-BAPTA, 1 $MgCl_2$, 0.5 $CaCl_2$, pH 7.2. 2 ATP was added immediately before recording each day. Because many of the modulators were prone to contaminating the cells and sticking to the tubing of the flowpipe, most experiments had to be performed separately with different tubing each time, preventing the reliable use of both glutamate and modulator on any individual cell. Thus, there were ten different flowpipe solutions. The vehicle-control barrel contained (in mM): 145 NaCl, 5.4 KCl, 5 HEPES, 1 $MgCl_2$, 1.8 $CaCl_2 \cdot H_2O$, and

0.01 mg/ml phenol red, pH 7.3. Except for glutamate alone experiments, appropriate modulator was added to the control barrel to pre-incubate receptors. The drug-containing barrels included glutamate (10 mM) in the presence and absence of 100 μM CTZ, 100 μM CX614, 1000 μM CX546, 10μM LY506091 or LY2152080. Modulators were dissolved in DMSO before dilution in extracellular solutions; final DMSO concentrations were 0.3-1%. Continuous solution flow was driven by a syringe pump (KD Scientific, New Hope, PA) at a rate of 0.2 ml/min. After clamping the cell at -60 mV, outside-out patchs were pulled and lifted up to a flow pipe constructed from θ tubing (Sutter Instrument Company, Novato, CA). The patch pipet tip was positioned in the stream containing control extracellular solution, and then moved near the interface between the stream of control and glutamate (and/or drug)-containing solutions. For assessing the response to drug, the patch pipet was jumped rapidly from the control into the drug solution. Rapid solution exchanges of 1 or 500 ms were driven by a piezoelectric device (Burleigh Instruments, Fishers, NY). Solution exchange rates were determined at the end of each experiment by open-tip junction currents. The rate of deactivation was estimated by fitting a single exponential (τ_{deact}) to responses evoked by a 1 ms drug pulse. The rate of onset of desensitization was estimated by fitting the decay of the response to a 500 ms drug pulse from 95% of peak to the steady state with a single-exponential function (τ_{des}). Additional fits to higher exponentials were tried as needed. Values were calculated using Synapse. Current traces and graphs were plotted using KaleidaGraph 3.6 (Synergy Software, Reading PA).

3.4 Results

LY506091 and LY2152080 bind between two subunits at the clamshell hinges

Two high-affinity positive allosteric modulators of AMPA receptors were identified, a bis-alkylsulfonamide (LY506091) and a bis-carboxythiophene (LY2152080). Displacement binding assays revealed similar, high affinities of the two compounds for both the flip and the flop isoforms of AMPA receptors: for LY506091 the $IC50_{flip}$=45 nM and $IC50_{flop}$=64 nM, whereas for LY2152080 the $IC50_{flip}$=123 nM and $IC50_{flop}$=483 nM. Both compounds are derivatives of the biarylpropylsulfonamides (Vandergriff, Huff et al. 2001; Shepherd, Aikins et al. 2002) but are composed of a single central aryl ring with symmetrical R-groups. The alkylsulfonamide R-groups of LY506091 and the nitrile/thiophene R-groups of LY2152080 reach above the plane of the aryl ring, while only the carboxy groups of LY2152080 reach below the plane of the aryl ring (Figure 3.1).

Co-crystal structures of the isolated GluR2 flop ligand-binding core with L-glutamate and either LY506091 or LY2152080 were solved. Like the AMPAkine CX614 (Jin, Clark et al. 2005), both LY506091 and LY2152080 bind as a single molecule within the solvent-filled crevice, situated at the interdomain hinge on the molecular twofold axis (Figure 3.2).

N1 and N2 of the alkylsulfonamide groups of LY506091 form hydrogen bonds with the main chain oxygens on residue P_{494} of both protomers. O2 and O4 form hydrogen bonds with the nitrogens on G_{731} for both protomers (Figure 3.3 A & B). Residues P_{494} and G_{731} lie within the two interdomain β-strands of the AMPA receptor, making up the "clamshell" hinges (Hinge 1, residues 494-498; Hinge 2, residues 729-733). The two carboxy groups of LY2152080 also form hydrogen bonds with the interdomain hinges through the main chain nitrogen of residue S_{497} in Protomer B and through water-mediated hydrogen bonds with the main chain oxygen of F_{495} of Protomer B, main chain oxygen and nitrogen of K_{730} and main and side chains of S_{729} of Protomer A and B (Figure 3.3 C - E).

Binding of LY506091 and LY2152080 to GluR2 flop ligand binding core shares similar characteristics with CTZ and CX614 binding

Previous crystallographic studies have revealed a "common" modulator-binding site in which CTZ and CX614 (and its parent compound, aniracetam) bind. CTZ binds two molecules per dimer perpendicular to, while CX614 binds one molecule per dimer parallel to the molecular twofold axis (Sun, Olson et al. 2002; Jin, Banke et al. 2003). Superpositions of the crystal structures of the LBC bound to either CTZ or CX614 demonstrate that LY506091 and LY2152080 also overlap the common binding site. With one molecule per dimer, their single aromatic rings are oriented like the central aromatic ring of CX614 but with additional

functional groups oriented in a similar manner to both molecules of CTZ (Figure 3.4). Although CTZ and CX614 bind within a common region, they have different functional, isoform-specific consequences on AMPA receptors. CTZ blocks desensitization with only a modest effect on deactivation of GluR2 flip with much less of an effect on desensitization and deactivation of GluR2 flop. CX614, on the other hand, is less efficacious than CTZ at slowing desensitization of GluR2 flip; more efficacious than CTZ at slowing desensitization of GluR2 flop; and more efficacious at slowing deactivation than CTZ in both GluR2 flip and flop. Because the LY506091 and LY2152080 interactions with the receptor share characteristics of the interactions of both CTZ and CX614, we were interested in defining pharmacophores for each drug, comparing individual binding sites which may predict modulator function and, thus, the structural underpinnings of receptor desensitization and deactivation.

A striking feature of this analysis is the extent to which all four compounds (CTZ, CX614, LY506091 and LY2152080) interact with the same sets of residues but through differing types of interactions (Figure 3.5). For example, P_{494} forms direct hydrogen bonds with LY506091 and CTZ, water-mediated bonds with CX614, and has a hydrophobic interaction with LY2152080; S_{497} forms direct hydrogen bonds with LY2152080, water-mediated hydrogen bonds with CX614, and has a hydrophobic interaction with LY506091; and, S_{729} forms a direct hydrogen bond with CTZ, water-mediated bonds with LY2152080 and CX614, and has a hydrophobic interaction with LY506091. Since all three of these example

residues form part of the two hinge regions, it would be hard to predict from this analysis the relative efficacies of modulation of deactivation of the four drugs, and even harder to predict their effects on receptor desensitization. Overall, CTZ has the most complicated residue-interaction profile, with the most numerous direct and water-mediated hydrogen bonds, spanning all regions of the ligand-binding core except Domain 2. In fact, of all the residues contacting all four modulators, only G_{731} does not contact CTZ. The residues that interact with all four compounds are composed largely of those constituting the hinge β-strands that connect the upper (Domain 1) ligand-binding clamshell to the lower (Domain 2) clamshell. The interaction between LY506091 and LY2152080 and the hinges might suggest that they would act to stabilize the closed-clamshell conformation of the protein, as proposed for CX614, resulting in the slowing of receptor deactivation as well as receptor desensitization. However, since LY506091 and LY2152080 also have moieties that overlap with CTZ, modulation of deactivation might be superceded by effects on dimer interface stability.

Functional analysis of LY506091 and LY2152080 reveals potent modulation of deactivation

To assess the effects of the modulators on channel activity, we measured responses evoked by ultrafast perfusion of glutamate to outside-out membrane patches from HEK293 cells expressing recombinant AMPA receptors. Long (500 ms) pulses of 10 mM glutamate, in the presence and absence of each of the four

modulators, permitted assessment of modulation of desensitization; brief (1 ms) pulses allowed us to assess their effects on deactivation. Both the flip (i) and flop (o) isoforms of GluR2 were tested, in order to determine whether the drugs showed isoform selectivity.

Low concentrations (10 μM) of LY506091 and LY2152080 markedly modulated receptor desensitization of the flip isoform of GluR2, virtually blocking the macroscopic onset of desensitization (Figure 3.6, Table 3.1). Thus, the high-affinity binding of the drugs accurately predicted the efficacious modulation of desensitization. However, removal of the functional group below the plane of the aromatic ring seemed to largely remove the flip-specificity, even increasing flop specificity for LY506091, whereas LY2152080, which makes most of its contacts below the aromatic ring, retained the flip selectivity. It has been proposed that binding of the flop residue N_{754} across the dimer interface (at Hinge 2) prevents CTZ from fully reaching its binding site (Sun, Olson et al. 2002). Our results support this idea that the flip binding pocket is more easily accessible to modulators like CTZ and LY2152080, although a comparative analysis of a GluR2 flip ligand binding core crystal with or without modulator to a wild type GluR2 flop crystal bound is necessary for a definitive statement.

As predicted by interactions with the aromatic ring structure that superposes with the rings of CX614, both LY compounds also potently modulated channel deactivation (Figure 3.6). A surprising finding was the ability of both LY

compounds to profoundly slow deactivation for both flip and flop isoforms. Although LY2152080 makes contacts below the aromatic ring and displays isoform-specific slowing of desensitization for the flip isoform like CTZ, unlike CTZ, it slows deactivation even for the flop isoform.

Mutation of modulator binding-site subdomains reveals isoform-dependent differences in receptor function and modulation

Previous structural and functional studies have suggested that the functional consequence of CTZ binding is to stabilize the dimer interface, whereas the binding of CX614 stabilizes cleft closure around agonist. Because of each drug's unique effect on slowing desensitization and deactivation, this has become a simplified model for structurally distinguishing desensitization from deactivation. To further understand the functional groups of the AMPA receptor that are important for modulation of desensitization and deactivation, we made point mutations of residues that seemed relatively unique to each of the drugs. Specifically, we studied the flip/flop residue K_{763} which is closest to Domain 2 (and is unique to the CTZ pharmacophore) and Hinge 2 residue G_{731} (unique to the CX614 and LY506091 pharmacophores) and tested all four modulators on these mutant receptors for both flip and flop isoforms. Additionally, Hinge 1 residue S_{497} and Hinge 2 residue S_{729} have been shown to play an important role in modulation by both CTZ and CX614, so we also tested modulation by the LY compounds on these mutant receptors. One might predict that for a modulator of

desensitization, mutations of hinge region residues would not impair efficacious modulation and in contrast, for a modulator of deactivation, the same mutants would have a large impact on efficacious modulation. Further, one could use this experimental paradigm to assess whether mutations that altered deactivation (or its modulation) always (or never) also impaired modulation of desensitization.

Hinge 1 mutants: $S_{497}A$ and $S_{497}T$

Residue S_{497} is located within Hinge 1 of the ligand-binding core and forms direct hydrogen bonds with CTZ and LY2152080, but also has important hydrophobic interactions with CX614, forming part of the base of the modulator-binding pocket. It is important to note that although hydrogen bonds are predicted to be important for modulator function, previous reports underscore the significance of hydrophobic interactions, especially in the case of molecules like CX614, which slow deactivation (Jin, Clark et al. 2005). When mutated to a threonine, S_{497} has been shown to impair modulation by CTZ in GluR1 flip and GluR2 flop and also by AMPAkines CX546 and CX614 in GluR2 flop, while an alanine substitution at residue 497 is still robustly modulated by both CTZ and CX614 (Partin 2001; Leever, Clark et al. 2003; Jin, Clark et al. 2005). Analysis of the crystal structure of the apo ligand binding core versus that bound with ligand and modulator show that the side chain of S_{497} rotates out of the modulator binding pocket to prevent steric clash when modulator is bound; thus, mutation to the slightly bigger threonine would increase steric hindrance, while mutation to the smaller alanine

would greatly decrease it, consistent with the functional consequences of these mutations on CX614 (Jin, Clark et al. 2005).

We tested the effects of $S_{497}A$ and $S_{497}T$ mutants in GluR2 flip and flop on modulation of deactivation and desensitization by CTZ, CX614, LY506091 and LY2152080. As predicted, $S_{497}A$ had little effect on modulation by both LY compounds. The most striking findings were the isoform-dependent differences. Overall, $S_{497}A$ flip had little to no effect on modulation by LY2152080 or CTZ but actually slowed glutamate kinetics in the absence of modulator and enhanced the slowing of deactivation by both LY506091 and CX614. $S_{497}A$ flop, on the other hand, showed a similar trend at slowing deactivation, but only the enhancing effect on CX614 was significant. Additionally, $S_{497}A$ flop significantly diminished CTZ's modulation of the steady state to peak ratio (an indication of the extent of desensitization) (Figure 3.7a, Table 3.1).

$S_{497}T$ had more of an impact on the flop isoform, impairing modulation by all modulators, although not to the same extent as other similar experiments (Partin 2001; Jin, Clark et al. 2005), perhaps because of the different subunits and/or ligands used). Although $S_{497}T$ impaired modulation in flop, it slowed desensitization with glutamate alone. $S_{497}T$ when expressed in the flip isoform was more like wild type in all cases except that the mutation enhanced modulation of desensitization by LY506091 (Figure 3.7b, Table 3.1).

Hinge 2 mutants: $S_{729}A$ and $G_{731}A$

Along with S_{497}, S_{729} in the Hinge 2 region forms the base of the modulator-binding pocket and has been shown to be important for modulator function (Partin 2001; Jin, Clark et al. 2005). Where S_{497} moves out of the way of the modulator, S_{729} moves closer to form bonds with modulators and the extensive water network within the modulator-binding crevice. Additionally, there is an important main chain interaction of S_{729} across the dimer interface with N_{754} in the flop variant. This interaction is thought to hinder CTZ binding in the flop isoform and give CTZ its prominent flip selectivity.

Mutation of S_{729} to an alanine had some unpredicted, isoform-specific results. In the flip isoform, $S_{729}A$ enhanced modulation of deactivation and desensitization by LY506091, while enhancing modulation of desensitization by CX614 and impairing CX614's steady-state to peak ratio. Additionally, $S_{729}A$ flip slightly impaired CTZ's modulation of desensitization but slowed its modulation of deactivation. The same mutation in the flop receptor impaired modulation of desensitization for all modulators except LY2152080 in which case $S_{729}A$ actually enhanced modulation (Figure 3.8a, Table 3.1).

Residue G_{731}, within the Hinge 2 region forms a hydrogen bond with the main chain nitrogen of I_{481} (Domain 1) within the same protomer. I_{481} has been shown to be important for dimer stability; mutation of $I_{481}$to a valine causes the channel to more rapidly desensitize (Horning and Mayer 2004). In addition to I_{481}, G_{731}

binds to CX614 (one protomer) and LY506091 (both protomers). To test the importance of this residue on receptor function and modulation, we mutated G_{731} to an alanine, making the residue slightly bigger and more rigid. Although mutation of glycine to a larger sidechain is not predicted to interfere with main-chain interactions, preventing the flexibility of this residue may. Interestingly, $G_{731}A$ sped deactivation and desensitization for both flip and flop even in the absence of modulator. Although all modulators but CX614 could modulate the $G_{731}A$ receptor in flip (with impairment), only CTZ could modulate $G_{731}A$ in flop, drastically increasing its current amplitude (Figure 3.8b, Table 3.1). Because $G_{731}A$ sped the control glutamate response of GluR2, it is likely that this residue is also important for dimer stability, further implicating Hinge 2 in desensitization and deactivation.

Flip/Flop mutant: $K_{763}Q$

It has been hypothesized that CTZ has a dual action on receptor function, slowing or blocking desensitization while speeding receptor deactivation in the non-desensitizing $L_{483}Y$ mutant (N.A. Mitchell 2004). Of all four modulators, CTZ reaches the farthest to Domain 2 and has the least impact on receptor deactivation. The region of CTZ that is close to Domain 2 of the receptor might also be responsible for this effect of speeding deactivation. Residue K_{763} is located in Helix K of the flip/flop domain, its side chain hydrogen bonds to E_{713} of Domain 2, while forming a water-mediated hydrogen bond with CTZ through its main chain. Although mutating this residue to an alanine likely has more of an

effect on flip/flop interactions with Domain 2, we also hoped to perturb its interaction with CTZ since it is one of the only residues that bind to CTZ and no other modulator. Despite the fact that residue K_{763} is not located at the dimer interface (thought to be important for desensitization) or the receptor hinges (thought to be important for deactivation), mutation from a lysine to a glutamine had a considerable impact on desensitization and modulation of both flip and flop isoforms (Figure 3.8c, Table 3.1). Notably, $K_{763}Q$ sped desensitization in response to glutamate without an effect on deactivation for both isoforms. In most cases, mutation to a glutamine impaired modulation by CTZ and LY2152080 with the exception of *slowing* deactivation with CTZ in flip and with LY506091 and CX614 in flop. These data support the idea that flip/flop interactions with Domain 2 and modulator are important for receptor desensitization and modulation of desensitization. Additionally, these data lend support to the dual-action-of-CTZ theory with the flip but not the flop isoform.

3.5 Discussion

We describe here the characterization of two new positive allosteric modulators of AMPA receptors: the bis-alykylsulfonamide LY506091 and the bis-carboxythiophene LY2152080. Co-crystals of each compound with L-glutamate and the GluR2 flop ligand binding core have been solved and reveal that both compounds have overlapping binding sites with CTZ and CX614, within the previously described modulator binding pocket located at the inter-dimer interface and the clamshell "hinges". In an attempt to dissect the molecular

determinants of deactivation from those of desensitization, we tested modulation by all four compounds on both GluR2 flip and flop wild-type receptors and on receptors with mutations of two residues that bind uniquely to CTZ ($K_{763}Q$) or to CX614 and LY506091 ($G_{731}A$). Additionally, we revisited mutations of other residues within the common modulator-binding site that have previously been shown to be important for modulation by CTZ and CX614 ($S_{497}A$, $S_{497}T$, and $S_{729}A$) and measured their consequences on modulation by the LY compounds. In contrast to our hypothesis that unique molecular contacts would have effects only on one class of modulator, our studies indicate that any mutation in this general area can affect modulation of deactivation and/or desensitization by any of the four drugs studied. Thus, we conclude that the structural underpinnings of deactivation and desensitization cannot be separated by studying a single residue that interacts uniquely with a modulator of desensitization (CTZ) versus a modulator of deactivation (LY506091).

Computer modeling of putative mechanisms of positive allosteric modulation. Previous studies have suggested that CTZ interacts with residues at the dimer interface stabilizing subunit interactions and thereby prevents the structural rearrangement that results in receptor desensitization, whereas CX614 interacts with residues that form the clamshell hinges, thereby stabilizing the ligand-bound, closed-cleft receptor conformation and slowing channel deactivation. Thus, CTZ modulates only desensitization without modulating deactivation – or, CTZ modulates desensitization and negatively modulates

channel deactivation. However, it was left unclear whether the macroscopic modulation by CX614 of receptor desensitization arose independently or dependently on its effects on channel deactivation.

Three potential explanations for the dual effects of CX614 and LY506091 on receptor deactivation and desensitization may be considered. In the first model, CX614 independently modulates two kinetic processes: channel deactivation and desensitization. For example, like CTZ, CX614 and LY506091 interact with residues on both protomers at the dimer interface, and could serve to make structural rearrangements underlying receptor desensitization less likely. In fact, equilibrium sedimentation analysis indicated that, like CTZ, CX614 promotes dimerization of the isolated ligand-binding core (Sun, Olson et al. 2002; Jin, Clark et al. 2005). Thus, CX614 and LY506091 could modulate deactivation by stabilizing the closed cleft conformation, and independently modulate desensitization by preventing dimer interface rearrangements. A second model to be considered is that both deactivation and desensitization occur from a common structural precursor state, the ligand-bound, closed cleft conformation (Figure 9). If CX614 and LY506091 stabilize this state, the result could be a slowing of macroscopic rates of deactivation and desensitization. A third model is that CX614 and LY506091 modulate only channel closing, and their apparent modulation of deactivation and desensitization arise as a result of this single action on channel gating. Our current lack of understanding of AMPA receptor gating, and the absence of single channel studies, prevent a rigorous test of

these different models. However, the Robert and Howe model (Robert and Howe 2003; Robert, Armstrong et al. 2005) provide an excellent starting place to begin to address these issues. Thus, in Figure 9 we present data comparing models 2 and 3. To test model 2, we decreased the probability of a receptor exiting the ligand-bound, closed-cleft conformation by reducing the rates of agonist dissociation (k_{-1}), the rate of channel opening (β), and the rate of the onset of desensitization ($\delta 1$) each by two-fold. To test model 3, we simply slowed the rate of channel closing (α). We found that model 3 more closely fit the experimental data, that is, the modulation of receptor deactivation and concomitant block of receptor desensitization. If this is correct, we would predict that single channel analysis would demonstrate that CX614 and LY506091 directly modulate channel closing, rather than merely stabilizing the ligand-bound closed left conformation, thereby increasing the probability of a channel either opening or desensitizing.

Designing potent, high-affinity, isoform-selective positive allosteric modulators. An initial problem with modulators of AMPA receptors was the need to increase their affinity, as well as improve their subunit and splice isoform selectivity. In this regard, LY506091 and LY2152080 provide important new insight. First, it is clear that both drugs can bind to the modulatory site with higher affinity (nM) than previously-described modulators, indicating that the site is amenable to the development new, therapeutically-relevant compounds. Secondly, LY506091 and LY2152080 are very efficacious, suggesting that there

is a relationship between high-affinity binding to the site and efficacious modulation of receptor activity. Thirdly, LY506091 and LY2152080 have very surprising isoform selectivities that were not predicted from their binding characteristics. Although LY2152080 showed a slight preference for the flip isoform in binding, it was dramatically more efficacious at modulating the kinetics of flip isoforms than flop. The basis of this preference is not clear from the present studies. Co-crystals of the flip and flop interface of the GluR2 LBC with agonist are not markedly different (David Timms, data not shown), suggesting the limitations of the static crystal structure in detecting differences in isoform-specific kinetic properties and modulation.

The functional implications of the selectivity of LY2152080 may be very significant. One of the concerns about using AMPA receptor positive modulators clinically is our insufficient understanding of how enhancing the AMPA receptor component of excitatory synapses compares with the effects of enhancing AMPA receptors on inhibitory cells. For instance, the CA1 region of the hippocampus contains pyramidal neurons that are excitatory but also receive information from inhibitory interneurons which are themselves activated by excitatory neurons, confounding the predicted effects of any given AMPA modulator. In this case, the goal for rational drug design becomes the ability of a modulator to affect the overall tone of excitation or inhibition within the circuit. Effects of AMPAkines CX516 and CX546 (which are slightly flop-selective) on excitation have been shown to outweigh their effects on inhibition, while CTZ seems to have a similar

effect on both pyramidal cells and interneurons (Xia and Arai 2005). Importantly, principle neurons express AMPA receptors composed of predominantly flip isoforms, whereas interneurons express AMPA receptors with a substantial flop component. Thus, LY2152080 would be predicted to enhance the excitatory component of principal neurons, while not effectively modulating the AMPA receptors on inhibitory cells, whereas LY506091 would affect both types of cell equally. Thus, future studies in a slice preparation using LY506091 and LY2152080 could provide important new information relevant to the development of the AMPA receptor complex for therapeutic benefit.

GluR2 Flip	*Wild-type*	*S497A*	*S497T*	*S729A*	*G731A*	*K763Q*
500ms GLU	6.7 ± 0.4	11.1 ± 2.2	6.7 ± 0.2	6.2 ± 1.2	0.5 ± 0.03	4.6 ± 0.3
	(22)	(5)	(4)	(4)	(15)	(18)
SS/Pk GLU	0.04 ± 0.01	0.10 ± 0.05	0.02 ± 0.004	0.01 ± 0.005	0.03 ± 0.01	0.03 ± 0.01
	(22)	(5)	(4)	(4)	(15)	(18)
1ms GLU	0.8 ± 0.1	1.2 ± 0.4	1.0 ± 0.1	1.1 ± 0.3	0.4 ± 0.04	1.0 ± 0.1
	(21)	(4)	(4)	(3)	(15)	(15)
500 ms LY506091	116.5 ± 38.1	59.4 ± 0.00	non-desens	non-desens	9.3 ± 2.6	217.6 ± 50.2
	(5)	(1)	(3)	(2)	(6)	(5)
SS/Pk LY506091	0.92 ± 0.03	0.90 ± 0.00	0.98 ± 0.002	1.01 ± 0.004	0.04 ± 0.01	0.89 ± 0.03
	(5)	(1)	(3)	(2)	(6)	(6)
1 ms LY506091	1.8 ± 0.3	7.8 ± 0.00	4.6 ± 1.6	6.1 ± 0.7	0.4 ± 0.1	4.1 ± 0.9
	(5)	(1)	(3)	(2)	(6)	(5)
500 ms CX614	46.5 ± 12.0	39.2 ± 14.2	65.0 ± 18.0	114.0 ± 9.0	0.9 ± 0.1	62.9 ± 16.5
	(10)	(3)	(3)	(4)	(6)	(9)
SS/Pk CX614	0.66 ± 0.05	0.89 ± 0.01	0.79 ± 0.06	0.29 ± 0.03	0.05 ± 0.02	0.39 ± 0.03
	(9)	(4)	(3)	(4)	(6)	(9)
1 ms CX614	1.9 ± 0.7	4.2 ± 0.7	1.3 ± 0.02	1.3 ± 0.1	0.5 ± 0.1	2.2 ± 0.3
	(10)	(4)	(3)	(4)	(6)	(9)
500 ms LY2152080	49.0 ± 20.8	29.1 ± 2.8	8.0 ± 1.2	11.4 ± 1.9	6.3 ± 1.6	5.3 ± 0.2
	(7)	(3)	(3)	(3)	(8)	(7)
SS/Pk LY2152080	0.66 ± 0.11	0.66 ± 0.01	0.78 ± 0.02	0.87 ± 0.004	0.06 ± 0.01	0.05 ± 0.01
	(7)	(3)	(3)	(3)	(8)	(7)
1 ms LY2152080	5.6 ± 1.2	3.7 ± 0.4	4.5 ± 1.2	3.6 ± 0.5	0.5 ± 0.04	1.4 ± 0.3
	(7)	(3)	(3)	(3)	(8)	(7)
500 ms CTZ	Non-desens	non-desens	non-desens	318.9 ± 37.1	86.6 ± 35.6	37.8 ± 6.0
	(8)	(9)	(3)	(4)	(6)	(11)
SS/Pk CTZ	0.96 ± 0.02	0.92 ± 0.02	0.99 ± 0.01	0.91 ± 0.02	0.72 ± 0.06	0.76 ± 0.02
	(8)	(9)	(3)	(5)	(6)	(11)
1 ms CTZ	1.3 ± 0.3	1.4 ± 0.3	1.9 ± 0.2	2.6 ± 0.5	0.8 ± 0.1	2.5 ± 0.2
	(8)	(6)	(3)	(5)	(6)	(10)

GluR2 Flop	*Wild-type*	*S497A*	*S497T*	*S729A*	*G731A*	*K763Q*
500ms GLU	1.6 ± 0.1	2.1 ± 0.1	3.0 ± 0.7	1.0 ± 0.05	0.8 ± 0.04	1.0 ± 0.1
	(22)	(4)	(3)	(3)	(9)	(25)
SS/Pk GLU	0.03 ± 0.01	0.03 ± 0.02	0.02 ± 0.02	0.01 ± 0.002	0.03 ± 0.01	0.02 ± 0.003
	(22)	(4)	(3)	(3)	(9)	(25)
1ms GLU	0.7 ± 0.1	0.9 ± 0.1	1.0 ± 0.3	0.5 ± 0.1	0.5 ± 0.1	0.7 ± 0.05
	(18)	(4)	(3)	(3)	(9)	(23)
500 ms LY506091	non-desens	non-desens	15.6 ± 5.7	217.8 ± 73.2	1.1 ± 0.2	non-desens
	(12)	(5)	(3)	(4)	(7)	(6)
SS/Pk LY506091	0.94 ± 0.01	0.87 ± 0.01	0.60 ± 0.03	0.87 ± 0.03	0.02 ± 0.01	0.95 ± 0.01
	(12)	(5)	(3)	(4)	(7)	(6)
1 ms LY506091	2.8 ± 0.4	3.6 ± 0.6	3.5 ± 0.4	4.0 ± 1.1	0.3 ± 0.02	7.0 ± 1.2
	(12)	(5)	(3)	(4)	(7)	(6)
500 ms CX614	136.3 ± 26.7	134.8 ± 28.1	2.1 ± 0.5	164.9 ± 25.7	1.0 ± 0.1	120.8 ± 14.4
	(10)	(3)	(3)	(3)	(7)	(8)
SS/Pk CX614	0.67 ± 0.02	0.89 ± 0.02	0.05 ± 0.01	0.15 ± 0.03	0.06 ± 0.02	0.23 ± 0.02
	(13)	(3)	(3)	(3)	(8)	(8)
1 ms CX614	1.9 ± 0.2	6.1 ± 0.9	0.8 ± 0.1	3.1 ± 1.6	0.5 ± 0.1	4.3 ± 0.5
	(12)	(3)	(3)	(3)	(8)	(8)
500 ms LY2152080	2.3 ± 0.2	2.4 ± 0.4	1.9 ± 0.2	134.1 ± 45.4	1.5 ± 0.3	0.9 ± 0.1
	(11)	(3)	(3)	(3)	(8)	(8)
SS/Pk LY2152080	0.18 ± 0.04	0.25 ± 0.07	0.01 ± 0.005	0.56 ± 0.03	0.07 ± 0.03	0.03 ± 0.01
	(11)	(3)	(3)	(3)	(8)	(8)
1 ms LY2152080	3.7 ± 1.5	1.4 ± 0.2	0.9 ± 0.1	7.3 ± 1.8	0.3 ± 0.03	0.6 ± 0.03
	(7)	(2)	(3)	(3)	(8)	(7)
500 ms CTZ	152.9 ± 12.3	148.6 ± 13.5	91.2 ± 14.0	85.2 ± 9.7	50.5 ± 5.1	52.4 ± 4.9
	(8)	(6)	(4)	(2)	(6)	(8)
SS/Pk CTZ	0.33 ± 0.05	0.15 ± 0.03	0.05 ± 0.02	0.07 ± 0.02	0.03 ± 0.01	0.12 ± 0.06
	(8)	(6)	(4)	(2)	(6)	(8)
1 ms CTZ	0.6 ± 0.1	0.6 ± 0.1	0.9 ± 0.4	0.7 ± 0.1	0.9 ± 0.3	0.8 ± 0.1
	(8)	(6)	(4)	(2)	(6)	(8)

Table 3.1. Summary of electrophysiology data for homomeric GluR2 WT, $S_{497}A$, $S_{497}T$, $S_{729}A$, $G_{731}A$, and $K_{763}Q$, flip and flop receptors heterologously expressed in HEK293 cells exposed to glutamate alone or glutamate and each of 4 modulators. Data reported as mean ± SEM compared using ANOVA with Dunnett's test for multiple comparisons within each receptor type to L-glutamate "control", ([a], $p<0.0001$; [b], $p<0.001$; [c], $p<0.05$)or between wild type and mutant ([d], $p<0.0001$; [e], $p<0.001$; [f], $p<0.05$) . Data were fit with a double exponent and both fast (F) and slow (S) components were combined into a weighted average based on their respective amplitude contributions ($\%A_{Fast} \times \tau_{Fast} + \%A_{Slow} \times \tau_{Slow}$). Non-desens, cells that did not desensitize in response to modulator.

a

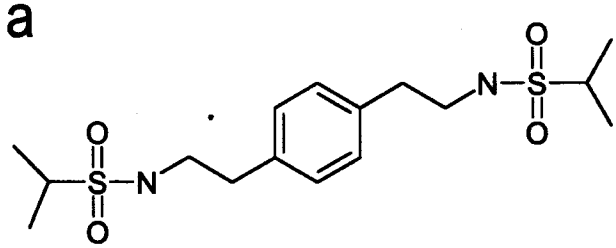

Bis-Alkylsulfonamide 506091

b

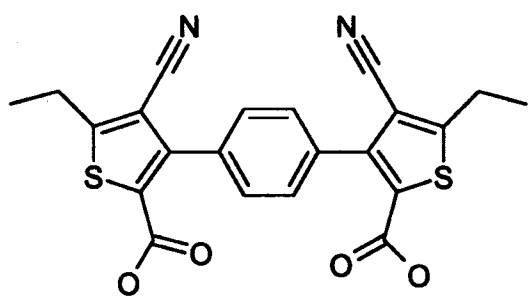

Bis-Carboxythiophene 2152080

Figure 1

Figure 3.1. Chemical structures (top) and omit electron density maps (bottom) of two positive allosteric modulators of AMPA receptors, a, Bis-Alkylsulfonamide 506091 (LY506091) and b, Bis-Carboxythiophene 2152080 (LY2152080). Omit density map for LY506091 (A) was calculated using $|F_o| - |F_c|$ coefficients, view is shown perpendicular to the two-fold axis. A simulated omit density map for LY2152080 is shown (B).

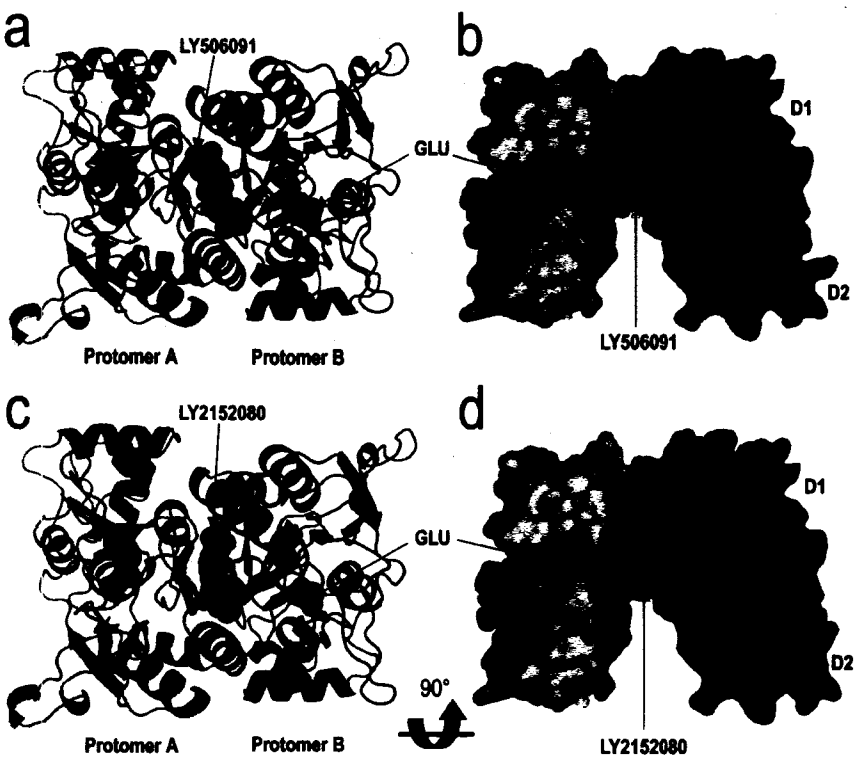

Figure 2

Figure 3.2. LY506091 and LY2152080 co-crystals with GluR2o S1SJ2 and L-glutamate. a, One molecule of LY506091 (magenta CPK) binds within the dimer interface at the clamshell hinges. View looking down the two-fold axis. Glutamate (GLU) is shown as red CPK. S1SJ2 is shown in cartoon representation. b, View of LY506091 perpendicular to the two-fold axis, S1SJ2 is shown in surface representation. c, One molecule of LY2152080 (pink CPK) binds within the dimer interface at the clamshell hinges. View looking down the two-fold axis. Glutamate is shown as red CPK. S1SJ2 is shown in cartoon representation. d, View of LY2152080 perpendicular to the two-fold axis, S1SJ2 is shown in surface representation. D1 and D2, Domains 1 and 2, respectively.

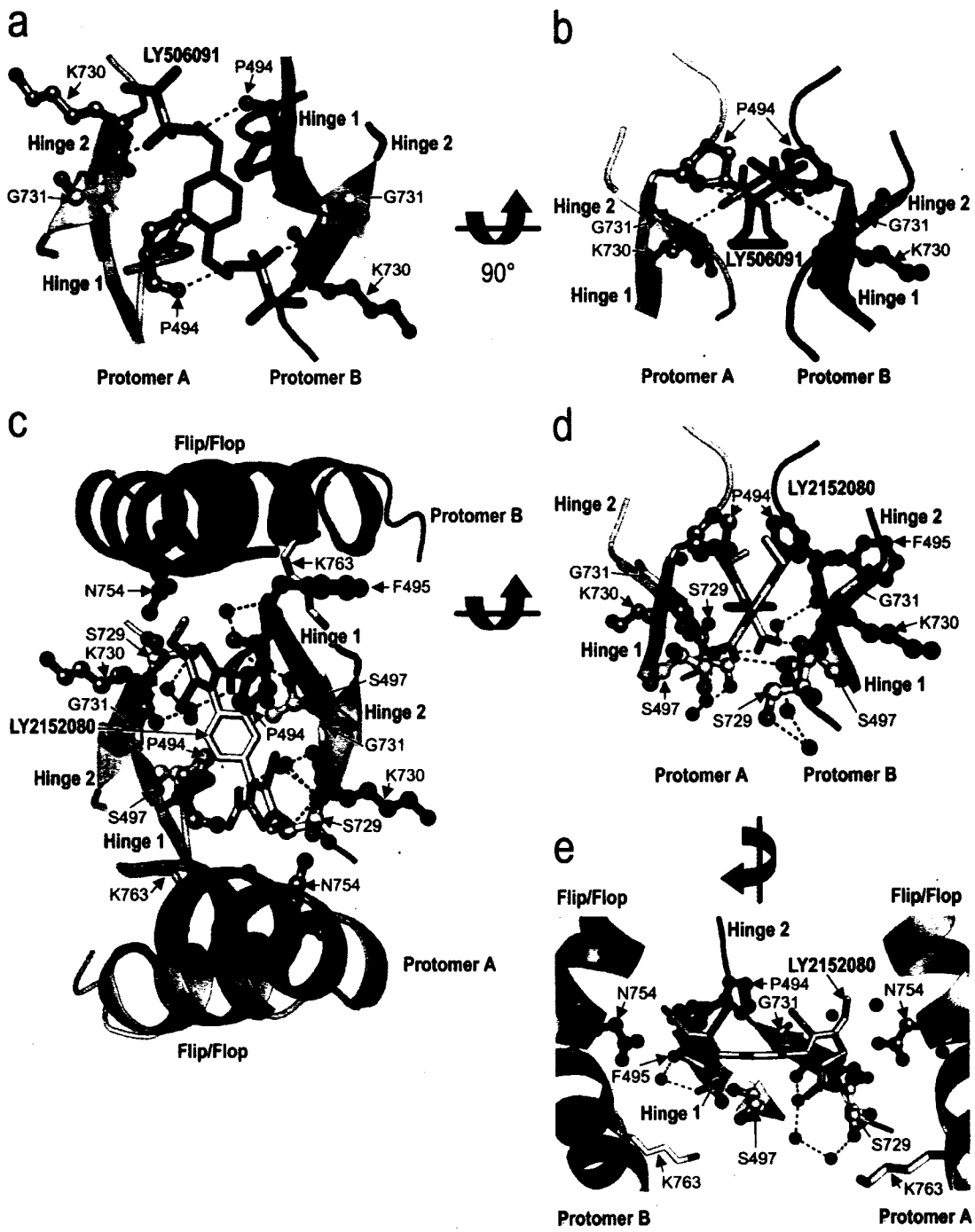

Figure 3

Figure 3.3. Although both LY modulators bind at the dimer interface and hinges, they make different contacts with the receptor. a, Top view of LY506091 (magenta stick) looking down the two-fold axis of symmetry showing the relationship of LY506091 to the hinge regions of S1SJ2 b, Side view of LY506091 rotated 90° about the x-axis from view A c, Top view of LY2152080 (pink stick) showing the relationship of LY2152080 to the flip/flop and hinge regions of S1SJ2 d, Side view of LY2152080 , rotated 90° about the x-axis from view c, omitting the flip/flop regions of Protomers A and B for clarity. e, Side view of LY2152080 rotated 90° about the y-axis from view d, omitting the hinges of Protomer B for clarity. Residues within 3.2Å of S1SJ2 are shown in ball-and-stick representation with CPK colors and carbons colored according to protomer (green, A and blue, B). Yellow residues indicate sites of point mutations. Residues K763 and G731 are represented in stick view in panels c-e, illustrating sites of these residues in relation to LY2152080 even though they do not form contacts with LY2152080. Water molecules are shown as cyan spheres. Calculated hydrogen bonds are shown as black dashed lines.

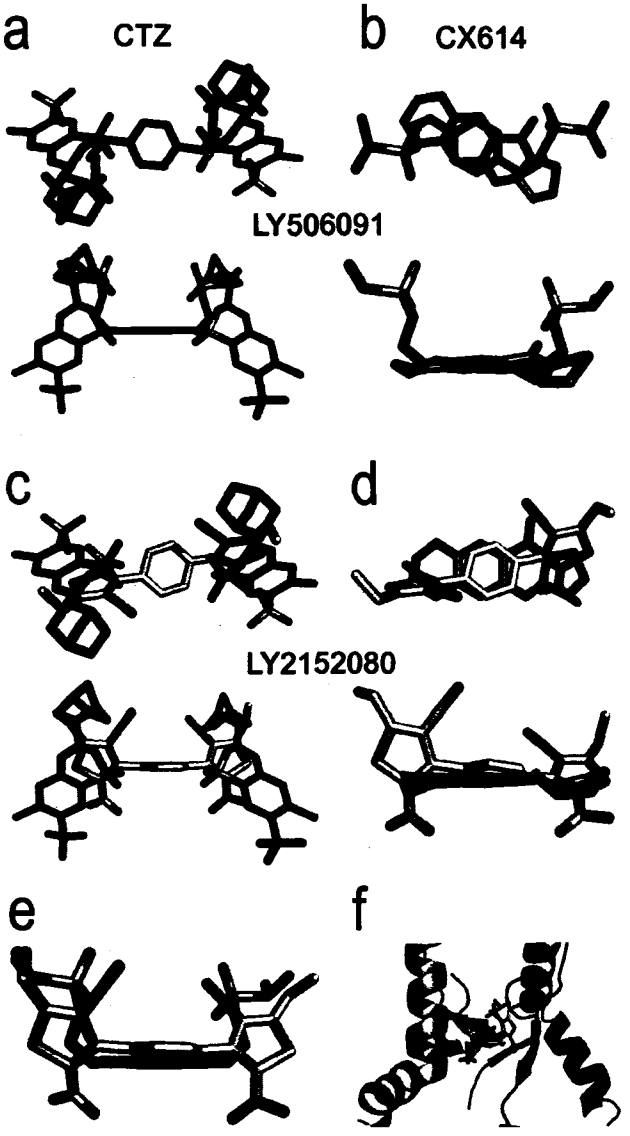

Figure 4

Figure 3.4. LY506091 (magenta stick, a and b) and LY2152080 (pink stick, c and d) share common groups with both classes of potentiators, cyclothiazide (CTZ, green stick, left panel) and Ampakine, CX614 (slate blue stick, right panel). Aside from carbons, colors are shown in CPK. Top (upper) and side (lower) views of each overlay are provided. e, Alignment of LY506091 and LY2152080. f, Side view of same alignment in panel E with -10° tilt about the x-axis illustrating the postion of both compounds at the Hinge 1 (chartreuse and purple beta sheets), Hinge 2 (green and blue beta sheets) and flip/flop (pale green and sky blue) regions for reference.

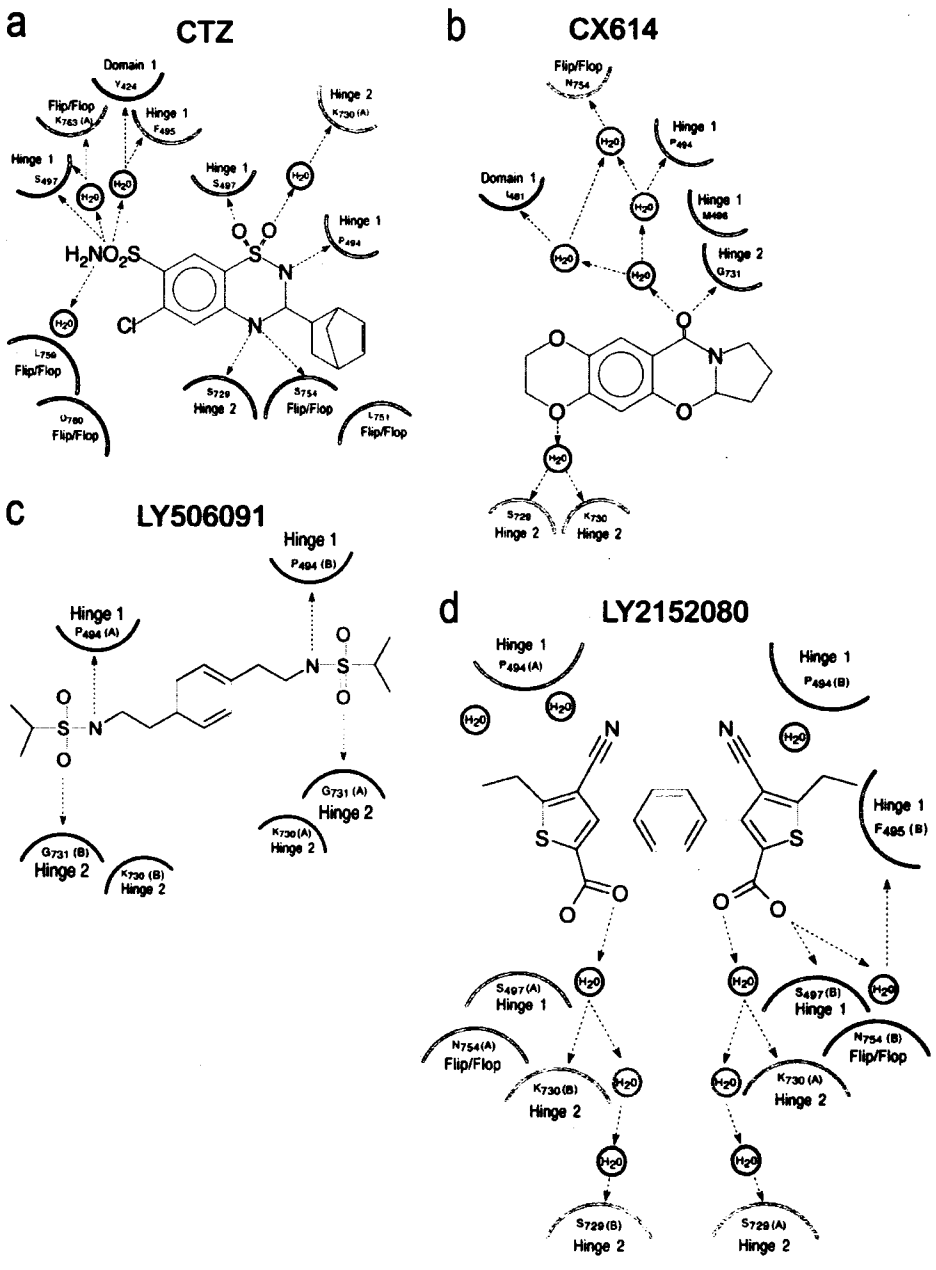

Figure 5

Figure 3.5. Pharmacophores of CTZ (a) , CX614 (b) , LY506091(c) and LY2152080 (d) show different profiles of drug binding. Residues within 3.2 Å of each compound are defined by red semi-circles, residues between 3.3 and 4.9 Å are defined by green semi-circles and water molecules participating in hydrogen bonds but greater than 5.0 Å from drug are defined by blue circles. Calculated hydrogen bonds are illustrated by black dashed arrows.

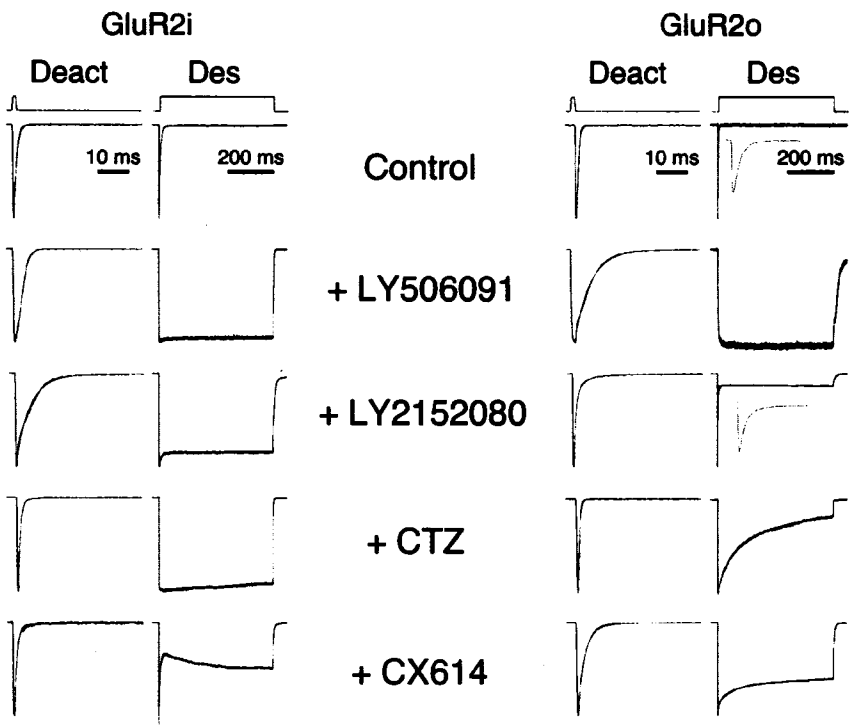

Figure 6

Figure 3.6. LY506091 and LY2152080 modulate deactivation and desensitization of GluR2 flip and flop. LY2152080 is isoform-specific for flip. Representative traces for homomeric WT GluR2 flip (i) (left panel) and flop (o) (right panel) receptors heterologously expressed in HEK293 cells exposed to 1ms (deactivation protocol) or 500 ms (desensitization protocol) of glutamate alone or glutamate plus each of 4 modulators. Inverted traces above Control traces are representative open-tip junctions. 2-exponential fits for decay times (see Table 2) are shown in red.

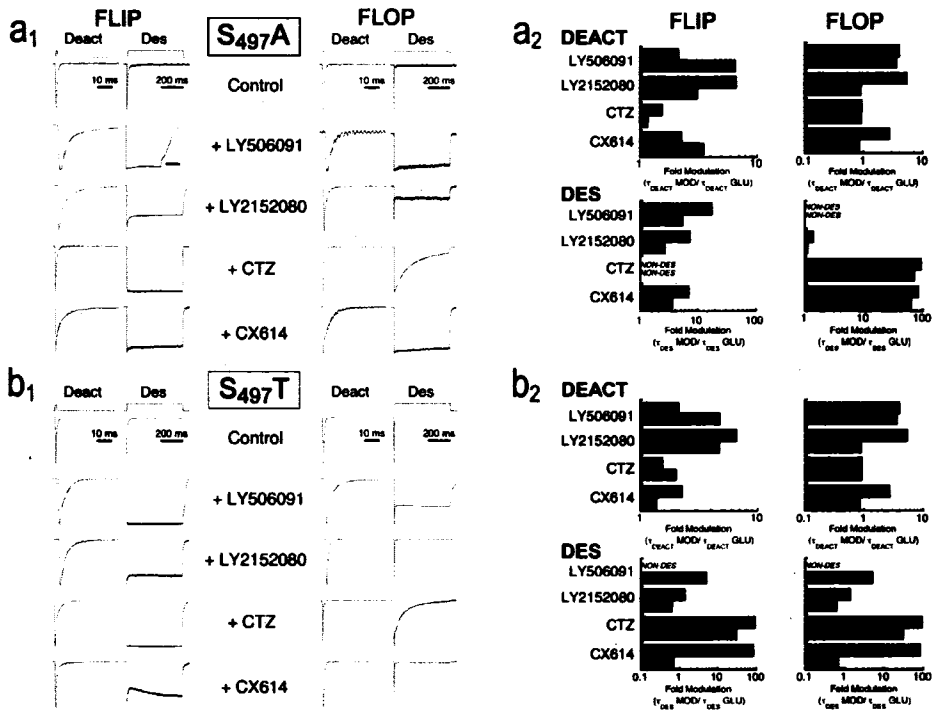

Figure 7

Figure 3.7. Effects of Hinge 1 mutations on GluR2 modulation. a_1, b_1, Representative traces for homomeric GluR2 $S_{497}A$ (a_1) and $S_{497}T$ (b_1), flip (i) (left panel) and flop (o) (right panel) receptors heterologously expressed in HEK293 cells exposed to 1ms (deactivaiton protocol) or 500 ms (desensitization protocol) of glutamate alone or glutamate plus each of 4 modulators. Inverted traces above Control traces are representative open-tip junctions. 2-exponential fits for decay times (see Table 2) are shown in red. a_2, b_2, Fold modulation of deactivation (top) and desensitization (bottom) of GluR2 wild-type (black bars) and GluR2 $S_{497}A$ (a_2, gray bars) or GluR2 $S_{497}T$ (b_2, gray bars) by each of 4 modulators. Flip, left; Flop, right. Fold modulation is the ratio of decay time constant, τ, with modulator (MOD) to τ without modulator (GLU). Because these are fold changes of means (no single cell was exposed to both modulator and control), no error/error bars can be reported.

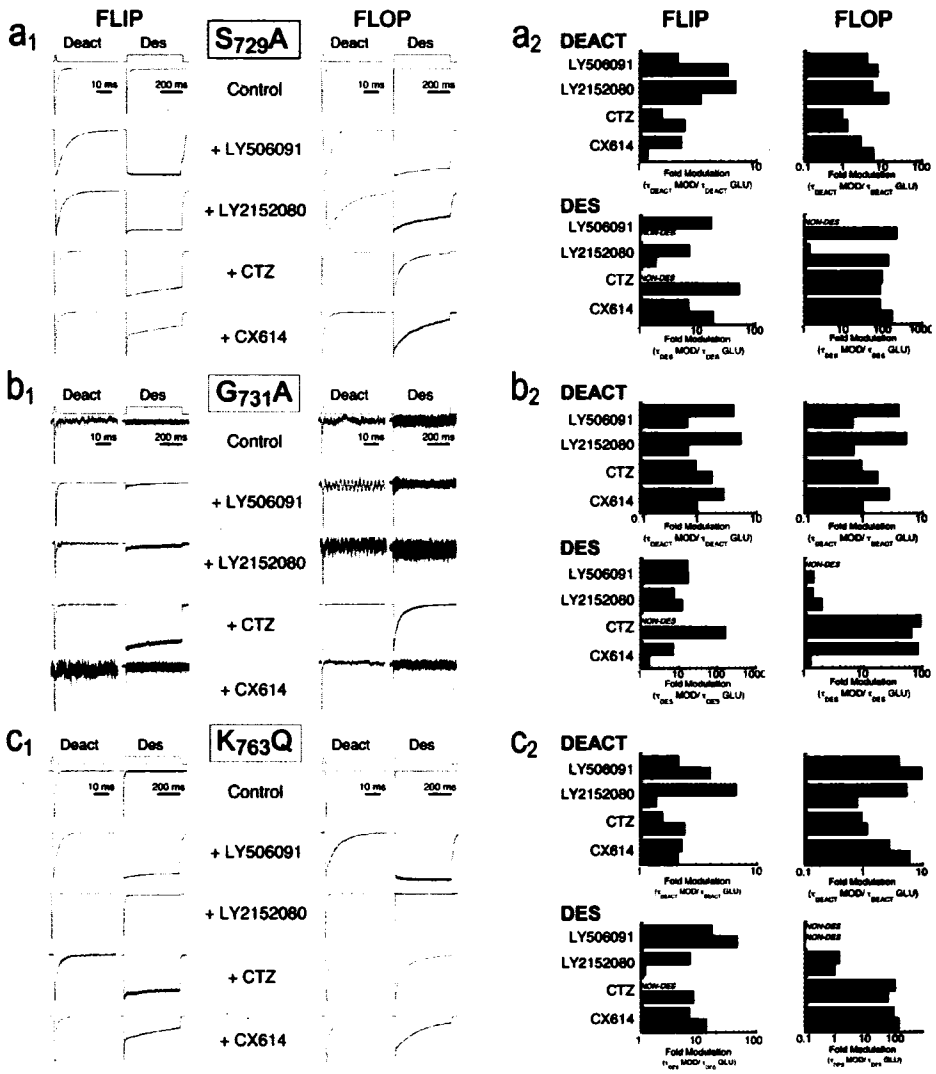

Figure 8

Figure 3.8. Effects of Hinge 2 and i/o mutations on GluR2 modulation. a_1, b_1, c_1, Representative traces for homomeric GluR2 $S_{729}A$ (a_1) ; $G_{731}A$ (b_1); and $K_{763}Q$ (c_1); flip (i) (left panel) and flop (o) (right panel) receptors heterologously expressed in HEK293 cells exposed to 1ms (deactivaiton protocol) or 500 ms (desensitization protocol) of glutamate alone or glutamate plus each of 4 modulators. Inverted traces above Control traces are representative open-tip junctions. 2-exponential fits for decay times (see Table 2) are shown in red. a_2, b_2, c_1, Fold modulation of deactivation (top) and desensitization (bottom) of GluR2 wild-type (black bars) and GluR2 $S_{729}A$ (a_2, gray bars); GluR2 $G_{731}A$ (b_2, gray bars); or GluR2 $K_{763}Q$ (c_2, gray bars)by each of 4 modulators. Flip, left; Flop, right. Fold modulation is the ratio of decay time constant, τ, with modulator (MOD) to τ without modulator (GLU). Because these are fold changes of means (no single cell was exposed to both modulator and control), no error/error bars can be reported.

CHAPTER 4: DISSERTATION SUMMARY AND FUTURE DIRECTIONS

4.1 Dissertation Summary

Much research has been conducted on AMPA receptor structure, function and modulation. Solving of the crystal structure of the isolated GluR2 ligand binding core has provided valuable insight into the structural determinants of these mechanisms; however, interpretations of the crystal structure alone are limited. Functional data has also greatly contributed to the structural studies, but until now has been incomplete. This is the first body of work that looks at 4 major classes of modulator, taking into account isoform differences in the same AMPA receptor subunit (GluR2) and tests 3 subdomains of the ligand binding core previously hypothesized to be distinctly responsible for AMPA receptor deactivation and desensitization. These data argue for a model in which the AMPA receptor depends upon global changes, using the same mechanism for closing the receptor in deactivation as is used for closing the receptor in desensitization. However, the exact mechanism the ligand binding core uses to contact and direct the activation gate remains unclear. The idea that using modulators to work backwards to understand innate AMPA receptor gating is interesting but not without flaw when modulators have overlapping binding sites

and actions; however until more distinctly acting drugs are designed (like LY2152080) or better methods are developed and experiments designed for testing AMPA receptor function in the intact receptor, this approach will have to do and is currently the best approach for the necessary design of more specific drugs.

4.2 Present Results Lead to Follow-up Studies

4.2.1 Computer Simulations And Single Channel Recording Offer Higher Resolution Techniques To Understanding Mechanisms Of AMPA Receptor Gating And Modulation.

Computer simulations have suggested that slowing cleft opening from around agonist (current proposed model of slowing deactivation) does not fully account for the effects seen by drugs such as CX614 which have a greater impact on deactivation rates than the benzamide drugs that primarily slow desensitization and prevent dimer dissociation. However, CX614 does have considerable impact on desensitization rates, so it may be that the states are distinct and our tools to resolve them are not, but because the hinge region of the clamshell is located at the dimer interface, it is more likely that there is at least some interaction between deactivation and desensitization.

The current model of AMPA receptor kinetics assumes that the time it takes the receptor to get from the resting to open state depends on agonist binding to each

subunit, with a graded opening to the fully-occupied, maximally open state. This idea is supported by three (and more recently, four) different conductance states (Rosenmund, Stern-Bach et al. 1998; Gebhardt and Cull-Candy 2006). Although the opening of the receptor is graded and dependent on subunit occupancy of agonist, the closing of the channel is assumed to be one step, independent of subunit occupancy. Although it is unlikely that agonist unbinds from the open state, closing of the channel may, in fact, also be a graded process with each subunit entering its own "closed" (deactivated or desensitized) state. Furthermore, it seems plausible that deactivation and desensitization could be part of the same process, with the ligand binding core acting as a barometer for glutamate concentration. In this sense, it would be valuable to use single channel analysis to test the experimental conditions of deactivation (1ms) vs. desenstization (500 ms) with glutamate in varying concentrations. If opening frequencies or duration times are different or occupancy time in individual conductance states are different (without affecting overall P_o), this might suggest a further relationship between deactivation and desensitization where deactivation is simply incomplete desensitization, and a comparable off time might be seen if you increase the concentration of glutamate for the 1 ms protocol compared to the 500 ms protocol. If this is the case, then, it is likely that, opposite to opening, each subunit has its own desensitized configuration, contributing to the closure of the pore and that if 3 or more of the subunits are in that configuration, then the channel will be closed. Deactivation and desensitization could be two distinct states or just a gradation of the same

closing process, where less agonist=less subunits that are desensitized that the channel must recover from before opening again.

4.2.2 Full Isoform Differences Have Yet To Be Elucidated

The developmental, structural and functional differences between AMPA receptor flip and flop splice isoforms is well characterized, demonstrating how two of the three regions that have different residues are important for receptor kinetics and modulation; however, little is known about the highly conserved Region 3 (GGGD in GluR1-4 flop; KDSG in GluR1-4 flip), proximal to TM4.

Although Region 3 does not affect rates of desensitization or rates of recovery from desensitization like Regions 1 & 2 (Quirk, Siuda et al. 2004), the possibility that it does not affect some aspect of AMPA receptor gating, assembly, modulation or signaling interaction is highly unlikely. Future experiments to understand the role of the Region 3 differences might include additional site-directed mutagenesis studies, testing the effects of swapping flip and flop residues in Region 3 paired with additional electrophysiological, optical, and immunoblot methods to look for functional differences, differences in cellular and subcellular localization, and differences in protein-protein interactions.

4.3 Future Directions: Use Of Other Techniques To View AMPA Receptor Dynamics

Most of the experiments from the present study were designed using as a guide x-ray crystallography structures of the isolated GluR2 flop ligand binding core co-crystallized with agonist and modulators, where structures were analyzed from a

solid, possibly constrained state and not necessarily in physiological conditions. Alternatively, because it takes advantage of proteins in solution, nuclear magnetic resonance (NMR) may reveal more about the dynamics of AMPA receptors in different states and exposed to different modulators. Another approach would be to use single-particle cryo-electron microscopy, although this technique lacks the high-resolution images of x-ray crystallography, it is capable of capturing images of proteins in multiple states. Fluorescence Resonance Energy Transfer (FRET) is another method that has and will continue to help the present studies. Together with electrophysiological data these structural visualization techniques likely will contribute to the ultimate goal of revealing the molecular determinants of AMPA receptor gating and modulation.

REFERENCES

Arai, A., M. Kessler, et al. (2000). "Effects of the potent ampakine CX614 on hippocampal and recombinant AMPA receptors: interactions with cyclothiazide and GYKI 52466." Molecular Pharmacology **58**(4): 802-813.

Arai, A., Y.-F. Xia, et al. (2002). "Benzamide-type AMPA receptor modulators form two subfamilies with distinct modes of action." Journal of Pharmacology and Experimental Therapeutics **303**(3): 1075-1085.

Arai, A. C., M. Kessler, et al. (2000). "Effects of the potent ampakine CX614 on hippocampal and recombinant AMPA receptors: interactions with cyclothiazide and GYKI 52466." Mol Pharmacol **58**(4): 802-13.

Bettler, B. and C. Mulle (1995). "Review: neurotransmitter receptors. II. AMPA and kainate receptors." Neuropharmacology **34**(2): 123-39.

Black, M. D. (2005). "Therapeutic potential of positive AMPA modulators and their relationship to AMPA receptor subunits. A review of preclinical data." Psychopharmacology (Berl) **179**(1): 154-63.

Colbourne, F., S. Y. Grooms, et al. (2003). "Hypothermia rescues hippocampal CA1 neurons and attenuates down-regulation of the AMPA receptor GluR2 subunit after forebrain ischemia." Proc Natl Acad Sci U S A **100**(5): 2906-10.

De Sarro, G., A. Siniscalchi, et al. (2000). "NMDA and AMPA/kainate receptors are involved in the anticonvulsant activity of riluzole in DBA/2 mice." Eur J Pharmacol **408**(1): 25-34.

Dingledine, R., K. Borges, et al. (1999). "The glutamate receptor ion channels." Pharmacology Reviews **51**: 7-61.

Gebhardt, C. and S. G. Cull-Candy (2006). "Influence of agonist concentration on AMPA and kainate channels in CA1 pyramidal cells in rat hippocampal slices." J Physiol **573**(Pt 2): 371-94.

Heurteaux, C., I. Lauritzen, et al. (1994). "Glutamate-induced overexpression of NMDA receptor messenger RNAs and protein triggered by activation of AMPA/kainate receptors in rat hippocampus following forebrain ischemia." Brain Res **659**(1-2): 67-74.

Horning, M. S. and M. L. Mayer (2004). "Regulation of AMPA receptor gating by ligand binding core dimers." Neuron **41**: 379-388.

Jin, R., T. G. Banke, et al. (2003). "Structural basis for partial agonist action at ionotropic glutamate receptors." Nat Neurosci **6**(8): 803-10.

Jin, R., S. Clark, et al. (2005). "Mechanism of positive allosteric modulators acting on AMPA receptors." J Neurosci **25**(39): 9027-36.

Klein, R. M. and J. R. Howe (2004). "Effects of the lurcher mutation on GluR1 desensitization and activation kinetics." J Neurosci **24**(21): 4941-51.

Koike, M., S. Tsukada, et al. (2000). "Regulation of kinetic properties of GluR2 AMPA receptor channels by alternative splicing." J Neurosci **20**(6): 2166-74.

Leever, D. L., S. Z. Clark, et al. (2003). "Identification of a site in GluR1 and GluR2 important for modulation of deactivation and desensitization." Molecular Pharmacology **(in press)**.

Liu, B., M. Liao, et al. (2006). "Ischemic insults direct glutamate receptor subunit 2-lacking AMPA receptors to synaptic sites." J Neurosci **26**(20): 5309-19.

Lomeli, H., J. Mosbacher, et al. (1994). "Control of kinetic properties of AMPA receptor channels by nuclear RNA editing." Science **266**: 1709-1713.

Lynch, G., R. Granger, et al. (1997). "Evidence that a positive modulator of AMPA-type glutamate receptors improves delayed recall in aged humans." Experimental Neurology **145**: 89-92.

Malinow, R. and R. C. Malenka (2002). "AMPA receptor trafficking and synaptic plasticity." Annu Rev Neurosci **25**: 103-26.

Mansour, M., N. Nagarajan, et al. (2001). "Heteromeric AMPA receptors assemble with a preferred subunit stoichiometry and spatial arrangement." Neuron **32**(5): 841-53.

N.A. Mitchell, M. W. F. (2004). Two Opposing Actions Of Cyclothiazide On GluR1 AMPA Receptors. Society for Neuroscience, Washington, DC.

Nagarajan, N., C. Quast, et al. (2001). "Mechanism and impact of allosteric AMPA receptor modulation by the ampakine CX546." Neuropharmacology **41**(6): 650-63.

Nagarajan, N., C. Quast, et al. (2001). "Mechanism and impact of allosteric AMPA receptor modulation by the Ampakine® CX546." Neuropharmacology **31**: 650-663.

Opitz, T., S. Y. Grooms, et al. (2000). "Remodeling of alpha-amino-3-hydroxy-5-methyl-4-isoxazole-propionic acid receptor subunit composition in

hippocampal neurons after global ischemia." Proc Natl Acad Sci U S A **97**(24): 13360-5.

Oswald, R. E. (2004). "Ionotropic glutamate receptor recognition and activation." Adv Protein Chem **68**: 313-49.

Partin, K. M. (2001). "Domains regulating AMPA receptor desensitization." Journal of Neuroscience **21**: 1939-1948.

Partin, K. M., D. Bowie, et al. (1995). "Structural determinants of allosteric regulation in alternatively spliced AMPA receptors." Neuron **14**: 833-843.

Partin, K. M., M. F. Fleck, et al. (1996). "AMPA receptor flip/flop mutants affecting deactivation, desensitization and modulation by cyclothiazide, aniracetam and thiocyanate." Journal of Neuroscience **16**: 6634-6647.

Partin, K. M., D. K. Patneau, et al. (1994). "Cyclothiazide differentially modulates desensitization of AMPA receptor splice variants." Molecular Pharmacology **46**: 129-138.

Pellegrini-Giampietro, D. E., J. A. Gorter, et al. (1997). "The GluR2 (GluR-B) hypothesis: Ca(2+)-permeable AMPA receptors in neurological disorders." Trends Neurosci **20**(10): 464-70.

Pollard, H., A. Heron, et al. (1993). "Alterations of the GluR-B AMPA receptor subunit flip/flop expression in kainate-induced epilepsy and ischemia." Neuroscience **57**: 545-554.

Quirk, J. C. and E. S. Nisenbaum (2003). "Multiple molecular determinants for allosteric modulation of alternatively spliced AMPA receptors." J Neurosci **23**(34): 10953-62.

Quirk, J. C., E. R. Siuda, et al. (2004). "Molecular determinants responsible for differences in desensitization kinetics of AMPA receptor splice variants." Journal of Neuroscience **24**(50): 11413-11420.

Ramanoudjame, G., M. Du, et al. (2006). "Allosteric mechanism in AMPA receptors: A FRET-based investigation of conformational changes." Proc Natl Acad Sci U S A.

Robert, A., N. Armstrong, et al. (2005). "AMPA receptor binding cleft mutations that alter affinity, efficacy, and recovery from desensitization." J Neurosci **25**(15): 3752-62.

Robert, A. and J. R. Howe (2003). "How AMPA receptor desensitization depends on receptor occupancy." J Neurosci **23**(3): 847-58.

Rosenmund, C., Y. Stern-Bach, et al. (1998). "The tetrameric structure of a glutamate receptor channel." Science **280**: 1596-1599.

Shepherd, T. A., J. A. Aikins, et al. (2002). "Design and synthesis of a novel series of 1,2-disubstituted cyclopentanes as small, potent potentiators of 2-amino-3-(3-hydroxy-5-methyl-isoxazol-4-yl)propanoic acid (AMPA) receptors." J Med Chem **45**(10): 2101-11.

Sommer, B., K. Keinänen, et al. (1990). "Flip and flop: a cell-specific functional switch in glutamate-operated channels of the CNS." Science **249**: 1580-1585.

Staubli, U., G. Rogers, et al. (1994). "Facilitation of glutamate receptors enhances memory." Proceedings of the National Academy of Sciences of the United States of America **91**: 777-781.

Stern-Bach, Y., B. Bettler, et al. (1994). "Agonist selectivity of glutamate receptors is specified by two domains structurally related to bacterial amino acid-binding proteins." Neuron **13**(6): 1345-57.

Stern-Bach, Y., S. Russo, et al. (1998). "A point mutation in the glutamate binding site blocks desensitization of AMPA receptors." Neuron **21**: 907-918.

Sun, Y., R. Olson, et al. (2002). "Mechanism of glutamate receptor desensitization." Nature **417**(6886): 245-53.

Sun, Y., R. Olson, et al. (2002). "Mechanism of glutamate receptor desensitization." Nature **417**: 245-253.

Suppiramaniam, V., B. A. Bahr, et al. (2001). "Member of the Ampakine class of memory enhancers prolongs the single channel open time of reconstituted AMPA receptors." Synapse **40**(2): 154-8.

Tanaka, H., S. Y. Grooms, et al. (2000). "The AMPAR subunit GluR2: still front and center-stage." Brain Res **886**(1-2): 190-207.

Vandergriff, J., K. Huff, et al. (2001). "Potentiation of responses to AMPA on central neurones by LY392098 and LY404187 in vivo." Neuropharmacology **40**(8): 1003-9.

Wollmuth, L. P., T. Kuner, et al. (2000). "The Lurcher mutation identifies delta 2 as an AMPA/kainate receptor-like channel that is potentiated by Ca(2+)." J Neurosci **20**(16): 5973-80.

Xia, Y. F. and A. C. Arai (2005). "AMPA receptor modulators have different impact on hippocampal pyramidal cells and interneurons." Neuroscience **135**(2): 555-67.

Ying, H. S., J. H. Weishaupt, et al. (1997). "Sublethal oxygen-glucose deprivation alters hippocampal neuronal AMPA receptor expression and vulnerability to kainate-induced death." J Neurosci **17**(24): 9536-44.

APPENDICES

APPENDIX 1: COPIES OF CONTRIBUTING MANUSCRIPTS

1.1 Identification of a site in GluR1 and GluR2 that is important for modulation of deactivation and desensitization (Leever et al., 2003)

1.2 Mechanism of Positive Allosteric Modulators Acting on AMPA receptors (Jin et al., 2005)

1.3 Kynurenic acid has a dual action on AMPA receptor responses (Prescott et al., 2006)

1.4 The proximal cytoplasmic tail of AMPA receptors is required for stargazin-mediated trafficking (Bedoukian et al., 2006)

0026-895X/03/6401-5–10$7.00
MOLECULAR PHARMACOLOGY
Copyright © 2003 The American Society for Pharmacology and Experimental Therapeutics
Mol Pharmacol 64:5–10, 2003

Vol. 64, No. 1
2430/1071078
Printed in U.S.A.

ACCELERATED COMMUNICATION

Identification of a Site in GluR1 and GluR2 That Is Important for Modulation of Deactivation and Desensitization

J. DUNCAN LEEVER, SUZANNE CLARK, AUTUMN M. WEEKS, and KATHRYN M. PARTIN

Department of Biomedical Sciences, Colorado State University, Fort Collins, Colorado

Received January 27, 2003; accepted March 19, 2003

This article is available online at http://molpharm.aspetjournals.org

ABSTRACT

The α-amino-3-hydroxy-5-methyl-4-isoxazolepropionic acid subtype of ionotropic glutamate receptors consists of rapidly gating ion channels. Positive modulation of channel gating may slow gating kinetics through at least two distinct mechanisms, evidenced by the predominant slowing of either the rate of receptor desensitization or the rate of offset after agonist withdrawal (deactivation). This study compares the actions of two positive allosteric modulators [cyclothiazide, which modulates desensitization, and 1-(1,4-benzodioxan-6-ylcarbonyl)piperidine (CX546), which modulates deactivation] in a mutant shown previously to impede modulation by cyclothiazide. These experiments test the hypothesis that the point mutation, GluR1(S493T), would also cause a loss of modulation by CX546. Wild-type GluR1 through -4 receptors were modulated by CX546, as assayed by the potentiation of steady-state currents in the *Xenopus laevis* oocyte expression system. CX546 potentiated steady-state currents of both splice isoforms of GluR1. Modulation by CX546 was completely abolished in GluR1(S493T) and its homolog, GluR2(S497T), although this mutation did not affect apparent agonist affinity in the absence of CX546. Thus, the GluR1(S493T) mutation has a similar impairment of modulation by either cyclothiazide or CX546, indicating that some residues at the subunit interface of glutamate receptors play an important role in channel deactivation and desensitization.

Ionotropic glutamate receptors are responsible for fast excitatory synaptic transmission in the central nervous system (Dingledine et al., 1999). Subtypes of glutamate receptors contribute to neuroplasticity: in animal models of learning and memory, *N*-methyl-D-aspartate receptors induce neuroplasticity, whereas the α-amino-3-hydroxy-5-methyl-4-isoxazolepropionic acid (AMPA) subtype of ionotropic glutamate receptors maintain the potentiated state (Huang and Stevens, 1998). In some cases, the potentiated state is maintained through cellular mechanisms that increase both the number and activity of AMPA receptors (Isaac et al., 1999). Thus, both *N*-methyl-D-aspartate and AMPA receptors may be important targets for the development of pharmacological agents that improve cognitive function and thereby treat brain damage or disease (Lynch, 1998).

This work was supported by American Heart Association Scientist Development grant 0030100N and National Institutes of Health grant R01-MH64700-02 (to K.M.P.). J.D.L. is a Hughes Undergraduate Research Scholar.

Preliminary findings related to this work were previously published in *Soc Neurosci Abstr* 27:480.12, 2001.

Two known classes of drugs act on AMPA receptors and have cognition-enhancing actions: the benzamides, including the AMPAkine CX546 and aniracetam; and the benzothiadiazides (BTDs), including cyclothiazide (CTZ) and IDRA21 (Isaacson and Nicoll, 1991; Yamada and Rothman, 1992; Zivkovic et al., 1995; Arai et al., 2002a). The AMPAkines have shown promise in improving cognitive function in laboratory animals and humans (Granger et al., 1993; Staubli et al., 1994; Arai et al., 1996b; Ingvar et al., 1997; Lynch et al., 1997). In particular, there are several recent reports on the mechanism of action of the AMPAkines CX516, CX546, and CX614 (Arai et al., 1996a; Arai et al., 2000, 2002b; Nagarajan et al., 2001). A potential problem for therapeutic use of cognition-enhancing drugs is that excessive AMPA receptor activity may induce hyperexcitability and seizures (Pelletier and Hablitz, 1996; Yamada, 1998). Thus, the development of brain-region–specific and subtype-specific drugs is an important goal that may require understanding the molecular mechanisms of these drugs.

Cognition-enhancing drugs modulate AMPA receptor gat-

ABBREVIATIONS: AMPA, α-amino-3-hydroxy-5-methyl-4-isoxazolepropionic acid; CTZ, cyclothiazide; CX546, 1-(1,4-benzodioxan-6-ylcarbonyl)piperidine; BTD, benzothiadiazide; GluR, ionotropic glutamate receptor; IDRA21, 7-chloro-3-methyl-3,4-dihydro-2H-1,2,4-benzothiadiazine 1,1-dioxide; BAPTA, 1,2-bis(2-aminophenoxy)ethane-*N*,*N*,*N*′,*N*′-tetraacetic acid; HEK, human embryonic kidney; DMSO, dimethyl sulfoxide; WT, wild type.

ing, including channel desensitization and deactivation; they also may modulate agonist affinity. Desensitization is the process by which the channel moves to a nonconducting state, although the agonist remains bound, thereby uncoupling ligand binding from channel opening. In contrast, deactivation is channel closure in the absence of desensitization; experimentally, this is measured as the offset of current after the withdrawal of the agonist (τ_{deact}). Thus, measurements of deactivation do not resolve channel closure from agonist unbinding. Generally, drugs such as benzamides are believed to modulate AMPA receptors by slowing deactivation. However, it has been proposed that there are different subfamilies of benzamides having distinct modulatory properties (Arai et al., 2002b). These investigators proposed that CX546 is a member of the subfamily that primarily slows channel closing rates (increasing τ_{deact}); this delays entry into the desensitized state, resulting in a secondary slowing of the macroscopic rate of channel desensitization (increasing τ_{des}). Alternatively, Nagarajan et al. (2001) suggested that CX546 slows agonist unbinding and increases the rate out of the desensitized state. Their hypothesis was supported by their findings that a nondesensitizing mutant receptor was still modulated by CX546, by virtue of the increase in agonist affinity. Either of these actions of benzamides is in contrast to the proposed actions of BTDs, including CTZ, which slow or block entry into the desensitized state with only a modest secondary effect on channel deactivation (Partin et al., 1996).

Consistent with the conventional idea that allosteric transitions involve intersubunit interactions, Sun et al. (2002) proposed that movement of AMPA receptor subunits at a dimer interface mediates desensitization. Using the isolated GluR2 agonist-binding domain, they found that CTZ spans this interface by forming hydrogen bonds and nonpolar contacts with amino acids from both subunits. CTZ may stabilize the interface and subsequently block transition of the receptor into the desensitized state. Thus, CTZ stabilizes the ligand-bound, nondesensitized conformation of AMPA receptors.

We previously mutated a residue at the subunit interface, GluR1(S493T), that impedes CTZ modulation of desensitization (Partin, 2001). These results are supported by structural data, which show that the homologous residue in GluR2, Ser497, hydrogen bonds with CTZ (Sun et al., 2002). Taken together, these data further implicate the subunit interface in desensitization and BTD action. In contrast, the binding site(s) of modulators of deactivation (e.g., CX546) have not been characterized. Modulator binding is presumed to be extracellular and coupled allosterically to the agonist-binding domain because the effects of CX546 depend on agonist concentration (Nagarajan et al., 2001).

The present study tests the hypothesis that the mutation of GluR1(S493T) also alters modulation by CX546. This assumes that channel deactivation (channel closing) requires a concerted conformational change at a dimer interface. To test this hypothesis, we compared CX546 and CTZ modulation on mutant and wild-type AMPA receptors. The results indicate that GluR1 Ser493 mutations severely impair modulation by CX546 as well as by CTZ, suggesting that a common binding site exists.

Materials and Methods

Plasmids and Mutants. Plasmids encoding cDNAs for flip (i) and flop (o) variants of wild-type GluR1 through -4 were gifts of Dr. Peter Seeburg (University of Heidelberg, Heidelberg, Germany) and Dr. Stephen Heinemann (Salk Institute, La Jolla, CA). Site-directed mutagenesis (QuikChange Mutagenesis Kit; Stratagene, La Jolla, CA) was performed to generate GluR1(S493T) and GluR2(S497T) mutations, which were confirmed by DNA sequencing (Macromolecular Resources Facility, Colorado State University; Fort Collins, CO).

Oocyte Expression. Capped mRNA was synthesized in vitro from linearized AMPA receptor cDNAs using T3 (GluR3) or T7 (GluR1, -2, and -4) polymerase (mMessage Machine; Ambion, Austin, TX). Oocytes were surgically obtained from adult *Xenopus laevis* (Nasco, Fort Atkinson, WI) anesthetized by immersion in 3% Tricaine (Sigma, St. Louis, MO) for 15 min and then placed on an ice bed. Animal care and surgical procedures conformed to institutional Animal Care and Use Committee standards and practices and were carried out in accordance with the National Institutes of Health's *Guide for the Care and Use of Laboratory Animals*. Harvested ovarian lobes were cut into small pieces and incubated with 1.5 mg/ml collagenase A (Roche Diagnostics, Indianapolis, IN) in calcium-free buffer (82.5 mM NaCl, 2 mM KCl, 1 mM $MgCl_2$, and 5 mM HEPES, pH 7.5) for 90 min at room temperature on a Nutator (Clay Adams, Parsippany, NJ). After thorough washing [88 mM NaCl, 1 mM KCl, 2.4 mM $NaHCO_3$, 0.3 mM $Ca(NO_3)_2$, 0.41 mM $CaCl_2$, 0.82 mM $MgSO_4$, and 15 mM HEPES, pH 7.6], selected eggs were stored at 18°C and injected 16 to 24 h later. RNA (46 nl) at 0.5 to 1.0 $\mu g/\mu l$ was injected into the oocyte cytoplasm with the use of a Drummond positive-displacement injector using micropipettes pulled to a diameter of <10 μm. To increase the channel conductance of homooligomeric WT GluR2, RNA was made from the pore mutant GluR2(R607Q) (the same mutation also referred to as "$GluR2_Q$" by Nagarajan et al., 2001). The receptors made from this mutant conducted robust current and had an inwardly rectifying current-voltage relationship. GluR2(S497T) was constructed within this pore mutant background and therefore is a double mutant.

Oocyte Electrophysiology. Experiments on oocytes were performed under two-electrode voltage clamp (Axoclamp 2A or GeneClamp 500B; Axon Instruments, Union City, CA) at a holding potential of −60 mV in a continuously perfused chamber of approximately 5 μl volume. The extracellular solution was calcium-free [88 mM NaCl, 1 mM KCl, 2.4 mM $NaHCO_3$, 0.3 mM $Ba(NO_3)_2$, 0.41 mM $BaCl_2$, 0.82 mM $MgSO_4$, and 15 mM HEPES, pH 7.6], to which was added glutamate, cyclothiazide (20 mM stock solution dissolved in DMSO), or CX546 (40 mM stock solution dissolved in DMSO) (all drugs were purchased from Sigma/RBI (Natick, MA). Drug concentrations used to determine the EC_{50} values in Table 1 were: CTZ, 1–300 μM; CX546, 1–1500 μM; and glutamate, 0.1–10,000 μM. Solution exchange was controlled via an electronic BPS-8 valve control system (ALA Scientific, Westbury, NY) and electronic valves (The Lee Co., Westbrook, CT). Drugs were applied for 60 s. Currents were measured at steady-state levels at the end of each application of drug. Electrodes of 0.1 to 3 MΩ resistance were filled with 1 M CsCl and 5 mM EGTA. Current responses were filtered at 100 Hz (Cygnus Technology, Delaware Water Gap, PA) and acquired by a Power Macintosh 7600/132 computer with an ITC-16 (InstruTECH Corporation, Port Washington, NY) interface under control of the program Synapse (Synergistic Research Systems, Silver Spring, MD).

Oocyte Data Analysis. Data were analyzed and graphed using KaleidaGraph (Abelbeck/Synergy Software, Reading, PA). Dose-response analysis was with either glutamate or CX546, as appropriate. The lack of solubility of CX546 limited the ability to test its effects beyond 1500 μM. Responses were fitted to the logistic equation $I = I_{max} \times (1/(1 + (EC_{50}/[ligand])^{n_H}))$, where I_{max} is the response at a saturating concentration of ligand, EC_{50} is the concentration of ligand producing a half-maximal response, and n_H is the Hill coefficient. Statistical analysis of the significance of differences between groups (single-factor analysis of variance) was performed using Microsoft Excel software (Microsoft, Redmond, WA).

Transient Transfections. Human embryonic kidney (HEK) 293 fibroblasts (American Type Culture Collection, Manassas, VA) were cultured as described previously (Partin et al., 1996). Briefly, cells were cultured in DMEM supplemented with 10% fetal bovine serum (Gemini, Irvine, CA), penicillin/streptomycin (100 units/ml each), and 1% GlutaMax-1 (both from Invitrogen, Carlsbad, CA). Cells were transiently transfected using FuGene 6 reagent (Roche Diagnostics) with GluR2o cDNA and enhanced green fluorescent protein cDNA (0.5 and 0.1 μg/35-mm dish, respectively).

Outside-Out Patch Recordings. Currents were recorded 48 to 96 h after transfection. During recordings, cells were perfused with extracellular solution containing 20 mM sucrose, 145 mM NaCl, 5.4 mM KCl, 5 mM HEPES, 1 mM $MgCl_2$, 1.8 mM $CaCl_2 \cdot H_2O$, and 0.01 mg/ml phenol red, pH 7.3. Outside-out membrane patches from transfected HEK293 cells were voltage-clamped at a holding potential of −60 mV using an Axopatch 200B amplifier (Axon Instruments). Synapse software (ver. 3.6d; Synergistic Research Systems) was used to control piezoelectric movement, data acquisition, and trace analysis. Responses were filtered at 5 kHz, digitized at 10 to 500 μs/point, and stored on a Power Macintosh computer using an ITC-16 interface (InstruTECH). Thin-walled borosilicate glass micropipettes (World Precision Instruments, New Haven, CT) with a resistance of 2 to 5 MΩ were filled with 135 mM CsCl, 10 mM CsF, 10 mM HEPES, 5 mM Cs-BAPTA, 1 mM $MgCl_2$, and 0.5 mM $CaCl_2$, pH 7.2, 292 mOsm. Patches were perfused with a θ tube (Sutter Instrument Co., Novato, CA) flowpipe using two pairs of solutions. The first pair assessed baseline responses to glutamate. The vehicle-control barrel contained 145 mM NaCl, 5.4 mM KCl, 5 mM HEPES, 1 mM $MgCl_2$, 1.8 mM $CaCl_2 \cdot 2H_2O$, DMSO (0.3–1%), and 0.01 mg/ml phenol red, pH 7.3; the glutamate-containing barrel included glutamate (10 mM) in addition to the above components. The pair of solutions used for testing CX546 were as above, but with CX546 (300 μM) added to both the control (CX546-control) and glutamate-containing (CX546 + glutamate) barrels. A higher concentration of CX546 (1 mM) was used in several pilot studies, but a 300 μM concentration was used for subsequent experiments because of problems with response run-down, patch stability, and concerns about the high DMSO concentrations. CX546 stock (100 mM) was dissolved in DMSO. The flowpipe solutions were driven continuously by a syringe pump (KD Scientific, New Hope, PA) at 0.3 ml/min. After going into voltage clamp, an outside-out patch was pulled and then lifted up to the flowpipe. The pipette tip was positioned in the stream containing control extracellular solution near the interface between the glutamate-free and glutamate-containing solutions. To assess the response to glutamate alone, the patch pipette was jumped rapidly from the vehicle-control into the glutamate solution; for assessing the drug effect, the pipette was jumped from CX546-control into CX546 + glutamate. Rapid solution exchanges of 1 or 100 ms were driven by a piezoelectric device (Burleigh Instruments, Fishers, NY). Solution exchange rates were determined at the end of each experiment by open-tip junction currents. The average 10 to 90% rise times of the 1-ms pulses were 0.29 to 0.32 ms per experimental group (range, 0.19 to 0.44 ms). Data were excluded with rise times of >0.5 ms.

Analysis of Rapid Responses. The rate of deactivation was estimated by fitting a single exponential (τ_{deact}) to responses evoked by a 1-ms pulse of glutamate. The rate of desensitization was estimated by fitting the decay of the response to a 100-ms glutamate pulse from 95% of peak to the steady state with a single-exponential function (τ_{des}). There was substantial desensitization during the initial component of responses to 1-ms glutamate pulses. Accordingly, the rate of deactivation was estimated from fits to the subsequent fast decay after the end of the glutamate pulse. In all cases, deactivation was faster than desensitization, such that there was a clear increase in the rate of decay after removal of glutamate. For all responses, deactivation kinetics were measured from that point out to 4 to 6 ms from the peak amplitude. This measurement accounted for 100% of the current decay in all patches, except for responses in WT patches treated with CX546. In those patches, the measurements accounted for 72 to 98% of the current decay, so the majority of the decay was included in the fit; points beyond this cutoff were disrupted by a solution artifact in some experiments. Current traces and graphs were plotted using KaleidaGraph 3.5 (Abelbeck/Synergy). Patch responses are averages of 3 to 20 successive glutamate applications.

Results and Discussion

Effects of the S493T Point Mutation on Modulation by CTZ and CX546. The GluR1i(S493T) mutation was shown previously to impair the modulation of desensitization by 100 μM CTZ (Partin, 2001), which is consistent with the fact that the homologous residue in GluR2, Ser497, lies at the subunit interface and interacts with CTZ (Sun et al., 2002). Figure 1 demonstrates that the GluR1(S493T) mutation impairs modulation by CX546 (Fig. 1A) and CTZ (Fig. 1B) in both splice isoforms, as assayed by slow perfusion in *X. laevis* oocytes.

CTZ had a higher apparent affinity for GluR1i (EC_{50} = 58 μM) versus GluR1o (EC_{50} = 237 μM) for potentiating glutamate-evoked responses (Table 1), as has been demonstrated previously using kainate as the agonist (Partin et al., 1994). As expected, CTZ was also more efficacious at GluR1i, potentiating glutamate-evoked responses with 300 μM CTZ 40-fold, whereas GluR1o responses were potentiated only 8-fold. The Ser493

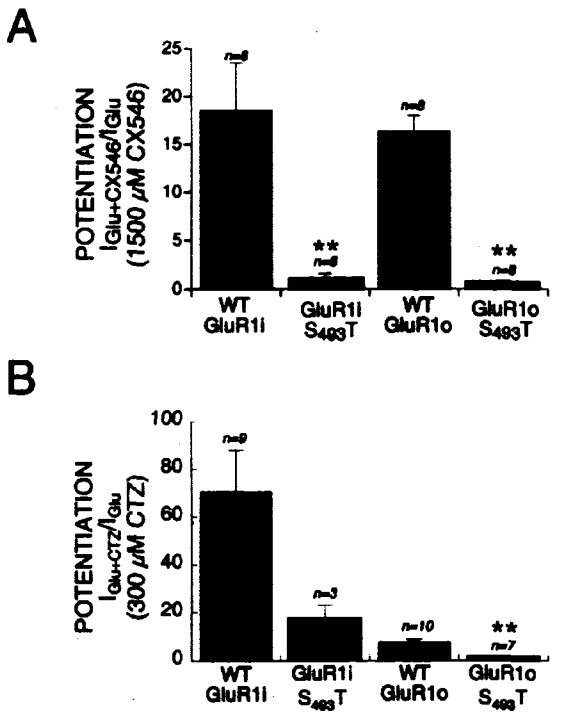

Fig. 1. The S493T mutation impedes the modulation of desensitization and deactivation in flip and flop AMPA receptor isoforms. A, mean potentiation of steady-state current evoked by 300 μM glutamate with 1500 μM CX546 for GluR1i and GluR1o wild-type (■) and the Ser493 mutant (▨), expressed in oocytes. For both splice isoforms, this mutation significantly blocks modulation by CX546 ($p < 0.05$). B, mean potentiation by CTZ. For both splice isoforms, this mutation also impedes the action of CTZ.

TABLE 1

Loss of modulation of GluR1(S493T) by CTZ and CX546

Loss of modulation by both CX546 and CTZ occurs when mutations are made at either position 493 (this article) or position 750 (this article and Partin et al., 1995) in GluR1. Values represent mean ± S.E.M.; n = 5 to 14 oocytes, but most data points represent n = 8. Hill values are given in parentheses below the value for EC_{50}.

	CTZ		CX546		Glutamate
	EC_{50}	Potentiation (300 μM CTZ) $I_{GLU+CTZ}/I_{GLU}$	EC_{50}	Potentiation (1500 μM CX546) $I_{GLU+CX546}/I_{GLU}$	EC_{50}
	μM		μM		μM
WT GluR1i	58.0 ± 1.9 (2.2)	39.6 ± 7.2	503 ± 73 (1.6)	18.5 ± 4.9	27.1 ± 8.9
GluR1i(S493T)	N.D.	17.9 ± 5.2	N.D.	1.1 ± 0.5	21.9 ± 7.3
WT GluR1o	237 ± 104 (0.9)	8.7 ± 1.7	595 ± 315 (1.0)	16.3 ± 1.7	11.1 ± 7.4
GluR1o(S493T)	N.D.	1.8 ± 0.1	N.D.	0.7 ± 0.1	28.3 ± 11.8
GluR1o(S750Q)	N.D.	1.0 ± 0.1[a]	N.D.	1.8 ± 0.2	N.D.

N.D., not determined (i.e., data could not be fit reliably with logistic equation because of small current amplitudes).
[a] Data from Partin et al. (1995).

mutation had a similar effect on both GluR1i and GluR1o receptors, reducing the level of maximal potentiation to 18- and 2-fold, respectively (Fig. 1B). These data indicate that mutation of Ser493 in either the flip or flop isoform of GluR1 has a deleterious effect on allosteric modulation by CTZ. This finding is consistent with the structural data for the S1/S2 domain complexed with both agonist and CTZ (Sun et al., 2002).

To test the hypothesis that the mutation affecting CTZ modulation would also affect CX546 modulation, similar analyses on WT and mutant GluR1i and GluR1o receptors were performed (Table 1). There was no difference in apparent affinity of CX546 for GluR1o (EC_{50} = 595 μM) versus GluR1i (EC_{50} = 503 μM), and the responses were potentiated to a similar extent (Fig. 1A). For both splice isoforms, the Ser493 mutation completely abolished potentiation by CX546. Thus, the Ser493 point mutation impaired modulation by both CX546 and CTZ, although these two drugs are believed to act through distinct mechanisms.

Previous experiments demonstrated that the AMPA receptor alternatively spliced flip/flop region was responsible for the differential sensitivity to CTZ and aniracetam (Partin et al., 1996). The differential sensitivity could be mapped to one critical residue, Ser750 (or Asn750 in the flop isoform) and, in fact, modulation could be abolished with the mutation GluR1(S750Q). Because CX546 is structurally related to aniracetam, one might predict that modulation by CX546 would be impaired by mutation of Ser750. Indeed, Table 1 shows that modulation of GluR1o(S750Q) by CX546 is reduced to 1.8-fold. Thus, there is a significant loss of modulation by both CX546 and CTZ upon mutation of both Ser493 and Ser750.

The loss of modulation by the Ser493 mutation could be a secondary consequence of a reduction in agonist affinity. To test this idea, glutamate dose-response analyses were performed on WT and mutant GluR1i and GluR1o receptors. The Ser493 mutation did not significantly change the apparent affinity of glutamate (Table 1). The EC_{50} for WT GluR1i was 27 μM and 22 μM for GluR1i(S493T); for WT GluR1o, the EC_{50} was 11 μM and 28 μM for the mutation. In addition, the mutation did not significantly change the efficacy of glutamate, because the mean peak current for WT GluR1i in 1000 μM glutamate was 414 ± 60 nA (n = 20) versus 569 ± 72 nA (n = 16) for GluR1i(S493T) (p = 0.10). Thus, the Ser493 mutation impairs modulation by CTZ and CX546, similar to the effects of the GluR1o(S750Q) mutation (Table 1), which impairs modulation by CTZ and aniracetam (Partin et al., 1996), without affecting inherent agonist affinity.

TABLE 2

Modulation of AMPA subunits by CX546

CX546 modulates the glutamate-evoked currents of the flop (o) isoform of all AMPA subunits. Values reported are the fit of the data from dose-response analysis using 1 to 1500 μM CX546, with n = 8 oocytes per determination. The left column shows the mean EC_{50}; given the limited solubility of CX546, these values may represent a lower estimate of the actual value (see also Nagarajan et al., 2001). Right column shows the mean potentiation of the current evoked by 300 μM glutamate and 1500 μM CX546.

	EC_{50} CX546	1500 μM CX546 $I_{GLU+CX546}/I_{GLU}$
	μM	
GluR1o	595 ± 315 (1.0)	24.7 ± 5.6
GluR2o (R607Q)	176 ± 26 (1.6)	9.9 ± 0.5
GluR3o	554 ± 159 (2.4)	30.9 ± 5.3
GluR4o	681 ± 566 (1.3)	8.8 ± 3.5

Modulation of All AMPA Receptor Subtypes by CX546. A dose-response analysis was used to test the efficacy of CX546 modulation on different AMPA receptor subtypes (Table 2). For these experiments, the flop splice isoform was used. Responses from GluR1 to -4 receptors were potentiated by CX546. There were 2- to 3-fold differences in the apparent affinities (EC_{50} values ranged from 176 to 681 μM) and 3-fold differences in the efficacy (maximal potentiation ranged from 10- to 31-fold) of CX546. Thus, CX546 positively modulates the flop isoform of all AMPA receptors. To interpret the electrophysiological experiments in light of the published crystal structural data of GluR2, we next performed kinetic experiments using GluR2o.

Kinetic Analysis of GluR2o(S497T). Nagarajan et al. (2001) have shown previously that CX546 modulation of "$GluR2i_Q$" caused a small but significant increase of the time constant of deactivation. In Fig. 2A, a similar result is shown for GluR2o, as assayed in outside-out patches of transiently transfected HEK293 cells, using ultrafast solution perfusion. CX546 slowed deactivation (i.e., increased τ_{deact}) from 0.71 ± 0.05 to 1.10 ± 0.08 ms (p = 0.001) (Fig. $2C_1$) without significantly changing τ_{des} (Fig. $2C_2$). In addition, CX546 significantly increased the ratio of steady-state to peak current from 0.06 ± 0.03 to 0.43 ± 0.04 ($p < 0.001$) (Fig. 2, A_2 and C_2). This modulation most likely arises as an indirect effect of CX546, which alters equilibrium desensitization by slowing channel deactivation rather than directly affecting the rate of desensitization (Partin et al., 1996; Arai et al., 2002b). The fact that CX546 did not alter τ_{des} may reflect that our experiments were performed in subsaturating concentrations of CX546 (300 μM). When we performed pilot experiments at a higher concentration of CX546 (1000 μM), the steady-state/peak ratio increased to near unity (S. Clark and K. M. Partin, unpublished observations).

The homolog of GluR1(S493T) is GluR2(S497T). Kinetic analysis of GluR2o(S497T) is shown in Fig. 2B. The ability of CX546 to modulate deactivation is completely lost in GluR2o(S497T). The loss of modulation also was evident as a decrease in equilibrium desensitization, as measured by the change in $I_{ss/peak}$ (Fig. 2C_3).

Identification of a Site Important for the Modulation of Deactivation and Desensitization. The data shown above indicate that mutation of Ser493 in GluR1 or Ser497 in GluR2 impairs AMPA receptor modulation by either class of drug. Fig. 3 shows the crystal structure of a dimer of the S1/S2 agonist-binding domain of GluR2o with glutamate bound (Armstrong et al., 1999). Ser497 lies at the dimer interface that has been shown to participate in CTZ binding. Mutation from serine to threonine impairs modulation by CTZ. The mutation also disrupts modulation by CX546, suggesting either that CX546 also binds at this site or that mutation of this residue perturbs the receptor structure and/or function in such a manner as to make it insensitive to allosteric drugs.

Summary. Oligomeric ligand-binding proteins rely on subunit interface interactions for the regulation of allosteric transitions (Creighton, 1993). For ionotropic glutamate re-

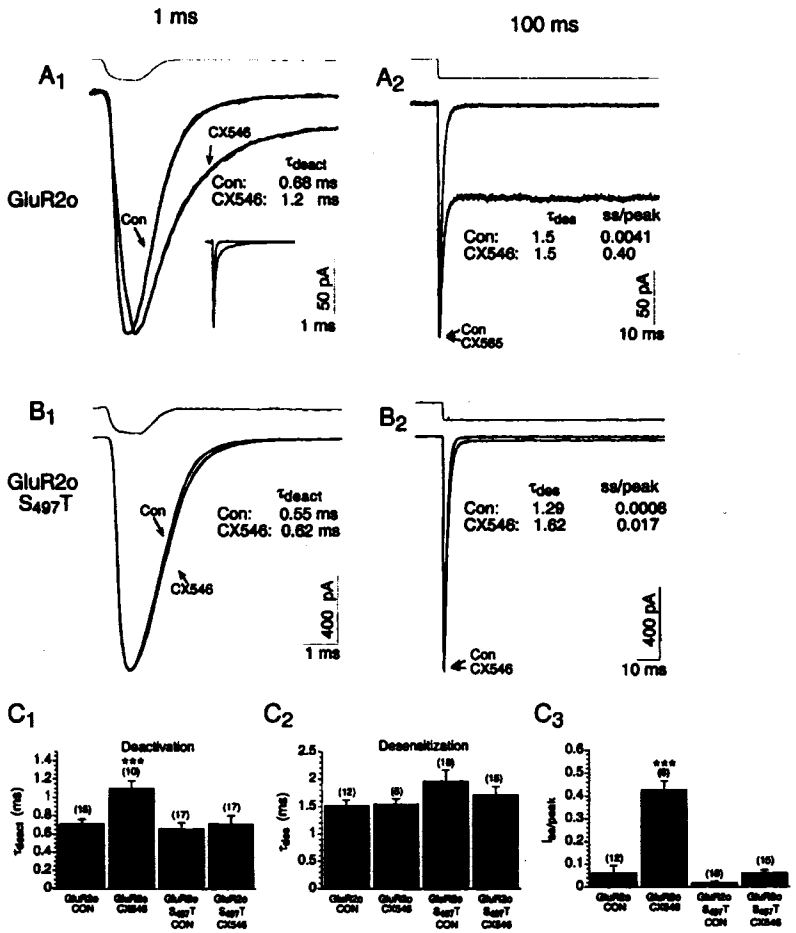

Fig. 2. Kinetic analysis of GluR2oand GluR2o(S497T). A, responses in outside-out patches of HEK293 cells expressing GluR2o, with a 1-ms (A_1) or 100-ms (A_2) pulses of glutamate (10 mM) (Con) or glutamate (10 mM) + CX546 (300 μM) (CX546). Inset traces in A_1 show that the decay in CX546 returns to baseline within 70 ms. CX546 slowed deactivation (τ_{deact}), increased $I_{ss/peak}$, but did not alter τ_{des}. All four traces are from the same patch. B, responses in GluR2o(S497T) patches. As shown, CX546 no longer modulated deactivation (B_1), nor potentiated the steady-state/peak current ratio (B_2). All four traces are from the same GluR2o(S497T) patch. Fits for individual waveforms are displayed; arrows indicate the single-exponential fits for analysis of deactivation or desensitization. For each pair of traces, inset values show time constants for deactivation and desensitization, as well as the steady-state/peak current ratios for each trace. Traces are normalized to peak amplitudes to correct for rundown. For each pair of traces, the amplitude of the smaller response (and fit) was scaled to the larger. (Accordingly, the calibration bars apply only to unscaled traces.) Scaling factors are as follows: GluR2o, 1 ms (1.047) and 100 ms (1.61); and GluR2o(S497T) 1 ms (1.055) and 100 ms (1.060). Shown above the current traces for A and B are open-tip junction currents. C, bar graphs for deactivation (C_1), desensitization (C_2), and steady-state/peak current ratios (C_3). Data given are group means (± S.E.M.); values in parentheses indicate the number of patches analyzed. C_1: ***, CX546 significantly slowed deactivation in GluR2o ($p \leq 0.001$). In contrast, GluR2o(S497T) abolished modulation of deactivation by CX546. C_2, desensitization rates were not affected by CX546. C_3, the modulatory effect of CX546 with respect to $I_{ss/peak}$ was greatly attenuated by the GluR2o(S497T) point mutation. ***, CX546 significantly increased the ss/peak ratio in GluR2o ($p \leq 0.001$). GluR2o refers to GluR2o(R607Q), as discussed under *Materials and Methods*.

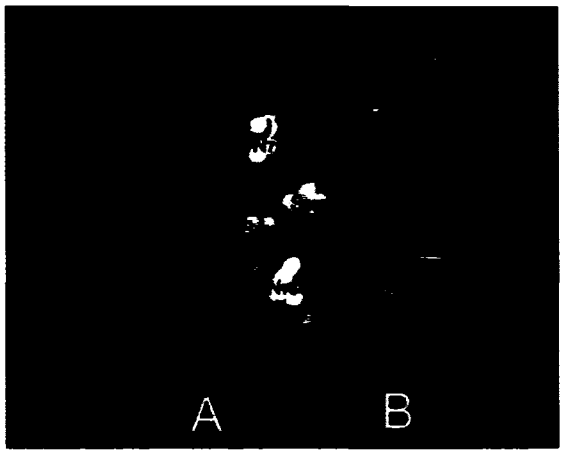

Fig. 3. Structure of the GluR2o S1/S2 agonist-binding domain, with glutamate bound. Ser497 lies at the interface between subunits A and B, as does Asn754 [homologous to GluR1o(Asn750) within the flip/flop splice region (Armstrong and Gouaux, 1999; structure is PDB file "1FTJ")]. Mutation of either residue impairs modulation by either CTZ or CX546, suggesting a common or overlapping binding site.

ceptors, such transitions after ligand binding include channel activation, deactivation, and desensitization. It is assumed that these transitions are coupled (Partin et al., 1996; Trussell and Otis, 1996), although this process is poorly understood. We have shown that one residue, GluR1(S493T) or GluR2(S497T), plays a critical role in permitting allosteric modulation of these gating transitions, presumably by participating directly in the drug-protein interaction. The role of this residue in regulating allosteric modulation seems to be similar to that of GluR1(Ser750) or GluR2(Ser754), the mutation of which also results in a receptor that is poorly modulated by either CTZ or aniracetam (Partin et al., 1995, 1996). Both of these residues (Ser493 and Ser750) directly participate in the binding of CTZ (Sun et al., 2002). The present studies suggest that modulation by CX546 may also be directed by these two residues. However, mutation of GluR1(S493T) had a more profound impact on modulation by CX546 than by CTZ (Table 1). This could suggest either that there are fewer contacts between CX546 and the receptor (so each contact is relatively more significant) or perhaps that Ser493 is a uniquely important contact for modulation of deactivation. In summary, mutations at the subunit interface of glutamate receptors impede the actions of drugs that modulate both deactivation and desensitization. It remains to be seen whether all such residues also participate in gating transitions and the extent to which they are involved in coupling these distinct allosteric processes.

Acknowledgments

We thank Dr. M. C. Kuehl-Kovarik for her technical expertise and for critically reading this manuscript. We thank Dr. Kurt Beam for his stimulating scientific discussions.

References

Arai A, Kessler M, Ambros-Ingerson J, Quan A, Yigster E, Rogers G, and Lynch G (1996a) Effects of a centrally active benzoylpyrrolidine drug on AMPA receptor kinetics. *Neuroscience* **75**:573–585.

Arai A, Kessler M, Rogers G, and Lynch G (1996b) Effects of a memory-enhancing drug on DL-α-amino-3-hydroxy-5-methyl-4-isoxazolepropionic acid receptor currents and synaptic transmission in the hippocampus. *J Pharmacol Exp Ther* **278**:627–638.

Arai A, Kessler M, Rogers G, and Lynch G (2000) Effects of the potent ampakine CX614 on hippocampal and recombinant AMPA receptors: interactions with cyclothiazide and GYKI 52466. *Mol Pharmacol* **58**:802–813.

Arai AC, Xia YF, Kessler M, Phillips D, Granger R, and Lynch G (2002a) Effects of 5′-alkyl-benzothiadiazides on (*R,S*)-α-amino-3-hydroxy-5-methyl-4-isoxazolepropionic acid (AMPA) receptor biophysics and synaptic responses. *Mol Pharmacol* **62**:566–577.

Arai A, Xia YF, Rogers G, Lynch G, and Kessler M (2002b) Benzamide-type AMPA receptor modulators form two subfamilies with distinct modes of action. *J Pharmacol Exp Ther* **303**:1075–1085.

Armstrong N, Sun Y, Chen GQ, and Gouaux E (1999) Structure of a glutamate-receptor ligand-binding core in complex with kainate. *Nature (Lond)* **395**:913–917.

Creighton TE (1993) *Proteins: Structures and Molecular Properties*, W.H. Freeman and Co., New York.

Dingledine R, Borges K, Bowie D, and Traynelis SF (1999) The glutamate receptor ion channels. *Pharmacol Rev* **51**:7–61.

Granger R, Staubli U, Davis M, Perez Y, Nilsson L, Rogers G, and Lynch G (1993) A drug that facilitates glutamatergic transmission reduces exploratory activity and improves performance in a learning-dependent task. *Synapse* **15**:326–329.

Huang EP and Stevens CF (1996) The matter of mind: molecular control of memory. *Essays Biochem* **30**:165–178.

Ingvar M, Ambros-Ingerson J, Davis M, Granger R, Kessler M, Rogers G, Schehr R, and Lynch G (1997) Enhancement by an ampakine of memory encoding in humans. *Exp Neurol* **146**:553–559.

Isaac JT, Nicoll RA, and Malenka RC (1999) Silent glutamatergic synapses in the mammalian brain. *Can J Physiol Pharmacol* **77**:735–737.

Isaacson JS and Nicoll RA (1991) Aniracetam reduces glutamate receptor desensitization and slows the decay of fast excitatory synaptic currents in the hippocampus. *Proc Natl Acad Sci USA* **88**:10936–10940.

Lynch G (1998) Memory and the brain: unexpected chemistries and a new pharmacology. *Neurobiol Learn Mem* **70**:82–100.

Lynch G, Granger R, Ambros-Ingerson J, Davis MC, Kessler M, and Schehr R (1997) Evidence that a positive modulator of AMPA-type glutamate receptors improves delayed recall in aged humans. *Exp Neurol* **145**:89–92.

Nagarajan N, Quast C, Boxall AR, Shahid M, and Rosenmund C (2001) Mechanism and impact of allosteric AMPA receptor modulation by the ampakine CX546. *Neuropharmacology* **41**:650–663.

Partin KM (2001) Domains regulating AMPA receptor desensitization. *J Neurosci* **21**:1939–1948.

Partin KM, Bowie D, and Mayer ML (1995) Structural determinants of allosteric regulation in alternatively spliced AMPA receptors. *Neuron* **14**:833–843.

Partin KM, Fleck MF, and Mayer ML (1996) AMPA receptor flip/flop mutants affecting deactivation, desensitization and modulation by cyclothiazide, aniracetam and thiocyanate. *J Neurosci* **16**:6634–6647.

Partin KM, Patneau DK, and Mayer ML (1994) Cyclothiazide differentially modulates desensitization of AMPA receptor splice variants. *Mol Pharmacol* **46**:129–138.

Pelletier MR and Hablitz JJ (1996) Altered desensitization produces enhancement of EPSPs in neocortical neurons. *J Neurophysiol* **75**:1032–1036.

Staubli U, Perez Y, Xu FB, Rogers G, Ingvar M, Stone-Elander S, and Lynch G (1994) Centrally active modulators of glutamate receptors facilitate the induction of long-term potentiation in vivo. *Proc Natl Acad Sci USA* **91**:11158–11162.

Sun Y, Olson R, Horning M, Armstrong N, Mayer ML, and Gouaux E (2002) Mechanism of glutamate receptor desensitization. *Nature (Lond)* **417**:245–253.

Trussell LO and Otis TS (1996) Physiology of AMPA receptors: biophysical characteristics that subserve integrative roles of synapses, in *Excitatory Amino Acids and the Cerebral Cortex* (Conti F and Hicks TP eds) pp 63–72, MIT Press, Cambridge, MA.

Yamada K (1998) Modulating excitatory synaptic transmission: potential treatment for neurologic disease? *Neurobiol Dis* **5**:67–80.

Yamada KA and Rothman SM (1992) Diazoxide reversibly blocks glutamate desensitization and prolongs excitatory postsynaptic currents in rat hippocampal neurons. *J Physiol (Lond)* **458**:385–407.

Zivkovic D, Thompson DM, Bertolino M, DiBella M, Costa E, and Guidotti A (1995) 7-chloro-3-methyl-3–4-dihydro-2H-1,2,4-benzothiadiazine-S,S-dioxide (IDRA21): a benzothiadiazine derivative that enhances cognition by attenuating DL-amino-2,3-dihydro-5-methyl-3-oxo-4-isoxazolepropanoic acid (AMPA) receptor desensitization. *J Pharmacol Exp Ther* **272**:300–309.

Address correspondence to: Dr. Kathryn M. Partin, Department of Biomedical Sciences, Colorado State University, 200 West Lake Street, Fort Collins, CO 80523-1617. E-mail: kathy.partin@colostate.edu

Cellular/Molecular

Mechanism of Positive Allosteric Modulators Acting on AMPA Receptors

Rongsheng Jin,[1] Suzanne Clark,[4] Autumn M. Weeks,[4] Joshua T. Dudman,[2] Eric Gouaux,[1,3] and Kathryn M. Partin[4]

[1]Department of Biochemistry and Molecular Biophysics, [2]Center for Neurobiology and Behavior, and [3]Howard Hughes Medical Institute, Columbia University, New York, New York 10032, and [4]Department of Biomedical Sciences, Division of Neuroscience, Colorado State University, Fort Collins, Colorado 80523

Ligand-gated ion channels involved in the modulation of synaptic strength are the AMPA, kainate, and NMDA glutamate receptors. Small molecules that potentiate AMPA receptor currents relieve cognitive deficits caused by neurodegenerative diseases such as Alzheimer's disease and show promise in the treatment of depression. Previously, there has been limited understanding of the molecular mechanism of action for AMPA receptor potentiators. Here we present cocrystal structures of the glutamate receptor GluR2 S1S2 ligand-binding domain in complex with aniracetam [1-(4-methoxybenzoyl)-2-pyrrolidinone] or CX614 (pyrrolidino-1,3-oxazino benzo-1,4-dioxan-10-one), two AMPA receptor potentiators that preferentially slow AMPA receptor deactivation. Both potentiators bind within the dimer interface of the nondesensitized receptor at a common site located on the twofold axis of molecular symmetry. Importantly, the potentiator binding site is adjacent to the "hinge" in the ligand-binding core "clamshell" that undergoes conformational rearrangement after glutamate binding. Using rapid solution exchange, patch-clamp electrophysiology experiments, we show that point mutations of residues that interact with potentiators in the cocrystal disrupt potentiator function. We suggest that the potentiators slow deactivation by stabilizing the clamshell in its closed-cleft, glutamate-bound conformation.

Key words: **glutamate receptor; desensitization; deactivation; kinetics; crystallography; cyclothiazide; aniracetam; CX614**

Introduction

At the cellular level, short- and long-term memory storage involves the strengthening and weakening of synapses (Kandel, 2001). Key molecules located at chemical synapses are ionotropic glutamate receptors (iGluRs), ligand-gated ion channels that mediate the majority of fast-synaptic signal transduction in the mammalian brain (Dingledine et al., 1999). Experiments in transgenic mice (Tsien et al., 1996), as well as pharmacological studies in rodents and humans (Morris et al., 1986; Rammsayer, 2001), underscore the importance of AMPA- and NMDA-sensitive iGluRs in learning and memory. In fact, positive allosteric modulators that slow deactivation of AMPA receptors improve short-term memory in humans (Ingvar et al., 1997) and may also prove useful for the treatment of depression and other disorders and diseases of the nervous system (O'Neill et al., 2004).

In studies using recombinant receptors and rapid perfusion, patch-clamp electrophysiology experiments, positive allosteric modulators such as aniracetam [1-(4-methoxybenzoyl)-2-pyrrolidinone] (Ani) and CX614 (pyrrolidino-1,3-oxazino benzo-1,4-dioxan-10-one) (CX) slow deactivation of AMPA receptors, or the rate at which the ion channel closes after the removal of glutamate (Vyklicky et al., 1991; Partin et al., 1996; Arai et al., 2000; Lawrence et al., 2003). However, aniracetam, CX614, and *N*-2-[4-(4-cyanophenyl)phenyl]propyl 2-propanesulfonamide (LY404187), as well as other related positive allosteric modulators (Miu et al., 2001; Quirk and Nisenbaum, 2003), also slow desensitization, a process by which the receptor ion channel closes although glutamate remains tightly bound (Isaacson and Nicoll, 1991; Tang et al., 1991; Arai et al., 2000; Sun et al., 2002). On the basis of experiments in rodents and humans, the cognitive enhancing properties of therapeutic agents such as aniracetam and CX614 are primarily attributable to their slowing of deactivation (Arai and Lynch, 1998). Therefore, it is of substantial interest to determine how positive modulators slow deactivation.

At the present time, there is no information, at the level of molecular detail, on how small molecules modulate the deactivation kinetics of any ligand-gated ion channel, although we have recently learned a great deal about how small molecules and specific mutations such as cyclothiazide and the leucine 483 to tyrosine mutation slow desensitization of AMPA receptors, respectively (Sun et al., 2002; Fleck et al., 2003; Leever et al., 2003;

Received June 22, 2005; revised Aug. 12, 2005; accepted Aug. 16, 2005.

This work was supported by the National Institutes of Health (K.M.P., E.G.) and the American Heart Association (K.M.P.), and E.G. is an investigator with the Howard Hughes Medical Institute. J.T.D. was supported by a National Science Foundation Graduate Research Fellowship. Diffraction data sets were collected at beam lines X4A at the National Synchrotron Radiation Source with the assistance of C. Ogata, R. Abramowitz, and X. Yang. R. Olsen performed the sedimentation equilibrium experiments using an XL-I centrifuge purchased using funds provided by the National Institutes of Health. We thank G. Rogers for providing CX614. K.M.P. thanks K. Beam for insightful scientific discussions.

Correspondence should be addressed to either of the following: Dr. Eric Gouaux, Howard Hughes Medical Institute/Vollum Institute, Oregon Health and Sciences University, Portland, OR 97239, E-mail: gouauxe@ohsu.edu; or Dr. Kathryn M. Partin, Department of Biomedical Sciences, Division of Neuroscience, 200 West Lake Street, Colorado State University, Fort Collins, CO 80523, E-mail: kpartin@lamar.colostate.edu.

R. Jin's present address: Howard Hughes Medical Institute, Stanford University, James H. Clark Center, E300, 318 Campus Drive, Stanford, CA 94305.

DOI:10.1523/JNEUROSCI.2567-05.2005

 0270-6474/05/259027-10$15.00/0

Horning and Mayer, 2004). Because modulators of desensitization act at the interface between glutamate binding subunits of AMPA receptors, we reasoned that molecules that slowed deactivation might also bind in the context of the glutamate binding domains. To map the binding site(s) and determine the mechanism by which aniracetam and CX614 modulate deactivation in AMPA receptors, we have determined the cocrystal structures of the GluR2 ligand-binding core in complex with the modulators, and we have tested specific receptor–modulator interactions using site-directed mutagenesis and rapid perfusion, patch-clamp electrophysiology experiments.

Materials and Methods

Materials. Aniracetam, L-quisqualic acid (Quis), and NBQX were obtained from Tocris Bioscience (Ellisville, MO), kynurenic acid was from Sigma (St. Louis, MO), cyclothiazide (CTZ) was from Alexis Biochemicals (San Diego, CA), and CX614 was generously provided by Cortex Pharmaceuticals (Irvine, CA). The rat GluR2 S1S2J construct used in this study was derived from GluR2 flop (Boulter et al., 1990; Keinänen et al., 1990) and has been described previously (Armstrong and Gouaux, 2000). Protein expression, refolding, and purification were performed using previously described methods (Chen and Gouaux, 1997). Before crystallization, glutamate was removed by dialyzing the GluR2 S1S2J protein extensively against a buffer composed of 10 mM HEPES, pH 7.0, 20 mM NaCl, and 1 mM EDTA, and the protein was concentrated to ~10 mg/ml (calculated ϵ_{280} of 39,640 M^{-1} cm^{-1}).

Crystallization and measurement of diffraction data. Before crystallization, the following ligands were added to the protein solution (final concentrations): 5 mM fluorowillardiine and 10 mM aniracetam, or 5 mM quisqualate and 5 mM CX614. Crystals were grown at 4°C by vapor diffusion, and each drop contained a 1:1 ratio of protein and reservoir solution. The reservoir solution for the aniracetam complex was 12–14% polyethylene glycol (PEG) 8000, 0.25–0.35 M ammonium sulfate, and 0.1 M sodium citrate, pH 5.5–6.0; the CX614 crystals were obtained from a reservoir solution composed of 10–14% PEG 8000, 0.1–0.15 M zinc acetate, and 0.1 M sodium acetate, pH 5.5.

Crystals were soaked in corresponding crystallization buffers supplemented with ligands and 12–16% glycerol before flash cooling in liquid nitrogen. Both data sets were collected at 110 K at the NSLS X4A beam line. The diffraction data were processed with the HKL suite of programs. The CX614 cocrystals belonged to the $P2_12_12$ space group, and the cell was isomorphous to the zinc crystal form of the previously described quisqualate complex (Jin et al., 2002). The aniracetam cocrystals also belonged to the $P2_12_12$ space group. However, the symmetry for both cocrystals was reduced to $P2_1$ to facilitate crystallographic refinement of the complex because, in the $P2_12_12$ space group, CX614 or aniracetam was positioned on the crystallographic twofold axis.

Structure determination. The structure of the CX614/Quis complex was solved by difference Fourier techniques using phases calculated from the "zinc form" quisqualate structure (Jin et al., 2002). The Ani/fluorowillardiine (FW) complex structure was solved by molecular replacement using AmoRe (Navaza, 1994) using the FW complex structure without solvent molecules and ligand as a search model (Jin and Gouaux, 2003). Crystallographic refinements were performed with CNS (Brünger et al., 1998), and the program O was used for model building (Jones et al., 1991; Jones and Kjeldgaard, 1997). Strong noncrystallographic symmetry restraints (weight of 300) were applied to the six protomers in the CX614/Quis structure and the two protomers in the Ani/FW structure. Refinements were begun with rigid body minimization followed by a slow-cool, simulated-annealing protocol at 5000 K to reduce model bias, followed by iterative rounds of positional and individual B-factor refinement and manual model building into omit maps until the R_{free} value converged (Brünger, 1992). The crystal structure of aniracetam was obtained from the Cambridge Structural Database under entry code GIJVOK. The CX614 structure was constructed based on two small molecule crystal structures with codes of VIGFUM and GODWAX, and the resulting structure was subjected to energy minimization using PRODRG (van Aalten et al., 1996). Because the modulators bind on the molecular twofold axis, two modulator molecules were modeled for each binding site, each with occupancies of 0.5 and related by a noncrystallographic twofold axis. Least squares superpositions were calculated using LSQMAN (Kleywegt, 1999), and the extent of domain closure was determined using the program FIT (http://bioinfo1.mbfys.lu.SE/~guoguang/fit.html). The degree of domain closure was defined as the rotation required to fit in domain 2 (*Ile 500–Lys 506; Pro 632–Asp 728; Gly-Thr linker*) after superposition of α-carbon atoms in domain 1 (Val 395–Phe 495; Tyr 732–Tyr 768). MOLSCRIPT (Kraulis, 1991), BOBSCRIPT (Esnouf, 1999), Raster3D (Merritt and Murphy, 1994), and Pymol (Delano, 2005) were used to make the figures. Coordinates for the aniracetam and CX614 complexes have been deposited in the Protein Data Bank under accession numbers of 2AL5 and 2AL4, respectively.

Sedimentation equilibrium. Sedimentation equilibrium ultracentrifugation runs were performed in a Beckman Instruments (Fullerton, CA) XL-I analytical ultracentrifuge. The experimental setup and data analyses were performed as described previously (Sun et al., 2002). Purified GluR2 S1S2J samples at ~1.2 mg/ml were first dialyzed extensively against buffer A, which was composed of 20 mM Tris-HCl, pH 7.5, 200 mM NaCl, and 1 mM EDTA. For the three experiments presented in this study, the protein samples were finally dialyzed overnight against buffer A supplemented with the following: (1) 2 mM glutamate and 5 mM aniracetam; (2) 0.3 mM AMPA and 0.3 mM CX614; or (3) 0.3 mM CX614. We were unable to examine the effects of higher concentrations of aniracetam because of its limited solubility. These last dialysis buffers were used as the blank controls, and the data were measured using interference optics. The sedimentation equilibrium experiments were performed using three different loading concentrations of protein (0.75, 0.5, and 0.25 mg/ml for the aniracetam sample and 1.0, 0.75, and 0.4 mg/ml for the CX614 samples) and three different speeds (15,000, 20,000, and 27,000 rpm). All dialyses and sedimentation equilibrium experiments were performed at 4°C.

Transient transfections. Human embryonic kidney 293 (HEK 293) fibroblasts (CRL 1573; American Type Culture Collection, Rockville, MD) were cultured as described previously (Partin et al., 1996). Cells were transiently transfected using FuGene 6 reagent (Roche Products, Indianapolis, IN) with GluR2 cDNA and enhanced green fluorescent protein cDNA (0.5–2 and 0.1–0.15 μg/35 mm dish, respectively). After transfection, NBQX (10 μM) and kynurenic acid (1 mM) were added to the media.

Outside-out patch recordings. Currents were recorded 2–4 d after transfection, as described previously (Leever et al., 2003). Extracellular solutions (ECS) contained the following: 20 mM sucrose, 145 mM NaCl, 5.4 mM KCl, 5 mM HEPES, 1 mM $MgCl_2$, 1.8 mM $CaCl_2 \cdot H_2O$, and 0.01 mg/ml phenol red, pH 7.3. To protect cells from excesive bath exposure to agonists and modulators, ECS also contained NBQX (3 μM) with or without kynurenic acid (1 mM) or lowered calcium concentrations, and bath solutions were fully exchanged after drug exposures. Outside-out membrane patches were voltage clamped at −60 mV using an Axopatch 200B amplifier (Molecular Devices, Union City, CA). Synapse (version 3.6d; Synergy Research, Silver Spring, MD) controlled piezoelectric movement, data acquisition, and trace analysis. Responses were filtered at 5 kHz, digitized at 10–500 μs/point, and stored on a Power Macintosh computer (Apple Computers, Cupertino, CA) using an ITC-16 interface (InstruTech, Port Washington, NY). Micropipettes (TW150F; 2–5 MΩ; World Precision Instruments, Sarasota, FL) contained the following (in mM): 135 CsCl, 10 CsF, 10 HEPES, 5 Cs-BAPTA, 1 $MgCl_2$, and 0.5 $CaCl_2$, pH 7.2 (292 mOsm). Patches were perfused at 0.3 ml/min with solutions emitted from a *two-barrel flow pipe made with θ tubing* (BT150–10; Sutter Instruments, Novato, CA). For baseline agonist responses, one barrel contained vehicle control (control) composed of the following: 145 mM NaCl, 5.4 mM KCl, 5 mM HEPES, 1 mM $MgCl_2$, 1.8 mM $CaCl_2 \cdot H_2O$, with 1% DMSO and 0.01 mg/ml phenol red, pH 7.3. The other barrel had this solution plus Quis (3 mM). The flow pipe solutions used for testing CX were as above, only with CX614 (100 μM) added to both barrels (i.e., CX-control and CX+Quis). Similar configurations were used for aniracetam and CTZ. After going into voltage clamp, an outside-out patch was pulled, lifted up to the flow pipe, positioned near the interface between the Quis-free and Quis-containing solutions, and jumped rapidly from the vehicle control into Quis or from CX-control

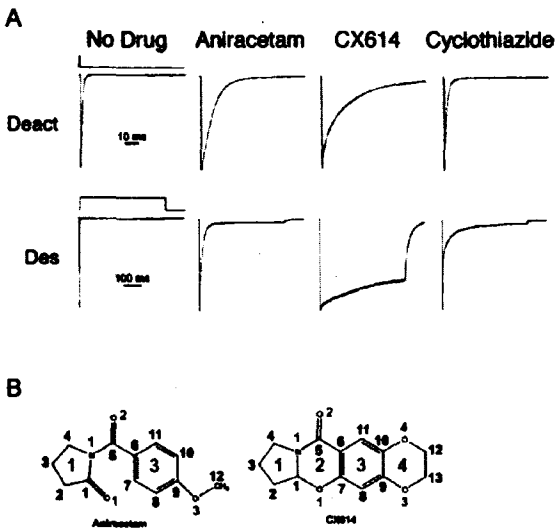

Figure 1. The positive allosteric modulators aniracetam and CX614 slow deactivation more profoundly than cyclothiazide at GluR2 (flop) receptors. *A*, Electrophysiological responses of GluR2 (flop) expressed on outside-out patches of transiently transfected HEK 293 cells. Top traces show the kinetics of deactivation, the decay of the peak response after a brief (1 ms) pulse of 3 mM quisqualate. Bottom traces show the kinetics of desensitization, the decay during a prolonged (500 ms) pulse of quisqualate. Responses are shown for patches with no drug or with 5 mM aniracetam, 100 μM CX614, or 100 μM cyclothiazide. Single-exponential fits are superimposed on the trace. Open-tip potentials are shown above the control traces. Note that desensitization by CTZ of GluR2o is only partially modulated compared with the flip isoform in which desensitization is virtually blocked. *B*, Chemical structures of aniracetam and CX614. The atoms of aniracetam and CX614 are numbered using smaller font, with oxygen atoms in red and carbon atoms in black, and the rings are numbered using a larger font.

into CX+Quis. Rapid solution exchanges of 1 or 500 ms were driven by a piezoelectric device (Burleigh Instruments, Fishers, NY). Solution exchange rates were determined at the end of each experiment by open-tip junction currents and excluded if rise times exceeded 0.5 ms.

Analysis of rapid responses. Deactivation rates were estimated by fitting a single exponential (τ_{deact}) to the 1 ms response decay; desensitization rates were estimated by fitting a single- or double-exponential function (τ_{des}) to the 500 ms response decay (from 95% of peak to steady state). Because modulators were slowly reversible, only cells naive to modulator were used for baseline Quis applications. Three to 20 responses per patch were averaged for analysis. Current traces and graphs were plotted using KaleidaGraph 3.5 (Synergy Software, Reading, PA).

Table 1. X-ray diffraction data collection statistics

	Aniracetam[a]	CX614[a]
Space group	$P2_1$	$P2_1$
Unit cell dimensions (Å)	$a = 48.1, b = 64.1, c = 108.0; \beta = 90.1°$	$a = 114.3, b = 163.7, c = 47.3; \beta = 90.0°$
# Molecules per A.U.[b]	2	6
Wavelength (λ, Å)	0.9763	0.9795
d_{min} (Å)[c]	1.65 (1.75)	1.70 (1.76)
Mean redundancy	2.8	2.5
R_{merge} (%)[d,e]	5.4 (37.4)	7.2 (14.8)
Completeness[e]	84.7 (66.1)	89.8 (52.1)

[a]Aniracetam was cocrystallized with fluorowillardiine, whereas CX614 was cocrystallized with quisqualate.
[b]Number of protein molecules per asymmetric unit (A.U.).
[c]Values in parentheses define the low-resolution limits for the highest-resolution shell of data.
[d]$R_{merge} = (\Sigma|I_i - \langle I_i \rangle|)/\Sigma|I_i|$, where $\langle I_i \rangle$ is the mean I_i over all symmetry-equivalent reflections.
[e]Values in parentheses are the statistics for the highest-resolution shell of data.

Table 2. Refinement statistics

	Aniracetam	CX614
Resolution (Å)	30.0–1.65	30.0–1.70
R_{work} (%)[a]	19.9	20.9
R_{free} (%)[b]	22.1	22.3
# Protein atoms	4024	11776
# Water molecules	711	776
# Ligand atoms	62	196
Mean B value (Å^2)	18.3	19.2
rms deviations from ideality: bonds/angles (Å/°)	0.005/1.22	0.005/1.20

[a]$R_{work} = (\Sigma||F_o| - |F_c||)/\Sigma|F_o|$, where F_o and F_c denote observed and calculated structure factors, respectively.
[b]Ten percent of the reflections were set aside for calculation of R_{free}.
[c]In the refinements, there were two aniracetam and two fluorowillardiine molecules in the Ani/FW complex and six CX614 and six quisqualate molecules in the CX614/Quis complex.

Results

Modulation of deactivation

Deactivation is the process by which the ion-conducting pore of glutamate receptors closes, allowing agonist to dissociate from the ligand-binding "clamshell." Deactivation is measured experimentally by exposing the receptor to such brief (1 ms) pulses of agonist that little receptor desensitization can occur. Desensitization is a long-lasting, agonist-bound, nonconducting state; it is measured experimentally by exposing the receptor to a prolonged (500 ms) pulse of agonist. CTZ prevents normal channel desensitization, the rearrangement of a dimer interface formed by adjacent subunits within a receptor complex that allows the ion-conducting pore to close in the continued presence of agonist (Sun et al., 2002). CTZ modulates desensitization to a far greater extent than it does deactivation, and it is more efficacious on flip isoforms. Unlike CTZ, aniracetam and CX614 slow channel deactivation (Fig. 1) and are selective for flop rather than flip splice isoforms. Modulators of deactivation can have little (aniracetam) or marked (CX614) additional effects on desensitization.

Structures of Ani/FW and CX/Quis complexes

To define the location of the modulator binding sites, we solved cocrystal structures of the GluR2 S1S2 ligand-binding core complex with Ani/FW and CX/Quis at 1.65 and 1.7 Å resolution, respectively. We used fluorowillardiine in the crystallographic studies with aniracetam because the Ani/FW complex diffracted to higher resolution than any of the other agonist-bound aniracetam complexes. Shown in Tables 1 and 2 are relevant crystallographic statistics. The Ani/FW and CX/Quis GluR2 S1S2 complexes crystallize as dimers with the same dimer interface as described previously (Armstrong and Gouaux, 2000; Sun et al., 2002; Mayer and Armstrong, 2004). There is a small but significant difference in the degree of domain closure in each protomeric clamshell: the Ani/FW and CX/Quis complexes are more closed by ~1° compared with the parent FW and Quis structures (Jin et al., 2002, 2003; Jin and Gouaux, 2003); however, the modulators do not produce any significant changes of binding site residues or water molecules within the agonist binding pockets.

Both modulators bind within the dimer interface of the nondesensitized conformation of the GluR2 S1S2 dimer (Sun et al., 2002); shown in Figure 2 are the electron densities associated with aniracetam and CX614. Strikingly, both modulators

occupy a single site, located on the molecular twofold axis that relates one protein subunit to another, as illustrated in Figure 3. Because the modulators bind on the molecular twofold axis, their respective electron densities are superpositions of the electron densities of the modulators bound in twofold disordered orientations, each with occupancies of 0.5. Despite this disorder, we were able to fit either orientation of aniracetam and CX614 to their associated electron densities because the crystals of the complexes diffract to high resolution and the maps have substantial atomic detail. In the crystallographic refinement, the modulator sites were occupied by two modulator molecules, each with an assigned occupancy of 0.5 and related by a noncrystallographic twofold axis of symmetry. Thus, although it appears from the crystallography that two modulator molecules are superimposed on each other, one dimer interface actually only binds a single modulator.

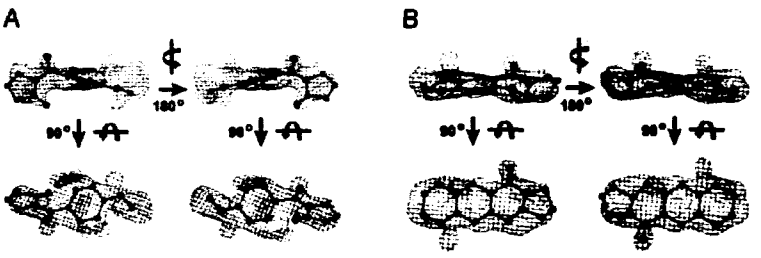

Figure 2. Omit electron density maps calculated using $|F_o| - |F_c|$ coefficients for aniracetam and CX614. *A*, Electron density for aniracetam contoured at 2.5 σ. *B*, Electron density for CX614, also contoured at 2.5 σ. For each modulator, the fit of the molecular structure to the electron density is shown for each of the twofold related positions of the modulator; on the top rows, the views are perpendicular to molecular twofold axis, whereas in the bottom rows, the views are parallel to the molecular twofold axis.

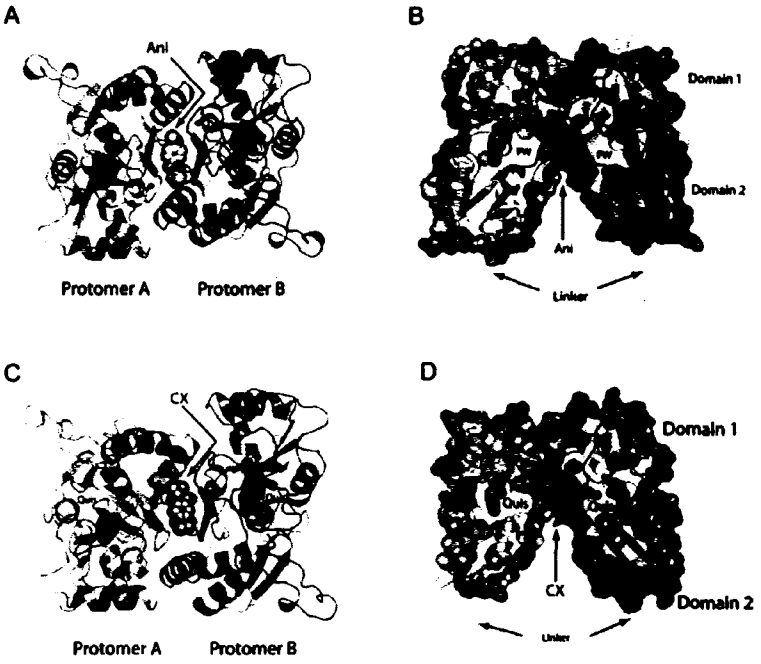

Figure 3. Aniracetam and CX614 bind in the dimer interface, in a crevice at the clamshell hinge. *A*, View down the twofold axis, showing the binding of aniracetam, in one of its two equivalent orientations. Protomer A is in green, protomer B is in blue, and aniracetam is drawn in Corey, Pauling, and Koltun (CPK) representation, as is the partial agonist fluorowillardiine. *B*, View of the Ani/FW complex perpendicular to the molecular twofold axis. Here, aniracetam is red and in CPK representation; the approximate positions of the "linker" that connects the ligand-binding cores to the transmembrane domains is shown. *C*, View of the CX614 complex, along the molecular twofold axis, with the protein subunits colored as in *A* and CX614 and quisqualate in CPK representation. *D*, Illustration of CX614 binding pocket using the same view as in *C*, with CX614 in red.

Modulator–protein interactions: the modulators bind in a dimer-interface, solvent-filled crevice

The binding site of both modulators is located in a solvent-filled crevice, in the dimer interface, and it is proximal to the transdomain β-strands that undergo conformational changes during agonist binding and domain closure (Armstrong and Gouaux, 2000). Strikingly, a key element of the modulator binding site involves a U-shaped crevice that is formed by main chain residues Pro 494 through Ser 497, and, as we show subsequently, many of the interactions between the modulators and the receptor are with atoms of the polypeptide main chain, a number of which are mediated by water molecules. Pro 494 forms the apex of the crevice, whereas Ser 497 and 729 define its base.

Two aniracetam molecules have been modeled into the Ani/FW crystal structure and are located on a non crystallographic twofold axis. Aniracetam oxygen atoms O1, O2, and O3 mediate the primary hydrogen bonding interactions between the modulator and the receptor, as depicted in Figure 4. Atom O2 forms water-mediated hydrogen bonds with the main chain oxygen atom of Pro A494, the ND2 atom of Asn A754, and the main chain oxygen atom of Ile B481. Both atoms O1 and O2 form water-mediated hydrogen bonds with Lys 730 and Ser 729, except that they interact with different protomers within a dimer, because of their position on a pseudo twofold axis of molecular symmetry. In addition to the hydrogen bonding interactions contributed by the three oxygen atoms, the aromatic ring of aniracetam is involved in nonpolar contacts with the ring of Pro 494. However, in comparing the interactions between the aromatic ring of aniracetam and Pro 494 with those between the equivalent rings in CX614 and Pro 494, we see that the interactions in the Ani/FW complex are not as extensive.

Six CX614 molecules have been modeled into the CX/Quis crystal structure. For each binding site, two CX614 molecules are modeled that are related by a noncrystallographic twofold axis. The interactions between CX614 and the GluR2 ligand-binding core are identical within experimental uncertainty for all six CX614 molecules. Atoms O2 and O3 of CX614 mediate most of the polar interactions between CX614 and the receptor. Atom O2 participates in a hydrogen bond with the main chain nitrogen atom of Gly 731, located on an interdomain β-strand near the clamshell "hinge." In addition, four water molecules (W1–W4)

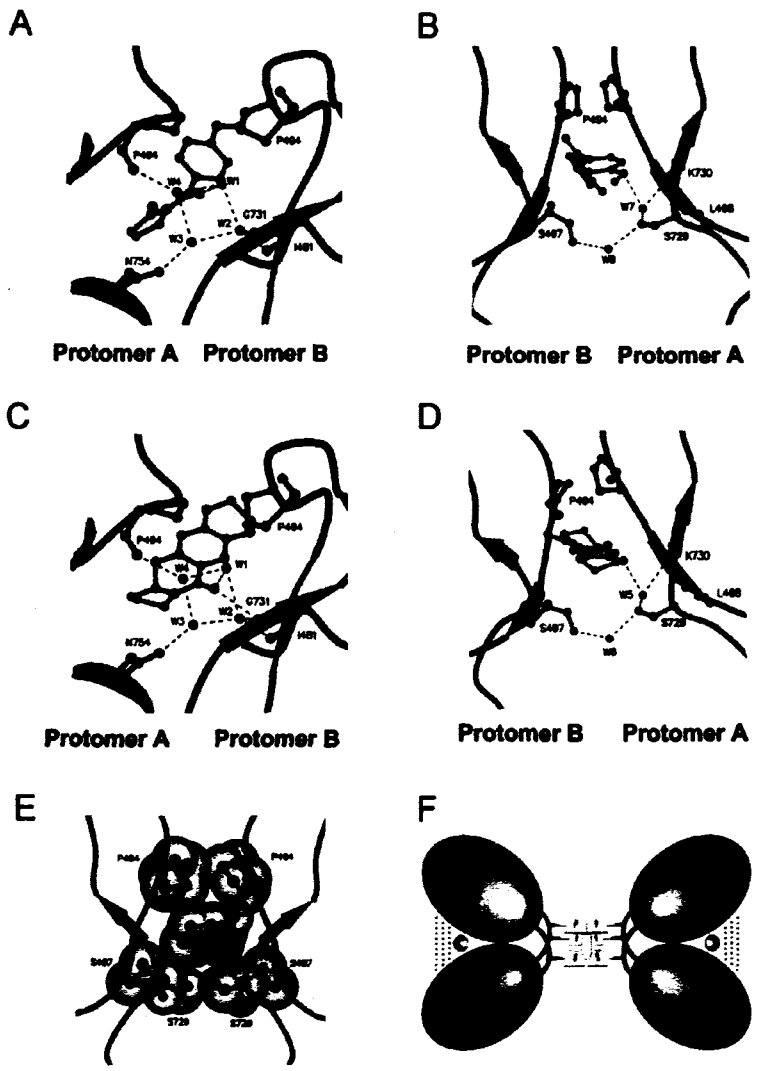

Figure 4. Hydrogen bonding interactions and binding modes of aniracetam and CX614. *A*, Top view of hydrogen bonding (dashed lines) between aniracetam, protein residues, and water molecules (blue spheres), in which the domains are color coded as shown in *F*. *B*, Side view of aniracetam hydrogen bonding interactions. *C*, View of hydrogen bonding interactions between CX614, protein, and water molecules from the top. *D*, CX614 interactions with protein and water molecules from the side. *E*, Binding of CX614 illustrated using CPK representation, showing residues Pro 494, Ser 497, and Ser 729 from each subunit, illustrating how the prolines form the "top" of the binding pocket and the serines form the base. *F*, A simple model to describe the mechanism of action of positive allosteric modulators such as aniracetam and CX614 on AMPA receptors. The diagram depicts a side view of the GluR2 ligand-binding core dimer in which domains 1 and 2 of protomer A are orange and blue, and domains 1 and 2 of protomer B are red and green, respectively. Agonists are represented by small blue spheres that bind between domains 1 and 2 and stabilize the closed-cleft conformation. Modulators, such as aniracetam and CX614 (yellow oval), bind on the backside of the ligand-binding core through interactions with a proline ceiling and a serine floor, at the interdomain hinge in the dimer interface, and stabilize the closed-cleft conformation of the ligand-binding core (dashed lines).

bridge the O2 atom of CX614 and oxygen or nitrogen atoms in residues Pro A494, Asn A754, and Ile B481, as illustrated in Figure 4. Atom O3 of CX614 forms a hydrogen bond with the side chain of Ser A729 and the main chain oxygen atom of Lys A730. In addition to polar interactions, the relatively hydrophobic modulators make numerous nonpolar, van der Waals contacts with the receptor. For example, the five-membered ring 1 of CX614 is oriented approximately parallel to the side chain ring of Pro 494, and the average distance between the two rings is ~5 Å. There are additional van der Waals contacts between CX614 and the receptor that include contacts with residues Pro 494–Ser 497 and Ser 729–Gly 731.

The "floor" of the aniracetam and CX614 binding site is formed by four serine residues: two from each subunit Ser 497 and Ser 729, as illustrated in Figure 4. During modulator binding, the side chain of Ser 729 reorients closer to the modulator so that it can participate in a hydrogen bond, whereas the side chain of Ser 497 moves away from the modulator so as to prevent a steric clash. As a consequence of these rearrangements, the four serine residues define a plane that is approximately perpendicular to the molecular twofold axis relating one protein subunit to the other. Indeed, a molecular surface representation of the modulator/GluR2 S1S2 complex shows that the four serine residues seal the floor of the modulator binding site and occlude the modulator from contact with bulk solvent, as seen in Figure 4.

Strikingly, the aniracetam and CX614 molecules bind to essentially the same site *in the dimer interface*, although *they differ* substantially in chemical structure. In fact, when a single protomer from the Ani/FW and CX/Quis dimers are superimposed, the resulting positions of the aniracetam and CX614 modulators overlap, as shown in Figure 5. Here we see that specific aromatic rings (Fig. 1, ring 3) of both modulators occupy the same position in the binding site, as does the five-membered, unsaturated ring. Because the nonpolar and polar atoms superimpose almost perfectly, both modulators make similar interactions with protein residues in the dimer interface. This conservation of binding therefore explains why both modulators share the functional behavior of slowing deactivation. Because CX614 has a larger surface area and makes additional polar and nonpolar contacts, it binds more tightly than aniracetam.

Mutation of side chains contacting modulator impairs modulation

We hypothesized that efficacious allosteric modulation by CX614 was mediated via hydrophobic interactions between the drug and Pro 494, and hydrogen bonding with the Ser 497 and Ser 729. To test the functional role of these interactions, we mutated each residue individually to alanine and measured deactivation and desensitization kinetics in the absence and presence of CX614 (Fig. 6, Table 3) (supplemental data, available at www.jneurosci.org as supplemental material), focusing on CX614 rather than aniracetam because the effects of CX614 on deactiva-

tion are more profound. The Ser 497 to Ala (S497A) mutant did not impair modulation, whereas the Ser 729 to Ala (S729A) mutant had a modest effect on modulation of desensitization. We then introduced a larger side chain by mutating the serines to threonines. Modulation was ablated for Ser 497 to Thr (S497T), whereas Ser 729 to Thr (S729T) was indistinguishable from wild type. The functional analyses support our interpretation of the structural data: because the Ser 497 side chain typically moves away from the binding site during modulator binding, making the side chain larger by introducing a threonine, causes steric hindrance between the threonine side chain and CX614, with a resulting loss of modulation. Substituting the S729 side chain with the smaller alanine would make it more difficult for this residue to reorient toward the drug, also resulting in the loss of modulation. The P494A mutation was not functional when assayed in a GluR2 flop background; however, the same mutation in a GluR2 flip background was functional, and, as expected, CX614 modulation was completely lost.

In addition to effects on modulation, mutation of these side chains in some cases altered the intrinsic kinetics of gating (deactivation) and desensitization (Table 3), consistent with a role for hinge domains in channel gating.

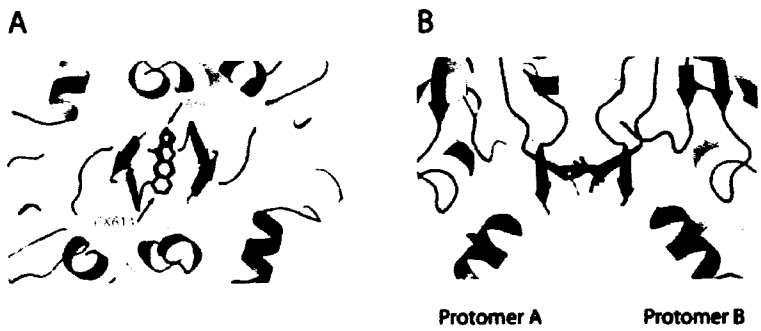

Figure 5. The binding sites of aniracetam and CX614 overlap. *A*, View parallel to the twofold axis showing that aniracetam (green) and CX614 (pink) overlap. In fact, rings 1 and 3 are nearly superimposable. *B*, View perpendicular to the twofold axis, showing that the modulators bind at the same "depth" in the dimer interface.

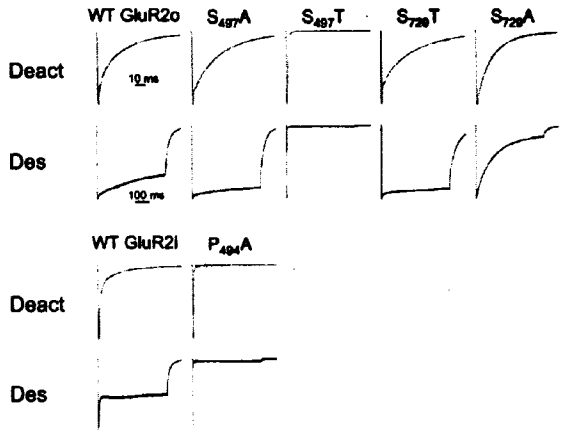

Figure 6. Mutations in modulator binding crevice impair modulation by CX614. Current responses, measured in outside-out patches of transiently transfected HEK 293 cells, of wild-type (WT) GluR2 (flop), and point mutations of residues that interact with CX614 are shown. Top traces show impairment of modulation of deactivation (Deact) by 100 μM CX614 with 3 mM quisqualate; bottom traces show impairment of modulation of desensitization (Des). The P494A mutation was measured in a GluR2 (flip) receptor, because the concomitant mutation in GluR2 (flop) was nonfunctional.

Apo state and modulator/agonist-bound state comparison

When agonist binds to the GluR2 ligand-binding core, the domain 1/domain 2 clamshell closes by ~21°, enveloping the agonist in the binding cleft. As a consequence of this conformational change, there are substantial changes in the backbone dihedral angles in the β-strands that link domain 1 and domain 2 and that include residues Ser 497–Ile 500 and Leu 727–Gly 731. Because these residues overlap with the modulator binding site, we wanted to determine the extent to which the modulator binding site changes when agonists bind to the ligand-binding core. To do this, we superimposed the "apo" ligand-binding core and the agonist/modulator-bound ligand-binding core using α-carbons in domain 1, a portion of the structure that does change substantially during agonist binding. To our surprise, we found that the modulator binding site is mostly preserved in the agonist-free state, except for the conformation of the side chains of Ser 497 and Ser 729. The side chain of Ser 497 swings out of the binding pocket to make room for the modulators (Fig. 7), whereas the side chain of Ser 729 moves into the binding site to form interactions with the modulators and nearby water molecules.

There is also a small but significant compression of the modulator binding site attributable to the ~1.5 Å movement of main chain atoms of Pro 494, Phe 495, Met 496, and Ser 497 into the pocket during binding of agonist and closure of the clamshell. Shown in Figure 7 are superpositions of apo and agonist bound states, illustrating the movements of side chain and main chain atoms. Thus, in the agonist-bound, closed clamshell state, the modulator binding site is slightly smaller and better matches the chemical structures of aniracetam and CX614. We suggest, therefore, that this is the primary mechanism by which the modulators stabilize the agonist-bound, closed-clamshell state of the receptor.

Comparison of the aniracetam/CX614 and cyclothiazide complexes

Two CTZ molecules bind in the dimer interface, and the two binding sites are related by a molecular twofold axis, as shown in Figure 8. CTZ is oriented such that the long axis of the molecule spans the dimer interface and each end of CTZ interacts extensively, via both polar and nonpolar contacts, to domain 1 and domain 2 on each subunit in the dimer. In contrast, there is only one binding site for aniracetam and CX614, and the binding site is centered on the molecular twofold axis. In addition, the long axes of aniracetam and CX614 are oriented approximately parallel to the dimer interface; the modulators do not penetrate into either domain 1 or domain 2, and most of the interactions between the modulators and the receptor are nonpolar contacts, with only a few modulator–protein hydrogen bonds.

Structural comparison of the CTZ/Glu, Ani/FW, and CX/Quis complexes shows that the binding sites for aniracetam and CX614 on the one hand and CTZ on the other hand partially

Table 3. Effect of mutations on modulation of GluR2 by CX614

	Control (τ_{deact})	Control (τ_{des})	CX614 (τ_{deact})	CX614 (τ_{des})	Fold slowing (τ_{deact})	Fold slowing (τ_{des})	% Des + CX614
WT GluR2(flop)	0.87 ± 0.06 (21)	1.21 ± 0.05 (18)	23.5 ± 1.48 (13)	207 ± 28.2 (10)	27	171	37 ± 4[d]
WT GluR2(flip)	2.52 ± 0.53 (6)	4.76 ± 0.29 (6)	8.91 ± 1.05 (6)		4		48 ± 3
S497A	1.86 ± 0.38 (5)[a]	2.60 ± 0.53 (5)[a]	31.3 ± 1.68 (6)[c,a]	191 ± 28.4 (6)	17	73	14 ± 2
S497T	1.03 ± 0.14 (9)	1.34 ± 0.14 (8)	0.87 ± 0.06 (6)[c,a]	1.32 ± 0.13 (5)[c,a]	1	1	89 ± 3
S729A	0.93 ± 0.08 (10)	1.01 ± 0.06 (8)	19.5 ± 2.21 (6)	105 ± 10.8 (7)[c,a]	21	104	77 ± 5
S729T	0.75 ± 0.04 (5)	0.98 ± 0.02 (4)	25.4 ± 0.69 (4)	330 ± 62.4 (4)	34	337	10 ± 2
P494A i	0.37 ± 0.02 (21)[b]	0.52 ± 0.03 (28)[b]	0.49 ± 0.06 (7)	0.64 ± 0.05 (8)	1	1	88 ± 4

Mean ± SEM data for wild-type (WT) and mutant GluR2 receptors. Three functional parameters were measured in the absence and presence of CX614: the time constant of deactivation (τ_{deact}), the time constant of desensitization (τ_{des}), and the ability of CX614 to block desensitization (Des) during a 500 ms pulse of agonist [% des = (1 − ss/pk)(100)]. For example, mutations that impaired modulation by CX614 (i.e., S497T and S729A) desensitized to a greater extent in the presence of the drug.

[a]Significantly slower than wild-type control kinetics ($p \leq 0.0001$).

[b]Significantly faster than wild-type control kinetics ($p \leq 0.0001$).

[c]Significantly different from wild-type GluR2o kinetics in the presence of CX614. *$p \leq 0.0001$; #$p \leq 0.01$.

[d]Control percentage desensitization in the absence of drug is 94 ± 1%.

i, Flop variant was nonfunctional; therefore, flip variant was used.

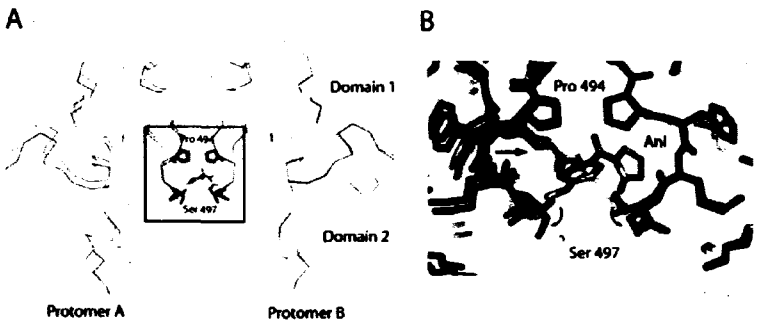

Figure 7. Conformational changes in the modulator binding site during agonist binding and clamshell closure. *A*, Shown here are α-carbon traces of the dimers from the Ani/FW complex and the apo state (Armstrong and Gouaux, 2000), in which the domain 1 from protomer B was superposed. In the boxed region, aniracetam is drawn, as are the side chain atoms for Pro 494 and Ser 497. *B*, Closeup view of the boxed region from *A*. The Ani/FW structure is blue, and the apo structure is gray. During agonist and modulator binding, the main chain atoms of residues Pro 494–Ser 497 move ~1.5 Å into the modulator binding site.

overlap. Specifically, the binding site for the endocyclic sulfonamide moiety of CTZ, located in the middle of the CTZ molecule, overlaps with the binding sites for the five-membered rings of aniracetam and CX614. In addition, the distal ring 4 of CX614 also overlaps with the endocyclic sulfonamide group of cyclothiazide.

Aniracetam and CX614 promote dimerization of the GluR2 ligand-binding core

To examine the effect of aniracetam and CX614 on dimerization of the GluR2 ligand-binding core, we performed sedimentation equilibrium experiments in the analytical ultracentrifuge, motivated by the studies of Sun et al. (2002) demonstrating that the dissociation constant of the ligand-binding core dimer was correlated with the extent of receptor desensitization. For CX614, we performed sedimentation equilibrium experiments in the presence and absence of the full agonist AMPA to determine whether the conformation of the clamshell affected the dimer dissociation constant. In both cases, CX614 shifted the dimer–monomer equilibrium substantially toward dimer. The centrifugation data could be best fit to a two-species, monomer–dimer model, and it yielded experimentally indistinguishable dimer–monomer K_d values of 26.1 μM in the presence of AMPA and 24.1 μM in the apo state. In contrast, aniracetam was less effective at stabilizing the dimer, and the measured dimer to monomer K_d value was 1.4 mM. Although both modulators decrease the dimer K_d value from its value of ~6 mM in the absence of modulator, CX614 stabilizes the dimer to a much greater extent that aniracetam. Shown in Figure 9 are residuals and fits from the sedimentation equilibrium analysis.

Discussion

Aniracetam and CX614 stabilize the agonist-bound state

The clamshell structure of the GluR2 ligand-binding core is composed of two domains that are connected by interdomain β-strands. The first interdomain β-strand is composed of Met 496–Leu 498 (β7), and the second spans residues Lys 730–Tyr 732 (β12). Structural analysis shows that the backbone dihedral angles in the regions of Ser 497–Ile 500 and Leu 727–Gly 731, together with the backbone torsion angles of Gly 499 and Lys 730, change significantly during agonist binding (Armstrong and Gouaux, 2000). Correspondingly, the axis that describes the domain closure that occurs during agonist binding runs through the two interdomain β-strands. Conformational fluctuations in the two interdomain β-strands is also supported by a recent nuclear magnetic resonance (NMR) study that showed that residues Leu 498, Gly 499, Leu 727, and Glu 728 exhibit chemical exchange (McFeeters and Oswald, 2002). Together, the crystallographic and NMR data reinforce the notion that regions Met 496–Ile 500 and Leu 727–Tyr 732 undergo conformational changes during

agonist binding. This region, therefore, is referred to as the interdomain hinge.

Among the six residues that make hydrogen bonding or van der Waals contacts with aniracetam and CX614, four are located in the interdomain hinge (Ser 497, Ser 729, Gly 731, and Lys 730). By binding to the hinge region, aniracetam and CX614 may stabilize the closed-cleft, agonist-bound conformation of the ligand-binding core. By stabilizing the closed-cleft, agonist-bound conformation, the modulators slow agonist unbinding and therefore ion channel deactivation, consistent with an increase in P_o in the presence of aniracetam (Lawrence et al., 2003). Destabilizing the closed-cleft conformation has the opposite effect, increasing the rate of channel deactivation (Robert et al., 2005).

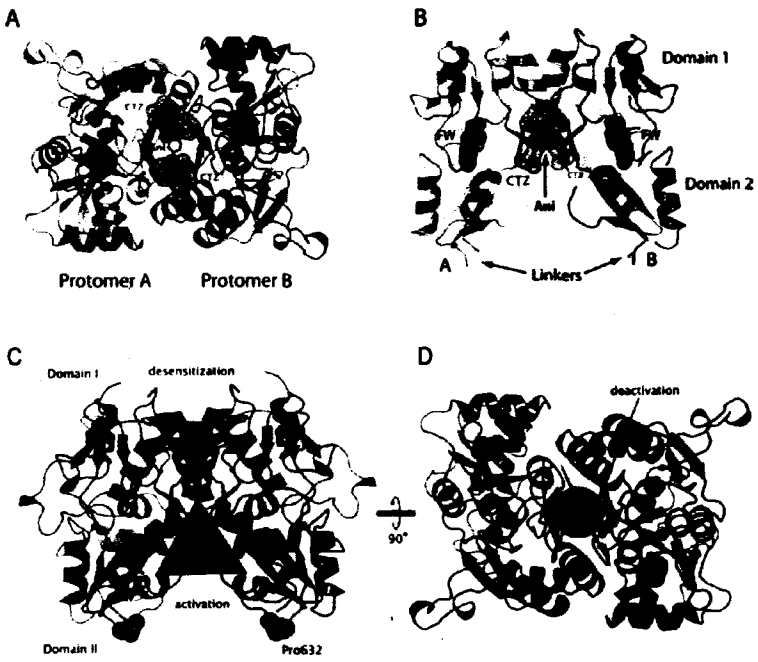

Figure 8. Comparison of the binding sites for aniracetam and CTZ. *A*, View down the twofold axis of the Ani/FW complex, showing aniracetam in red. Superimposed on the Ani/FW complex are the two CTZ molecules, taken from the GluR2 S1S2–CTZ cocrystal structure (Sun et al., 2002), after superposition of the protein structure on the Ani/FW protein structure. The molecular surfaces of the CTZ molecules are drawn as pink dots. *B*, View perpendicular to the molecular twofold axis. *C*, View perpendicular to the molecular twofold axis, as in *B*, relating drug-binding sites to their modes of action. Receptor activation increases the distance between domain II of each subunit (dark gray triangle). Subsequent to activation, channel desensitization occurs through rearrangements of domain I interactions (red triangle); this rearrangement is prevented when CTZ is bound. CX614 binds at the hinges between domains I and II (red circle). Rotating the view by 90° (*D*) allows a view of the CX614 interaction with the hinges, resulting in modulation of deactivation by stabilizing the closed-clamshell conformation.

Aniracetam and CX614 stabilize the ligand-binding core dimer

Sedimentation equilibrium experiments show that CX614 lowers the GluR2 S1S2 dimer K_d from ~6 mM to 26.1 μM. CTZ more effectively stabilizes the dimer, and, in the presence of saturating CTZ, the dimer K_d is 1.2 μM (Sun et al., 2002). In contrast, aniracetam provides minimal stabilization to the dimer and only lowers the dimer K_d to ~1.4 mM, although because of the limited solubility of aniracetam, we may not have saturated the binding site. Because stabilization of the dimer interface decreases the extent of receptor desensitization (Sun et al., 2002), we suggest that the effects that aniracetam and CX614 have on diminishing the rate of receptor desensitization are attributable to the degree to which they stabilize the dimer interface. We suggest, therefore, that the structural underpinning of receptor desensitization and deactivation are conceptually separable: stabilization of the dimer interface primarily affects receptor desensitization, whereas stabilization of the closed-clamshell state of the ligand-binding core slows deactivation. Although this model is appealing, it is an oversimplification because it does not explain why the L483Y mutation, which is relatively far from the interdomain hinge, slows receptor deactivation by ~10-fold (Sun et al., 2002). Furthermore, although CTZ and CX614 primarily effect desensitization and deactivation, respectively, CTZ also slows deactivation and CX614 slows desensitization. The inseparability of modulation of deactivation and desensitization arises because the interdomain hinges are located at the dimer interface (Partin et al., 1996; Lawrence et al., 2003). We suggest that these overlapping functional activities are attributable to the fact that the binding sites for these modulators partially overlap. Additional functional and structural experiments will be required to unravel the relationships between deactivation and desensitization.

Modulator binding is sensitive to functional states of the receptor

A striking feature of compounds such as aniracetam and CX614 is that they selectively modulate one functional state of a complex receptor that occupies many functional states. Indeed, recent electrophysiological studies using intact AMPA receptors and a related compound, 1-(1,4-benzodioxan-6-ylcarbonyl) piperidine (CX546), suggest that the modulator binds preferentially to the agonist-bound, nondesensitized state of the receptor, i.e., to the activated state (Nagarajan et al., 2001). Although we do not see large differences between the aniracetam and CX614 binding sites in the apo and agonist-bound states of the ligand-binding core, there is a compression of the modulator binding site and rearrangements of side chains and water molecules that accompany modulator binding. Because the ligand-binding core interface rearranges during receptor desensitization and the modulator binding site is situated in the middle of the nondesensitized dimer interface, dimer interface rearrangement during receptor desensitization will split the modulator binding site in half, thereby completely disrupting it.

Modulator pharmacology

Aniracetam, a weak binding modulator with an EC_{50} of >5 mM, was the lead compound for the development of the AMPAkine series of modulators (Tang et al., 1991). The early AMPAkine molecules, with potencies in the high micromolar range, were similar in architecture to aniracetam and contained two separate ring structures connected by a carbonyl group, with representative members being 1-(1,3-benzodioxol-5-ylcarbonyl)piperidine (BDP; CX465), 1-(quinoxalin-6-ylcarbonyl)piperidine (BDP-12; CX516), and CX546 (Arai et al., 1994, 1996b). A more recent generation of AMPAkines has two rings structures connected by

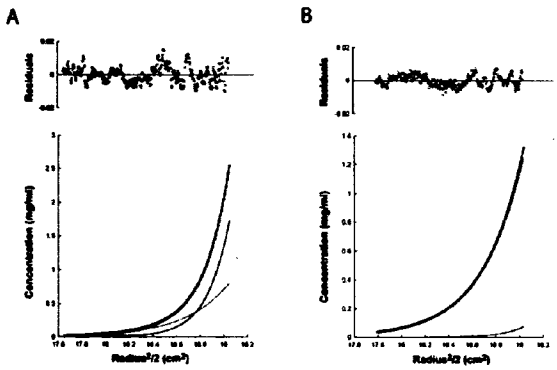

Figure 9. Sedimentation equilibrium data showing that CX614 and aniracetam stabilize the GluR2 dimer to different extents. *A*, Sedimentation equilibrium data taken in the presence of 0.3 mM AMPA and 0.3 mM CX614; the data shown here was collected at 27 K rpm and a protein concentration of 1.0 mg/mL. *B*, Sedimentation equilibrium data measured in the presence of 2 mM glutamate and 5 mM aniracetam. For the data shown here, the rotor speed was also 27 K rpm, and the loading protein concentration was 0.75 mg/mL. In both of the experiments involving CX614 and aniracetam, interference data from three loading protein concentrations and three rotor speeds were fit to a dimer–monomer equilibrium, yielding a protein dimer K_d of 26.1 μM in the case of CX614 and 1.4 mM for aniracetam. In *A* and *B*, the top panels show the residuals of the fit of the dimer–monomer model to the measured interference data, and the bottom panels show the measured interference data (open black circles), the fit to the data (solid black line), and the relative predicted concentrations of dimer (dark gray line) and monomer (light gray line). As seen in *A*, CX614 is much more effective in shifting the dimer–monomer toward dimer than aniracetam.

a fused six-atom heterocyclic ring, with representative examples being 1-(1,3-benzodioxol-5-ylcarbonyl)piperidine-20 (BDP-20; CX554) and CX614. On the basis of physiological and behavioral experiments, CX554 has a potency approximately an order of magnitude lower than the previous BDP compounds (EC_{50} of ~300 μM) (Arai et al., 1996a), whereas CX614 is more potent, with an EC_{50} of 20–40 μM (Arai et al., 2000). More recently, high-affinity modulators, such as LY404187, have been shown to modulate desensitization and appear to bind in the dimer interface (Quirk and Nisenbaum, 2003).

Because aniracetam and CX614 are representative of the weakest and most potent drugs in this series, respectively, the structures of their complexes with the GluR2 ligand-binding core provide a unique opportunity to investigate structure and function relationships. In general, the binding of aniracetam and CX614 is driven primarily by nonpolar, van der Waals contacts, the hydrophobic effect, and, to a lesser extent, hydrogen bonds. The modulator binding site, before modulator binding, is preorganized and filled with ordered solvent. Both aniracetam and CX614 are relatively hydrophobic molecules and have few polar atoms. Perhaps the most significant difference between aniracetam and CX614, however, is that CX614 is a substantially more rigid, constrained molecule. On the basis of the aniracetam structure, the planes of the two rings are staggered by ~60°. By joining rings 1 and 3, as in the case of CX614, the orientation of rings 1 and 3 are covalently constrained to a relative orientation that is favorable for binding. The conformational rigidity of the molecules may contribute to high potency by maximizing interactions with the receptors while minimizing unfavorable entropy loss during modulator binding. Modulator rigidity may also contribute to high potency by enabling optimal nonpolar contacts between ring 1 and Pro 494, and hydrogen bonding interactions involving O2 and O3.

The cocrystal structure with CX614 can also help to answer questions of structure and function relationships in other modulators, such as why CX614 is more potent than CX554, although they have nearly identical structures. Indeed, the only difference between CX614 and CX554 is that the two oxygen atoms extending from the benzene ring are connected by two methylene groups in CX614 and a single methylene group in CX554. In the CX614 structure, ring 4 is located in a hydrophobic pocket defined by residues Pro 494, Val 750, Leu 751, and Leu 759. Because CX614 has an additional methylene group, it can better fill the hydrophobic pocket and, in so doing, can also participate in additional van der Waals contacts. The slightly greater hydrophobicity of CX614 will also enhance binding.

A common feature of modulator binding in the dimer interface is the displacement of ordered water molecules. For example, before modulator binding, the aniracetam and CX614 binding sites are occupied by eight ordered water molecules, and, after the modulators bind, all eight water molecules are displaced; the hydrophobic pocket that is occupied by the bicyclic ring of CTZ is filled with four water molecules before CTZ binding, and similarly, these four waters are displaced during CTZ binding. In the Ani/FW and CX/Quis complexes, there is an ordered water molecule that mimics one of the oxygen atoms of the 7-sulfonamide group of CTZ.

Conclusions

The crystal structures of the GluR2 ligand-binding core Ani/FW and CX/Quis complexes reveal a new binding site for positive allosteric modulators of AMPA receptors. This binding site is located in the dimer interface and at the interdomain hinge. We suggest that aniracetam and CX614 stabilize the ligand-binding core in the agonist-bound, activated state, thereby slowing agonist release and ion channel deactivation. Aniracetam and CX614 also stabilize the ligand-binding core dimer and, through this effect, reduce the rate of receptor desensitization. The high resolution crystal structures presented here demonstrate, for the first time, how modulators can differentially affect deactivation and desensitization, they lend insight into the mechanism underlying modulator potency and efficacy, and they provide a structural basis from which to design a new generation of AMPA receptor modulators.

References

Arai A, Lynch G (1998) The waveform of synaptic transmission at hippocampal synapses is not determined by AMPA receptor desensitization. Brain Res 799:230–234.

Arai A, Kessler M, Xiao P, Ambros-Ingerson J, Rogers G, Lynch G (1994) A centrally active drug that modulates AMPA receptor gated currents. Brain Res 638:343–346.

Arai A, Kessler M, Ambros-Ingerson J, Quan A, Yigiter E, Rogers G, Lynch G (1996a) Effects of a centrally active benzoylpyrrolidine drug on AMPA receptors kinetics. Neuroscience 75:573–585.

Arai A, Kessler M, Rogers G, Lynch G (1996b) Effects of a memory-enhancing drug on D,L-alpha-amino-3-hydroxy-5-methyl-4-isoxazolepropionic acid receptor currents and synaptic transmission in hippocampus. J Pharmacol Exp Ther 278:627–638.

Arai AC, Kessler M, Rogers G, Lynch G (2000) Effects of the potent ampakine CX614 on hippocampal and recombinant AMPA receptors: interactions with cyclothiazide and GYKI 52466. Mol Pharmacol 58:802–813.

Armstrong N, Gouaux E (2000) Mechanisms for activation and antagonism of an AMPA-sensitive glutamate receptor: crystal structures of the GluR2 ligand binding core. Neuron 28:165–181.

Boulter J, Hollmann M, O'Shea-Greenfield A, Hartley M, Deneris E, Maron C, Heinemann S (1990) Molecular cloning and functional expression of glutamate receptor subunit genes. Science 249:1033–1037.

Brünger AT (1992) Free *R* value: a novel statistical quantity for assessing the accuracy of crystal structures. Nature 355:472–475.

Brünger AT, Adams PD, Clore GM, DeLano WL, Gros P, Grosse-Kunstleve RW, Jiang JS, Kuszewski J, Nilges M, Pannu NS, Read RJ, Rice LM, Simonson T, Warren GL (1998) Crystallography and NMR system: a new software suite for macromolecular structure determination. Acta Crystallogr D Biol Crystallogr 54:905–921.

Chen GQ, Gouaux E (1997) Overexpression of a glutamate receptor (GluR2) ligand binding domain in *Escherichia coli*: application of a novel protein folding screen. Proc Natl Acad Sci USA 94:13431–13436.

Delano WL (2005) The PyMOL molecular graphics system. San Carlos, CA: DeLano Scientific.

Dingledine R, Borges K, Bowie D, Traynelis SF (1999) The glutamate receptor ion channels. Pharmacol Rev 51:7–61.

Esnouf RM (1999) Further additions to MolScript version 1.4, including reading and contouring of electron density maps. Acta Crystallogr D Biol Crystallogr 55:938–940.

Fleck MW, Cornell E, Mah SJ (2003) Amino-acid residues involved in glutamate receptor 6 kainate receptor gating and desensitization. J Neurosci 23:1219–1227.

Horning M, Mayer M (2004) Regulation of AMPA receptor gating by ligand binding core dimers. Neuron 41:379–388.

Ingvar M, Ambros-Ingerson J, Davis M, Granger R, Kessler M, Rogers GA, Schehr RS, Lynch G (1997) Enhancement by an ampakine of memory encoding in humans. Exp Neurol 146:553–559.

Isaacson JS, Nicoll RA (1991) Aniracetam reduces glutamate receptor desensitization and slows the decay of fast excitatory synaptic currents in the hippocampus. Proc Natl Acad Sci USA 88:10936–10940.

Jin R, Gouaux E (2003) Probing the function, conformational plasticity and dimer-dimer contacts of the GluR2 ligand-binding core: studies of 5-substituted willardiines and GluR2 S1S2 in the crystal. Biochemistry 42:5201–5213.

Jin R, Horning M, Mayer ML, Gouaux E (2002) Mechanism of activation and selectivity in a ligand-gated ion channel: structural and functional studies of GluR2 and quisqualate. Biochemistry 41:15635–15643.

Jin R, Banke T, Mayer ML, Traynelis SF, Gouaux E (2003) Structural basis for partial agonist action at ionotropic glutamate receptors. Nat Neurosci 6:803–810.

Jones TA, Kjeldgaard M (1997) Electron-density map interpretation. Methods Enzymol 277:173–208.

Jones TA, Zou JY, Cowan SW (1991) Improved methods for building protein models in electron density maps and the location of errors in these models. Acta Crystallogr A 47:110–119.

Kandel ER (2001) The molecular biology of memory storage: a dialogue between genes and synapses. Science 294:1030–1038.

Keinänen K, Wisden W, Sommer B, Werner P, Herb A, Verdoorn TA, Sakmann B, Seeburg PH (1990) A family of AMPA-selective glutamate receptors. Science 249:556–560.

Kleywegt GJ (1999) Experimental assessment of differences between related protein crystal structures. Acta Crystallogr D Biol Crystallogr 55:1878–1884.

Kraulis PJ (1991) MOLSCRIPT: a program to produce both detailed and schematic plots of protein structures. J Appl Cryst 24:946–950.

Lawrence JJ, Brenowitz S, Trussell LO (2003) The mechanism of action of aniracetam at synaptic α-amino-3-hydroxy-5-methyl-4-isoxazolepropionic acid (AMPA) receptors: indirect and direct effects on desensitization. Mol Pharmacol 64:269–278.

Leever JD, Clark S, Weeks AM, Partin KM (2003) Identification of a site in GluR1 and GluR2 that is important for modulation of deactivation and desensitization. Mol Pharmacol 64:5–10.

Mayer ML, Armstrong N (2004) Structure and function of glutamate receptor ion channels. Annu Rev Physiol 66:161–181.

McFeeters RL, Oswald RE (2002) Structural mobility of the extracellular ligand-binding core of an ionotropic glutamate receptor. Analysis of NMR relaxation dynamics. Biochemistry 41:10472–10481.

Merritt EA, Murphy MEP (1994) Raster3D, version 2.0. A program for photorealistic molecular graphics. Acta Crystallogr D Biol Crystallogr 50:869–873.

Miu P, Jarvie KR, Radhakrishnan V, Gates MR, Ogden A, Ornstein PL, Zarrinmayeh H, Ho K, Peters D, Grabell J, Gupta A, Zimmerman DM, Bleakman D (2001) Novel AMPA receptor potentiators LY392098 and LY404187: effects on recombinant human AMPA receptors in vitro. Neuropharmacology 40:976–983.

Morris RG, Anderson E, Lynch GS, Baudry M (1986) Selective impairment of learning and blockage of long-term potentiation by an *N*-methyl-D-aspartate receptor antagonist, AP5. Nature 319:774–776.

Nagarajan N, Quast C, Boxall AR, Shahid M, Rosenmund C (2001) Mechanism and impact of allosteric AMPA receptor modulation by the ampakine CX546. Neuropharmacology 41:650–663.

Navaza J (1994) AMoRe: an automated package for molecular replacement. Acta Crystallogr A 50:157–163.

O'Neill MJ, Bleakman D, Zimmerman DM, Nisenbaum ES (2004) AMPA receptor potentiators for the treatment of CNS disorders. Curr Drug Targets 3:181–194.

Partin KM, Fleck MW, Mayer ML (1996) AMPA receptor flip/flop mutants affecting deactivation, desensitization, and modulation by cyclothiazide, aniracetam, and thiocyanate. J Neurosci 16:6634–6647.

Quirk JC, Nisenbaum ES (2003) Multiple molecular determinants for allosteric modulation of alternatively spliced AMPA receptors. J Neurosci 23:10953–10962.

Rammsayer TH (2001) Effects of pharmacologically induced changes in NMDA-receptor activity on long-term memory in humans. Learn Mem 8:20–25.

Robert A, Armstrong N, Gouaux E, Howe JR (2005) AMPA receptor binding cleft mutations that alter affinity, efficacy, and recovery from desensitization. J Neurosci 25:3752–3762.

Sun Y, Olson RA, Horning M, Armstrong N, Mayer ML, Gouaux E (2002) Mechanism of glutamate receptor desensitization. Nature 417:245–253.

Tang CM, Shi QY, Katchman A, Lynch G (1991) Modulation of the time course of fast EPSCs and glutamate channel kinetics by aniracetam. Science 254:288–290.

Tsien JZ, Huerta PT, Tonegawa S (1996) The essential role of hippocampal CA1 NMDA receptor-dependent synaptic plasticity in spatial memory. Cell 87:1327–1338.

van Aalten DM, Bywater R, Findlay JB, Hendlich M, Hooft RW, Vriend G (1996) PRODRG, a program for generating molecular topologies and unique molecular descriptors from coordinates of small molecules. J Comput Aided Mol Des 10:255–262.

Vyklicky LJ, Patneau DK, Mayer ML (1991) Modulation of excitatory synaptic transmission by drugs that reduce desensitization at AMPA/kainate receptors. Neuron 7:971–984.

Available online at www.sciencedirect.com
SCIENCE DIRECT
Neuroscience Letters 402 (2006) 108–112
Neuroscience Letters
www.elsevier.com/locate/neulet

Kynurenic acid has a dual action on AMPA receptor responses

Christina Prescott [b], Autumn M. Weeks [a], Kevin J. Staley [b], Kathryn M. Partin [a,*]

[a] Department of Biomedical Sciences, Neuroscience Division, Colorado State University, Fort Collins, CO 80523, USA
[b] Department of Neurology and Pediatrics, University of Colorado Health Sciences Center, Denver, CO 80262, USA

Received 31 January 2006; received in revised form 8 March 2006; accepted 22 March 2006

Abstract

Glutamate is the predominant excitatory neurotransmitter in the central nervous system. The receptors that bind glutamate, including *N*-methyl-D-aspartate (NMDA) and α-amino-3-hydroxy-5-methyl-4-isoxazole propionic acid (AMPA) receptor subtypes, are strongly implicated in higher cognitive processes, especially learning and memory. Loss of glutamate receptor function impairs the ability to acquire and retain information in some patients subsequent to stroke or brain injury, and positive allosteric modulators of glutamate receptors can restore learning and memory in some of these patients. Here we demonstrate that kynurenic acid (KYNA), an endogenous tryptophan metabolite, acts upon heterologous AMPA receptors via two distinct mechanisms. Low (nanomolar to micromolar) concentrations of KYNA facilitate AMPA receptor responses, whereas high (millimolar) concentrations of KYNA competitively antagonize glutamate receptors. Low concentrations of KYNA appear to increase current responses through allosteric modulation of desensitization of AMPA receptors. These findings suggest the possibility that low concentrations of endogenous KYNA acting at AMPA receptors may be a positive modulator of excitatory synaptic transmission.

Keywords: Glutamate receptor; Allosteric modulation; Desensitization; Electrophysiology; Pharmacology

KYNA is a neuroprotective endogenous tryptophan metabolite produced by astrocytes and neurons via the kynurenine pathway in both humans and rodents [6]. In human CSF, KYNA levels are in the low nanomolar range [4]; however, the KYNA levels that are measured in the CSF may not accurately reflect synaptic concentrations because the majority of neuronal KYNA is produced by astrocytes, many of which are directly associated with excitatory synapses and are capable of producing micromolar concentrations of KYNA [7,13]. KYNA levels are decreased in the frontal cortex in absence epilepsy, infantile spasms, and in the caudate nucleus in Huntington's disease, while KYNA levels are increased in Alzheimer's disease, Down's syndrome, Gilles de la Tourette syndrome, schizophrenia, some bacterial and viral infections, and old age [22,12]. Increasing evidence suggests that KYNA is an endogenous neuroprotective agent able to prevent neuronal loss following excitotoxic, ischemia-induced, and infectious neuronal injuries [20,15]. Specifically, KYNA's ability to act as a neuroprotectant in multiple epilepsy models has been well documented [3,27,19,25,16,9,26].

* Corresponding author. Tel.: +1 970.491 2263; fax: +1 970 491 7907.
E-mail address: kpartin@lamar.colostate.edu (K.M. Partin).

0304-3940/$ – see front matter © 2006 Elsevier Ireland Ltd. All rights reserved.
doi:10.1016/j.neulet.2006.03.051

The molecular mechanisms of action of KYNA in the CNS have been studied with mixed results. At non-physiologic (millimolar) concentrations, KYNA has been reported to act somewhat non-selectively at several different receptor types, but at lower (low micromolar) concentrations, KYNA acts as a competitive antagonist at the glycine-binding site of the NMDA receptor and as a non-competitive antagonist at the α-7 nicotinic receptor [8]. Therefore, a significant component of KYNA's neuroprotective ability arises from its actions as an antagonist of glutamate receptors in brain regions with neuronal damage and concomitant NMDA receptor hyperexcitability. Rationally-designed structural derivatives of KYNA that are more selective for the glycine-binding site of the NMDA receptor are successfully making their way into clinical use [2]. In addition, KYNA is a lower-affinity competitive antagonist of AMPA receptors, competing for binding at the glutamate-binding pocket in the extracellular ligand-binding domain.

In the course of performing concentration-response experiments using very low concentrations of KYNA to reduce glutamatergic activation of AMPA receptors, we made an unexpected observation that suggested to us in some cases KYNA might facilitate AMPA synaptic transmission. We hypothesized, based on these data that KYNA might act both as a competitive antagonist and a positive allosteric modulator of AMPA receptor

activity. Positive allosteric modulators of AMPA receptors, such as cyclothiazide or aniracetam, modulate receptor desensitization and thereby increase AMPA-mediated current responses. Co-crystallization of the ligand-binding core of GluR2 with cyclothiazide [23] or aniracetam [11] identified a positive modulatory binding site at the interface between two adjacent subunit dimers. KYNA has never been reported to interact with this site, however. The goal of the present work was to determine if low concentrations of KYNA facilitate responses of cloned, heterologously expressed rat AMPA receptors, and if so to explore the molecular mechanism of the facilitation.

Adult (4–6 weeks old) male Sprague–Dawley rats were anesthetized with 100 mg/kg pentobarbital and decapitated. The brain was rapidly dissected out and placed into ice-cold high sucrose solution containing (in mM) 0.5 $CaCl_2$, 7 $MgCl_2$, 2.5 KCl, 25 $NaHCO_3$, 87 NaCl, 1.25 NaH_2PO_4, 25 glucose, and 75 sucrose. Then, 400 μm-thick coronal hemibrain slices were cut using a Leica VT-1000E vibratome (Leica, Nussloch, Germany) and kept for at least 90 min in an interface chamber containing 50% high sucrose solution and 50% ACSF, containing (in mM) 2 $CaCl_2$, 2 $MgCl_2$, 2.5 KCl, 26 $NaHCO_3$, 126 NaCl, 1.25 NaH_2PO_4, and 10 glucose (pH 7.4). Slices were then transferred to a recording chamber, where they were bathed in a modified ACSF solution containing (in mM) 1.3 $CaCl_2$, 0.9 $MgCl_2$, 3.3 KCl, 26 $NaHCO_3$, 126 NaCl, 1.25 NaH_2PO_4, and 10 glucose (pH 7.4). All solutions were saturated with 95% O_2/5% CO_2 and both interface and recording chambers were maintained at 35 °C. Experiments were approved by the University of Colorado Health Science Center Institutional Animal Care and Use Committee.

Field excitatory postsynaptic potentials (fEPSPs) were recorded using glass electrodes (resistance 5–6 MΩ) filled with 150 mM NaCl placed in the stratum radiatum of the CA1 region or the CA3 pyramidal cell layer. A bipolar platinum–iridium stimulating electrode was placed approximately 0.5 mm lateral to the recording electrode in the CA1 or 0.5 mm medial to the recording electrode in the CA3. The strength of the electrical stimulus was modified to obtain the maximal fEPSP amplitude without evoking a population spike. Each individual stimulus was 20 μs in duration and the interstimulus interval was 10 s. Recordings were performed with an Axoclamp 2B amplifier (Axon Instruments, Foster City, CA) and digitized at 5 kHz using a PCI-DAS 1602/16 (Computer Boards, Middleboro, MA). The change in response was determined as the average fEPSP slope or amplitude during drug application (20 min) normalized to the average baseline (20 min) fEPSP slope or amplitude, respectively.

Recordings were collected using programs written in Visual Basic 6.0 by Dr. K.J. Staley. All data are presented as the mean of the normalized responses, with standard errors shown.

Wild type and mutant GluR2 cDNAs served as a template for in vitro transcription using T7 polymerase, and oocytes were prepared from anesthetized *Xenopus laevis* as previously described [14]. Forty-eight hours after injection, responses to varying concentrations of glutamate, with or without KYNA, were recorded. An electronic valve control system and electronic valves were used to exchange solutions. A Macintosh G4 computer with an A/D interface running the program Synapse (Synergistic Research Systems, Silver Springs, MD) was used to acquire the current response. Oocytes were perfused with a solution of 100 μM glutamate for 30 s, followed by 30 s with 100 μM glutamate plus different concentrations of KYNA. Oocyte responses were analyzed by measuring the average amplitude of the control response and the average amplitude of the response in the presence of KYNA. Potentiation was measured as $I_{Glu+KYNA}/I_{Glu}$. Differences were measured using an ANOVA test.

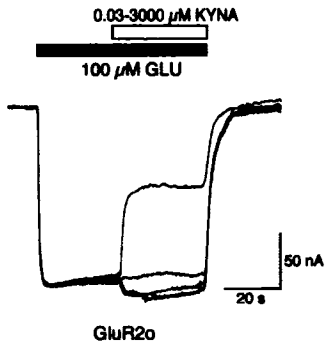

Fig. 1. KYNA has a dual effect on GluR2 glutamate-evoked currents. Overlay of six responses measured with two-electrode voltage clamp (TEVC) from an oocyte expressing GluR2o. After a 30 s exposure 100 μM glutamate, each oocyte was exposed to 30 s of a solution containing 100 μM glutamate and increasing concentrations of KYNA (0.03, 0.3, 3.0, 30, 300 and 3000 μM). Responses are normalized to the glutamate current immediately preceding application of KYNA, to negate the effects of receptor rundown over the 15–20 min needed to perform the entire experiment. $N = 6$–21 oocytes. Lower concentrations resulted in a modest potentiation of the glutamate-evoked currents, whereas concentrations of 300 and 3000 μM inhibited these currents.

All salts and drugs were obtained from Sigma (St. Louis, MO). Drugs were bath applied, unless otherwise stated.

We used a heterologous expression system in order to test the hypothesis that low concentrations of KYNA have positive allosteric effects on isolated AMPA receptors. We first examined the effects of KYNA on recombinant rat GluR2 responses. We found that concentration-dependent effects of KYNA were evident in the glutamate response of GluR2 receptors heterologously expressed in *Xenopus* oocytes, as measured by two-electode voltage clamp recording (TEVC) (Figs. 1 and 3). Low concentrations (0.03–30 μM) of KYNA potentiated steady-state responses to 100 μM glutamate of GluR2o by up to 110 ± 3% (3 μM KYNA), whereas high concentrations of KYNA inhibited responses to 40 ± 4% (3000 μM). Application of KYNA in the absence of agonist did not alter the holding current of the oocyte membrane. There was no significant difference in the ability of KYNA to potentiate the flop versus flip isoform (data not shown).

We reasoned that KYNA might be modulating receptor desensitization, as do other positive allosteric modulators. To determine if KYNA modulates desensitization, we tested a "non-desensitizing" GluR2o receptor mutant, $L_{483}Y$ [21]. Consistent with this hypothesis, KYNA was not able to potentiate responses of GluR2o $L_{483}Y$ (Figs. 2 and 3), but was still able to inhibit responses at the higher concentrations. We also tested a GluR2o

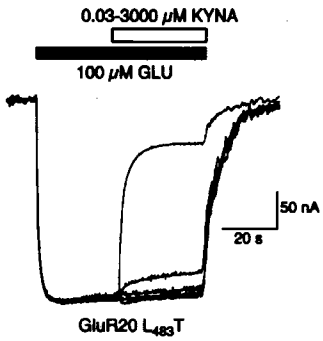

Fig. 2. KYNA may act by modulating channel desensitization. Overlay of six responses measured with TEVC from an oocyte expressing GluR2o $L_{483}Y$, with recording conditions similar to Fig. 1. The low-concentration, potentiating effect of KYNA was lost, whereas higher concentrations (300 and 3000 μM) remained inhibitory.

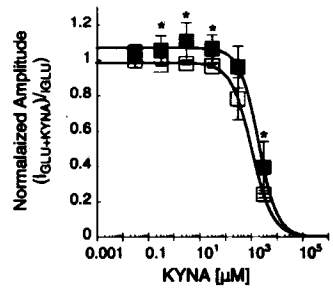

Fig. 3. KYNA dose–response relationship. Summary of mean TEVC dose–response data from oocytes expressing wild type GluR2o (closed squares) and the "non-desensitizing" GluR2o $L_{483}Y$ mutant receptors (open squares). The normalized amplitude is plotted versus increasing concentrations of KYNA. For all receptors, lower concentrations of KYNA facilitated the responses evoked by 100 μM glutamate. However, the effect of KYNA on GluR2o $L_{483}Y$ was less than for WT GluR2o, and this difference reached significance at 0.01 mM KYNA. The mutation had no effect on the ability of KYNA to inhibit responses at the higher concentrations. Data points are fit with a logistic equation (solid line), with I_{max} for WT receptors = 1.07 ± 0.01, whereas I_{max} for the mutated receptor = 0.99 ± 0.005; IC_{50}'s of the fit were calculated at 1.9 and 1.0 mM, respectively. Asterisks indicate significant differences in relative amplitude between wild type and the mutant receptor, $p < 0.05$. $N = 6$–21 oocytes. Data shown are mean ± S.E.M.

receptor mutant, $S_{497}T$, which impairs the ability of other positive allosteric modulators, such as cyclothiazide, to modulate desensitization [23,14,11]. GluR2o $S_{497}T$ impaired the ability of KYNA to potentiate the glutamate response, although not as effectively as the $L_{483}Y$ mutation (data not shown). As with the GluR2o $L_{483}Y$ mutant, the S497 mutant did not affect the ability of KYNA to inhibit responses at higher concentrations; the mutations only affected the ability of KYNA to potentiate responses at low concentrations. The most parsimonious interpretation of these data is that KYNA interacts with two distinct sites on the AMPA receptor: a lower affinity site that is most likely the ligand-binding site and a higher affinity site that at least overlaps the previously identified positive allosteric modulation site. KYNA is a sufficiently potent antagonist that at higher concentrations (such as the concentrations typically used experimentally to antagonize glutamate responses), the potentiation of glutamate responses is masked by the antagonist effect. Our experiments at low concentrations reveal a previously unrecognized positive allosteric action of KYNA.

The effects of KYNA on evoked excitatory transmission in the rat hippocampal slice preparation were measured at KYNA concentrations of 10–1000 μM. Low concentrations (10 μM) of KYNA typically potentiated the amplitude of the evoked response in both the CA1 and CA3 regions of the hippocampus (Fig. 4). However, the potentiation was very modest and differences did not reach statistical significance: the mean response was potentiated to 110 ± 9.5% (i.e., a 1.1-fold facilitation) in the CA1 and to 124 ± 17% in the CA3 ($p > 0.05$, paired t-test). High concentrations (1000 μM) of KYNA inhibited responses by up to 82%: the mean was 50 ± 13% in the CA1 and 34 ± 22% in the CA3. KYNA exerted similar dual effects on the fEPSP slope, with a mean increase of 100.5 ± 8.9% in the CA1 and 113 ± 7.5% in the CA3. A 1000 μM KYNA inhibited the response by up to 73%; the mean was 53 ± 8.1% in the CA1 and 15 ± 12% in the CA3. This potentiation occurred in 80% of experiments in the CA1 and 60% of experiments in the CA3, though the overall effect was not significant in either region. These results raised the possibility that under some conditions, KYNA positive modulation of native AMPA receptors could enhance synaptic transmission, although this effect varied widely. We hypothesized that the variability could be related to the expression of different AMPA receptor subunits, as well as the many KYNA receptor targets present in the hippocampal slice preparation that could induce confounding pre and postsynaptic alterations in fEPSPs.

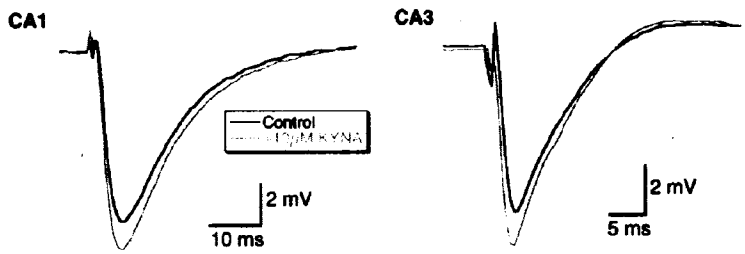

Fig. 4. Effect of kynurenic acid in the hippocampal slice preparation. Sample traces of fEPSP recordings from the CA1 and the CA3 areas of the hippocampus before (black lines) and during (grey lines) bath application of 10 μM KYNA.

We demonstrate a facilitation of AMPA receptor responses by low micromolar concentrations of kynurenate in a heterologous expression system. The molecular mechanism of the KYNA augmentation of currents is unclear. One formal possibility is that KYNA is competing for glutamate at the agonist-binding site, and when glutamate and KYNA together occupy binding sites on a common tetramer, the gating properties are changed (i.e., P_o increases), presumably by changing the agonist efficacy [10]. This explanation seems unlikely, given the fact that the affinity for KYNA at the agonist-binding site is much lower than for glutamate. Alternatively, KYNA may occupy a different, higher affinity site, and allosterically modulate receptor activity. One such site could be the previously identified binding site that lies at the interface between receptor subunits. The data with $GluR2S_{497}T$ are consistent with KYNA interacting at this site, as are the data from $GluR2oL_{483}Y$. At this binding site, KYNA may serve to destabilize the desensitized state, thus allowing KYNA-bound receptors to recover from desensitization and reopen, which would be seen as an increase in current amplitude. To directly determine if KYNA has an effect on desensitization, we measured the time constant of desensitization in the absence and presence of KYNA in transiently transfected HEK293 cells expressing recombinant GluR2, but found no statistically significant effect. Thus, because of the very modest facilitative action of KYNA, further experiments to pursue the molecular mechanism are not feasible.

A similar trend for low concentrations of KYNA to facilitate AMPA responses was seen in the slice preparation, although these results did not reach statistical significance. There are several possible explanations for the differences in results obtained from the oocyte and slice preparations: (1) the difference in the magnitude (100 μM in oocyte versus >1 mM in slice) of the glutamate exposure, (2) KYNA's effects on other receptors present in the slice preparation, including NMDA receptors and α-7 nicotinic acetylcholine receptors, (3) a difference between the AMPAR subunit composition in the two preparations, (4) differences in proteins that interact with the AMPAR such as stargazin, which can positively modulate the AMPA receptor and stargazin-like transmembrane AMPA receptor regulatory proteins that interact with the receptor in the two systems [24,18,5] and (5) the availability of endogenous KYNA in the hippocampus. If endogenous KYNA is sufficient to maximally modulate the AMPA receptor under normal conditions, then the modulatory effect of KYNA may only become apparent under conditions such as neuronal injury.

As far as we are aware, this is the first report that an endogenous antagonist can also act as a positive modulator through a distinct site. Our data with KYNA are consistent with actions of two synthetic antagonists, NBQX (2,3-dihydroxy-6-nitro-7-sulfamoyl-benzo(F)quinoxaline) and GYKI 52466 (1-(4-amino-phenyl)-4-methyl-7,8-methyl-endioxyl-5H-2,3-benzodiazepine). These antagonists were also found to have a dual effect on neuronal responses measured by fast perfusion, potentiating plateau responses at low concentrations and inhibiting peak responses at high concentrations, through an unknown mechanism [17,1]. The fact that an endogenous compound has dual effects on recombinant AMPA receptors leaves open the question as to whether endogenous ligands are meant to modulate AMPA receptor activity in vivo. Since much lower concentrations of KYNA are needed for facilitation than inhibition, we suggest that facilitation by KYNA of AMPA receptors may play a more significant role in vivo than does antagonism. Taken together, these findings suggest the possibility that there may be an in vivo role for KYNA acting at AMPA receptors, perhaps specific to the developing brain or to nervous tissue that has been injured and is being repaired. Although the in vivo significance of KYNA positive modulation of AMPA receptors remains to be determined, experimenters using very low doses of KYNA on cells containing AMPA receptors or in slice preparations (where the concentration of exogenously added KYNA cannot be well-controlled) should be cognizant of the dual effects of KYNA.

Acknowledgement

This work was supported by the National Institutes of Health and the American Heart Association (KMP).

References

[1] A.C. Arai, GYKI 52466 has positive modulatory effects on AMPA receptors, Brain Res. 892 (2001) 396–400.
[2] F.P. Bonina, L. Adenare, R. Ippolito, G. Boatto, G. Battaglia, V. Bruno, P. de Caprariis, Synthesis, pharmacokinetics and anticonvulsant activity of 7-chlorokynurenic acid prodrugs, Int. J. Pharmaceut. 202 (2000) 79–88.
[3] M.R. Domenici, S. Marinelli, S. Sagratella, Effects of felbamate, kynurenic acid derivatives and NMDA antagonists on in vitro kainate-induced epileptiform activity, Life Sci. 58 (26) (1996) 391–396.
[4] S. Erhardt, K. Blennow, C. Nordin, E. Skogh, L.H. Lindstrom, G. Engberg, Kynurenic acid levels are elevated in the cerebrospinal fluid of patients with schizophrenia, Neurosci. Lett. 313 (2001) 96–98.
[5] Y. Fukata, A.V. Tzingounis, J.C. Trinidad, M. Fukata, A.L. Burlingame, R.A. Nicoll, D.S. Bredt, Molecular constituents of neuronal AMPA receptors, J. Cell Biol. 169 (3) (2005) 399–404.
[6] G.I. Giles, C.A. Collins, T.W. Stone, C. Jacob, Electrochemical and in vitro evaluation of the redox-properties of kynurenine species, Biochem. Biophys. Res. Commun. 300 (2003) 719–724.
[7] G.J. Guillemin, S.J. Kerr, G.A. Smythe, D.G. Smith, V. Kapoor, P.J. Armati, J. Croitoru, B.J. Brew, Kynurenine pathway metabolism in human astrocytes: a paradox for neuronal protection, J. Neurochem. 78 (2001) 842–853.
[8] C. Hilmas, E.F.R. Pereira, M. Alkondon, A. Rassoulpour, R. Schwarcz, E.X. Albuquerque, The brain metabolite kynurenic acid inhibits α7 nicotinic receptor activity and increases non-α7 nicotinic receptor expression: physiopathological implications, J. Neurosci. 21 (2001) 7463–7473.
[9] S.Y. Ivanova, M.V. Storozhuk, I.V. Melnick, P.G. Kostyuk, Chronic treatment with ionotropic glutamate receptor antagonist kynurenate affects GABAergic synaptic transmission in rat hippocampal cell cultures, Neurosci. Lett. 341 (2003) 61–64.
[10] R. Jin, T.G. Banke, M.L. Mayer, S.F. Traynelis, E. Gouaux, Structural basis for partial agonist action at ionotropic glutamate receptors, Nat. Neurosci. 6 (8) (2003) 803–810.
[11] R. Jin, S. Clark, A.M. Weeks, J. Dudman, E. Gouaux, K.M. Partin, Mechanism of positive allosteric modulators acting on AMPA receptors, J. Neurosci. 25 (2005) 9027–9036.
[12] R.M. Kaminski, E. Zielinska, A. Dekundy, G. van Luijtelaar, W.A. Turski, Deficit of endogenous kynurenic acid in the frontal cortex of rats with a genetic form of absence epilepsy, Polish J. Pharmacol. 55 (2003) 741–746.

[13] C. Kiss, G. Ceresoli-Borroni, P. Guidetti, C.L. Zielke, H.R. Zielke, R. Schwarcz, Kynurenate production by human astrocytes, J. Neural Trans. 110 (2003) 1–14.
[14] J.D. Leever, S. Clark, A. Weeks, K.M. Partin, Identification of a site in GluR1 and GluR2 that is important for modulation of deactivation and desensitisation, Mol. Pharmacol. 64 (2003) 5–10.
[15] E. Luchowska, P. Luckowski, A. Sarnowska, M. Wielosz, W.A. Turski, E.M. Urbanska, Endogenous level of kynurenic acid and activities of kynurenine aminotransferases following transient global ischemia in the gerbil hippocampus, Polish J. Pharmacol. 55 (2003) 443–447.
[16] R. Meller, C.K. Schindler, X.P. Chu, Xiong Zg, J.A. Cameron, Simon Rp, D.C. Henshall, Seizure-like activity leads to the release of BAD from 14-3-3 protein and cell death in hippocampal neurons in vitro, Cell Death Differ. 10 (2003) 539–547.
[17] C.G. Parsons, R. Gruner, J. Rozenthal, Comparative patch clamp studies on the kinetics and selectivity of glutamate receptor antagonism by 2,3-dihydroxy-6-nitro-7-sulfamoyl-benzo(F)quinoxaline (NBQX) and 1-(4-amino-phenyl)-4-methyl-7,8-methyl-endioxyl-5H-2, 3-benzodiazepine (GYKI 52466), Neuropharmacology 33 (5) (1994) 589–604.
[18] A. Priel, A. Kolleker, G. Ayalon, M. Gillor, P. Osten, Y. Stern-Bach, Stargazin reduces desensitization and slows deactivation of the AMPA-type glutamate receptors, J. Neurosci. 25 (10) (2005) 2682–2686.
[19] H.E. Scharfman, J.H. Goodman, Effects of central and peripheral administration of kynurenic acid on hippocampal evoked responses in vivo and in vitro, Neuroscience 86 (3) (1998) 751–764.
[20] D.H. Smith, K. Okiyama, M.J. Thomas, T.K. McIntosh, Effects of the excitatory amino acid receptor antagonists kynurenate and indole-2-carboxylic acid on behavioral and neurochemical outcome following experimental brain injury, J. Neurosci. 13 (12) (1993) 5383–5392.
[21] Y. Stern-Bach, S. Russo, M. Neuman, C. Rosenmund, A point mutation in the glutamate binding site blocks desensitization of AMPA receptors, Neuron 21 (4) (1998) 907–918.
[22] T.W. Stone, Kynurenines in the CNS: from endogenous obscurity to therapeutic importance, Prog. Neurobiol. 64 (2001) 185–218.
[23] Y. Sun, R. Olson, M. Horning, N. Armstrong, M. Mayer, E. Gouaux, Mechanism of glutamate receptor desensitisation, Nature 417 (2002) 245–253.
[24] S. Tomita, H. Adesnik, M. Sekiguchi, W. Zhang, K. Wada, J.R. Howe, R.A. Nicoll, D.S. Bredt, Stargazin modulates AMPA receptor gating and trafficking by distinct domains, Nature 435 (23) (2005) 1052–1058.
[25] H. Wu, S. Lee, H.E. Scharfman, R. Schwarcz, L-4-chlorokynurenine attenuates kainate-induced seizures and lesions in the rat, Exp. Neurol. 177 (2002) 222–232.
[26] H. Wu, A. Rassoulpour, J.H. Goodman, H.E. Scharfman, E.H. Bertram, R. Schwarcz, Kynurenate and 7-chlorokynurenate formation in chronically epileptic rats, Epilepsia 46 (7) (2005) 1010–1016.
[27] H. Wu, R. Schwarcz, Seizure activity causes elevation of endogenous extracellular kynurenic acid in the rat brain, Brain Res. 39 (3) (1996) 155–162.

JBC Papers in Press. Published on June 22, 2006 as Manuscript M600679200
The latest version is at http://www.jbc.org/cgi/doi/10.1074/jbc.M600679200

DIFFERENT DOMAINS OF THE AMPA RECEPTOR DIRECT STARGAZIN-MEDIATED TRAFFICKING AND STARGAZIN-MEDIATED MODULATION OF KINETICS

Matthew A. Bedoukian, Autumn M. Weeks and Kathryn M. Partin
Dept. of Biomedical Sciences, Colorado State University, Fort Collins, CO 80521

Running Title: Interactions between stargazin and AMPA receptors

Address correspondence to: Kathryn M. Partin, Dept. of Biomedical Sciences, Div. of Neuroscience, Colorado State University, Fort Collins, CO 80523-1617. Tel.: 970-491-2263, Fax: 970-491-7907, E-mail: kpartin@lamar.colostate.edu

Stargazin is an accessory protein of AMPA receptors that enhances surface expression and also affects the biophysical properties of the receptor. AMPA receptor domains necessary for either of these two processes have not yet been identified. Here, we used confocal imaging and electrophysiology of heterologously expressed, fluorophore-tagged GluR1, GluR2 and stargazin to study surface expression and desensitization kinetics. Stargazin-mediated trafficking was sensitive to the nature of the AMPA receptor cytoplasmic domain. The insertion of YFP after residue 15 of the truncated cytoplasmic tail of GluR1i perturbed stargazin-mediated trafficking of the receptor but not its modulation of desensitization kinetics. This construct also failed to permit fluorescence resonance energy transfer (FRET) with stargazin in the ER, whereas FRET between fluorophore-tagged stargazin and non-truncated AMPA receptors demonstrated a specific interaction between these proteins, both in the ER and the plasma membrane. Rather than encoding a specific binding site, the fluorophore-tagged C-terminus may restrict access to one or more endoplasmic reticulum (ER) retention sites. Although perturbations of the C-terminus impeded stargazin-mediated trafficking to the plasma membrane, their effects on the biophysical properties of AMPA receptors (i.e., modulation of desensitization) remained intact. These data provide strong evidence that the AMPA receptor domains required for stargazin-modulation of gating and trafficking are separable.

INTRODUCTION

AMPA (-amino-3-hydroxy-5-methyl-isoxazole-4-propionate) receptors, a subtype of ionotropic glutamate receptors, are expressed at the postsynaptic membrane of neurons where they mediate rapid excitatory synaptic transmission (1-4). Native AMPA receptors are hetero-oligomers composed of four subunits (GluR1-4) that are either a flip (i) or flop (o) isorform (5). AMPA receptors play a critical role in neuronal signal transduction that is necessary for memory and learning. AMPA receptors cycle rapidly in and out of the plasma membrane in an activity-dependent manner (6-9) that requires assembly with auxiliary proteins such as stargazin (10).

Stargazin, also known as 2 or CACNG2, is a member of the transmembrane AMPA receptor regulatory protein (TARP) family (11-14). It was initially identified from the stargazer mouse, an inbred mouse strain with a phenotype of an unsteady gait, persistent head-raising ("star-gazing"), and frequent spike-wave discharges (12,15). Granule cells from the cerebellum of stargazer mice are missing functional AMPA receptors. A biochemical interaction between stargazin and both AMPA receptors and PSD-95 exists (16). The interaction between stargazin and AMPA receptors is essential for efficient delivery of receptors to the surface of cerebellar granule cells, whereas its interaction with PSD-95 is essential for clustering receptors to the postsynaptic membrane.

Stargazin enhances the total current of AMPA receptors, consistent with its ability to traffic more receptors to the plasma membrane

where current is measured (17-21). Recombinant AMPA receptors are poorly trafficked to the cell surface in the absence of stargazin and remain trapped in intracellular pools (22). Stargazin may facilitate AMPA receptor export from the ER (11) by masking ER retention signals of the tetrameric receptor in vivo (10). In addition to enhancing AMPA receptor trafficking, stargazin also slows AMPA receptor desensitization and deactivation (19-21) and increases the rate of channel opening (20). The domains of stargazin essential for modulating trafficking versus biophysical properties are partially separable. Stargazin is a four-pass transmembrane protein: the cytoplasmic C-terminal domain is required for receptor trafficking but the first extracellular domain controls stargazin's modulation of AMPA receptor biophysical properties (20,21). The stargazin extracellular domain may allosterically modulate the AMPA receptor's extracellular ligand-binding core, altering AMPA receptor subunit interactions (14). Single-particle electron microscopy indicates that stargazin associates primarily with the AMPA receptor transmembrane domains (23,24). However, there is little information about AMPA receptor domains involved in stargazin-mediated trafficking or modulation.

The present study uses functional deletions of AMPA receptors to identify domains necessary for effective trafficking and modulation of desensitization by stargazin. Because the intracellular C-terminus of stargazin is necessary for targeting AMPA receptors, we hypothesized that an intracellular region of the AMPA receptor such as the C-terminus might directly interact with stargazin. Consistent with this idea, the C-termini of AMPA receptors are known to bind a number of different proteins that effect trafficking and the stabilization of the channel at synapses (**Figure S1**). Our data suggest that stargazin requires access to a cytoplasmic binding site for effective trafficking to the surface membrane but does not require this same interaction for modulation of desensitization.

METHODS

Transient transfections for electrophysiology. Human embryonic kidney 293 (HEK 293) fibroblasts (CRL 1573; American Type Culture Collection, Rockville, MD) were cultured as described previously (25). Cells were transiently transfected using FuGene 6 reagent (Roche Products, Indianapolis, IN) or Lipofectamine 2000 (Invitrogen, Carlsbad, CA) with AMPA receptor cDNA (0.5–2 g/35 mm dish) and if channel was not tagged, soluble yellow fluorescent protein cDNA (0.1– 0.15 g/35 mm dish). When used, stargazin was always added in a 1:2 stargazin ratio (with total amounts of cDNA transfected ranging from 0.1-3 g). After transfection, 10-40 M NBQX was added to the media to prevent cell toxicity.

Transfections for confocal microscopy. Collagen or poly-d-lysine coated 14 mm glass bottom culture dishes (MatTek Corporation, Ashland, MA) were incubated with ECL Attachment Matrix (Upstate Cell Signaling Solutions, Lake Placid, NY) for 1hr at 37°C then washed with cMEM before plating cells. Cells were transfected using Lipofectamine 2000 (Invitrogen, Carlsbad, CA) when 60-90% confluent and incubated under identical conditions as cells used for standard electrophysiology. For each transfection 70 l of MEM was incubated with 3 l of Lipofectamine and in another tube 30 l of MEM was incubated with 0.1 to 3 g of total cDNA and thoroughly mixed. Contents of the tubes were combined, and after 20-30 minutes the solution was added to the cells along with 0-10 M NBQX. 4.5-24 hours later, the solution was exchanged with fresh cMEM with 20-40 M NBQX. All cells were imaged at room temperature 2-3 days after transfection. Immediately before imaging the solution was exchanged with cMEM containing no phenol red.

Outside-out patch recordings. Currents were recorded 2–3 days after transfection, as described previously (25). Extracellular solutions (ECS) contained the following: 20 mM sucrose, 145 mM NaCl, 5.4 mM KCl, 5 mM HEPES, 1 mM $MgCl_2$, 1.8 mM $CaCl_2 \cdot H_2O$, and 0.01 mg/ml phenol red, pH 7.3. Outside-out membrane patches were voltage clamped at -60 mV using an Axopatch 200B amplifier (Molecular Devices, Union City, CA). Synapse

(version 3.6d; Synergy Research, Silver Spring, MD) controlled piezoelectric movement, data acquisition, and trace analysis. Responses were filtered at 5 kHz, digitized at 10–500 s/point, and stored on a Power Macintosh computer (Apple Computers, Cupertino, CA) using an ITC-16 interface (InstruTech, Port Washington, NY). Micropipettes (TW150F; 2–5 M ; World Precision Instruments, Sarasota, FL) contained the following (in mM): 135 CsCl, 10 CsF, 10 HEPES, 5 Cs-BAPTA, 1 $MgCl_2$, and 0.5 $CaCl_2$, pH 7.2 (292 mOsm). Patches were perfused at 0.2 ml/min with solutions emitted from a two-barrel flow pipe made with tubing (BT150–10; Sutter Instruments, Novato, CA). One barrel contained vehicle (control) composed of the following: 145 mM NaCl, 5.4 mM KCl, 5 mM HEPES, 1 mM $MgCl_2$, 1.8 mM $CaCl_2 \cdot H_2O$, with 0.01 mg/ml phenol red, pH7.3. The other barrel had this solution plus L-glutamate (10 mM). After going into voltage clamp, an outside-out patch was pulled, lifted up to the flow pipe, positioned near the interface between the glutamate-free and glutamate-containing solution and jumped rapidly from the vehicle control into glutamate. Rapid solution exchanges of 1 or 500 ms were driven by a piezoelectric device (Burleigh Instruments, Fishers, NY). Solution exchange rates were determined at the end of each experiment by open-tip junction currents and excluded if rise times exceeded 0.5 ms.

Analysis of rapid responses. Desensitization rates were estimated by fitting a single-exponential function ($_{des}$) to the 500 ms response decay (from 95% of peak to steady state). Deactivation rates were estimated by fitting a single-exponential function ($_{deact}$) to the 1 ms response decay (from 95% of peak to steady state). Three to 20 responses per patch were averaged for analysis. Current traces and graphs were plotted using KaleidaGraph 3.5 (Synergy Software, Reading, PA).

Generation of constructs. The CMV expression plasmids (pRK) for GluR1, GluR2 ($R_{607}Q$) and GluR6 ($R_{621}Q$) were provided by Dr. Peter Seeburg (Max Planck Institute for Medical Research, Heidelberg, Germany). $R1_{81}$YFP was generated using overlapping PCR to make an in-frame fusion protein with CFP or YFP, using pECFP or pEYFP (Clontech, Palo Alto, CA) as templates. The first residue from the fluorescent protein followed immediately after the last amino acid in the sequence ATGL. $R1_{46}$YFP was made by inserting the restriction site MluI (ACGCGT) between amino acids GGG and SGE of the C-terminal domain using QuikChange II XL Site-Directed Mutagenesis Kit (Stratagene, La Jolla, CA). The final sequence at the fusion was GGGTR(YFP). $R1_{36}$YFP, $R1_{15}$YFP, $R1_7$YFP, $R1_2$YFP, $R2_{46}$YFP, and $R2_{16}$YFP were generated similarly (see **Figure S1** for the locations of insertion sites). All point mutations were made using the QuikChange II XL Site-Directed Mutagenesis Kit as was the insertion of a stop codon for $R1i_{14}$ after amino acids KRMK of the cytoplasmic tail. The insertion sequence of the $R1i_{15+38}$YFP, $R1i_{7+38}$YFP, and $R1i_{2+38}$YFP constructs had a 38 amino acid linker before fluorophore attachment with the sequence: TRGGSEQKLISEEDLSQFRVSPLDRTWNLG ETVELKTR. GluR2i and GluR2o ATD were constructed to delete 380 amino acids of the mature protein. The N-terminus thus began with LPS preceded by the Kozak sequence (ACC) and the GluR6 signal sequence. Stargazin constructs: StgEGFP/Gw1-CMV plasmid (British Biotechnology; (26)) was a generous gift from Dr. David Bredt (UCSF, San Francisco), as was pcDNA3-stg. StgCFP and stgYFP were inserted in frame at the BglII site in pcDNA3 (Stratagene) homologous to stgGFP but truncated after amino acid 269. GluR4i ATD and FLAG-GluR4i were kind gifts from Dr. Kari Keinanen (University of Helsinki; Helsinki, Finland; (27)) FLAG-GluR4i CTD was made by inserting a stop codon after EF, the first two amino acids of the cytoplasmic tail. Kv2.1 was a kind gift from Dr. Michael Tamkun (Colorado State University; Fort Collins, CO; (28)). The CD8 plasmid (MGC-34614) was purchased from American Type Culture Collection (Rockville, MD) and CD3CFP was a generous gift from Dr. Nicholas Gascoigne (The Scripps Research Institute; La Jolla, California (29)).

TABLE 1

Loss of modulation of GluR1(S493T) by CTZ and CX546

Loss of modulation by both CX546 and CTZ occurs when mutations are made at either position 493 (this article) or position 750 (this article and Partin et al., 1996) in GluR1. Values represent mean ± S.E.M.; n = 5 to 14 oocytes, but most data points represent n = 8. Hill values are given in parentheses below the value for EC_{50}.

	CTZ		CX546		Glutamate
	EC_{50}	Potentiation (300 μM CTZ) $I_{GLU+CTZ}/I_{GLU}$	EC_{50}	Potentiation (1500 μM CX546) $I_{GLU+CX546}/I_{GLU}$	EC_{50}
	μM		μM		μM
WT GluR1i	58.0 ± 1.9 (2.2)	39.6 ± 7.2	503 ± 73 (1.6)	18.5 ± 4.9	27.1 ± 8.9
GluR1i(S493T)	N.D.	17.9 ± 5.2	N.D.	1.1 ± 0.5	21.9 ± 7.3
WT GluR1o	237 ± 104 (0.9)	8.7 ± 1.7	595 ± 315 (1.0)	16.3 ± 1.7	11.1 ± 7.4
GluR1o(S493T)	N.D.	1.8 ± 0.1	N.D.	0.7 ± 0.1	28.3 ± 11.8
GluR1o(S750Q)	N.D.	1.0 ± 0.1[a]	N.D.	1.8 ± 0.2	N.D.

N.D., not determined (i.e., data could not be fit reliably with logistic equation because of small current amplitudes).
[a] Data from Partin et al. (1996).

mutation had a similar effect on both GluR1i and GluR1o receptors, reducing the level of maximal potentiation to 18- and 2-fold, respectively (Fig. 1B). These data indicate that mutation of Ser493 in either the flip or flop isoform of GluR1 has a deleterious effect on allosteric modulation by CTZ. This finding is consistent with the structural data for the S1/S2 domain complexed with both agonist and CTZ (Sun et al., 2002).

To test the hypothesis that the mutation affecting CTZ modulation would also affect CX546 modulation, similar analyses on WT and mutant GluR1i and GluR1o receptors were performed (Table 1). There was no difference in apparent affinity of CX546 for GluR1o (EC_{50} = 595 μM) versus GluR1i (EC_{50} = 503 μM), and the responses were potentiated to a similar extent (Fig. 1A). For both splice isoforms, the Ser493 mutation completely abolished potentiation by CX546. Thus, the Ser493 point mutation impaired modulation by both CX546 and CTZ, although these two drugs are believed to act through distinct mechanisms.

Previous experiments demonstrated that the AMPA receptor alternatively spliced flip/flop region was responsible for the differential sensitivity to CTZ and aniracetam (Partin et al., 1996). The differential sensitivity could be mapped to one critical residue, Ser750 (or Asn750 in the flop isoform) and, in fact, modulation could be abolished with the mutation GluR1(S750Q). Because CX546 is structurally related to aniracetam, one might predict that modulation by CX546 would be impaired by mutation of Ser750. Indeed, Table 1 shows that modulation of GluR1o(S750Q) by CX546 is reduced to 1.8-fold. Thus, there is a significant loss of modulation by both CX546 and CTZ upon mutation of both Ser493 and Ser750.

The loss of modulation by the Ser493 mutation could be a secondary consequence of a reduction in agonist affinity. To test this idea, glutamate dose-response analyses were performed on WT and mutant GluR1i and GluR1o receptors. The Ser493 mutation did not significantly change the apparent affinity of glutamate (Table 1). The EC_{50} for WT GluR1i was 27 μM and 22 μM for GluR1i(S493T); for WT GluR1o, the EC_{50} was 11 μM and 28 μM for the mutation. In addition, the mutation did not significantly change the efficacy of glutamate, because the mean peak current for WT GluR1i in 1000 μM glutamate was 414 ± 60 nA (n = 20) versus 569 ± 72 nA (n = 16) for GluR1i(S493T) (p = 0.10). Thus, the Ser493 mutation impairs modulation by CTZ and CX546, similar to the effects of the GluR1o(S750Q) mutation (Table 1), which impairs modulation by CTZ and aniracetam (Partin et al., 1996), without affecting inherent agonist affinity.

TABLE 2

Modulation of AMPA subunits by CX546

CX546 modulates the glutamate-evoked currents of the flop (o) isoform of all AMPA subunits. Values reported are the fit of the data from dose-response analysis using 1 to 1500 μM CX546, with n = 8 oocytes per determination. The left column shows the mean EC_{50}; given the limited solubility of CX546, these values may represent a lower estimate of the actual value (see also Nagarajan et al., 2001). Right column shows the mean potentiation of the current evoked by 300 μM glutamate and 1500 μM CX546.

	EC_{50} CX546	1500 μM CX546 $I_{GLU+CX546}/I_{GLU}$
	μM	
GluR1o	595 ± 315 (1.0)	24.7 ± 5.5
GluR2o (R607Q)	176 ± 26 (1.6)	9.9 ± 0.5
GluR3o	554 ± 159 (2.4)	30.9 ± 5.3
GluR4o	681 ± 566 (1.3)	8.8 ± 3.5

Modulation of All AMPA Receptor Subtypes by CX546. A dose-response analysis was used to test the efficacy of CX546 modulation on different AMPA receptor subtypes (Table 2). For these experiments, the flop splice isoform was used. Responses from GluR1 to -4 receptors were potentiated by CX546. There were 2- to 3-fold differences in the apparent affinities (EC_{50} values ranged from 176 to 681 μM) and 3-fold differences in the efficacy (maximal potentiation ranged from 10- to 31-fold) of CX546. Thus, CX546 positively modulates the flop isoform of all AMPA receptors. To interpret the electrophysiological experiments in light of the published crystal structural data of GluR2, we next performed kinetic experiments using GluR2o.

Kinetic Analysis of GluR2o(S497T). Nagarajan et al. (2001) have shown previously that CX546 modulation of "$GluR2i_Q$" caused a small but significant increase of the time constant of deactivation. In Fig. 2A, a similar result is shown for GluR2o, as assayed in outside-out patches of transiently transfected HEK293 cells, using ultrafast solution perfusion. CX546 slowed deactivation (i.e., increased τ_{deact}) from 0.71 ± 0.05 to 1.10 ± 0.08 ms (p = 0.001) (Fig. $2C_1$) without significantly changing τ_{des} (Fig. $2C_2$). In addition, CX546 significantly increased the ratio of steady-state to peak current from 0.06 ± 0.03 to 0.43 ± 0.04 ($p < 0.001$) (Fig. 2, A_2 and C_2). This modulation most likely arises as an indirect effect of CX546, which alters equilibrium desensitization by slowing channel deactivation rather than directly affecting the rate of desensitization (Partin et al., 1996; Arai et al., 2002b). The fact that CX546 did not alter τ_{des} may reflect that our experiments were performed in subsaturating concentrations of CX546 (300 μM). When we performed pilot experiments at a higher concentration of CX546 (1000 μM), the steady-state/peak ratio increased to near unity (S. Clark and K. M. Partin, unpublished observations).

absence of stargazin. However, these receptors could form fluorescent membrane surface rings when co-expressed with stargazin. No decrease in the frequency of surface rings or differences in the ratio of membrane to cytosolic intensity were found for these truncated proteins compared with the wild type C-terminus. However, a third fusion protein that deleted all but the first 15 amino acids of the C-terminus, $R1i_{15}$YFP, resulted in a receptor that never formed surface rings (10 independent transfections with >1000 counted fluorescent cells). Rings also did not form when $R1i_{15}$YFP was co-expressed with stgCFP (**Figure 2b**). Rings were not seen even at a 1:8 stargazin ratio.

The homologous deletion made in GluR2 ($R2i_{16}$) tagged with CFP or YFP was also tested for stargazin-mediated trafficking. Similar to $R1i_{15}$YFP, the expression of this protein was cytosolic in either the absence or presence of stargazin. In contrast, the C-terminal deletion mutation $R2i_{46}$YFP also formed surface expression rings (**Figure 4a**). Thus, the cytoplasmic requirements for trafficking of GluR1 or GluR2 by stargazin appear to be similar. All flop isoforms tested followed the same trend.

3. The intracellular interaction necessary for effective stargazin-mediated trafficking is not necessary for stargazin-mediated modulation of desensitization.

The inability of stargazin to traffic $R1_{15}$YFP or $R2_{16}$YFP to the surface membrane suggests that stargazin cannot interact with these proteins. To determine whether trunctions that impair trafficking also impair modulation of AMPA receptor function, we examined the electrophysiological properties of the mutated receptors. Outside-out patches of cells transfected with the C-terminal trunctions, $R1i_{15}$YFP or $R1i_{36}$YFP, demonstrated no significant difference in stargazin-mediated slowing of desensitization compared to the non-truncated $R1i_{81}$YFP (**Figure 2c, 2e**). Stargazin slowed the kinetics of $R1i_{81}$YFP from 3.2±0.1 to 5.8±0.7 ms, $R1i_{36}$YFP from 3.4±0.5 to 4.8±0.3 ms, and $R1i_{15}$YFP from 2.9±0.1 to 5.8±0.3 ms. It is important to note that cells with surface expression rings were not selected for in these experiments and are not paired with the data used for **Figure 1**.

As expected if the formation of surface expression (and reduced ER retention) is related to overall current density, $R1i_{15}$YFP showed only a two-fold increase in current amplitude when co-expressed with stargazin (370±113 vs. 733±175 pA), whereas both $R1i_{81}$YFP (198±69 vs, 694±301 pA) and $R1i_{36}$YFP (172±82 vs, 630±140 pA) showed a ~3.5-fold increase in current amplitude (**Figure 2d**). $R1i_{14}$, which lacked a fluorophore and had one less amino acid than $R1i_{15}$YFP, produced currents that were significantly smaller 30±3 pA, but when co-transfected with stargazin the mean current increased ~11–fold to 364±118 pA. Together, the data presented in Figures 1 and 2 suggest that the domains of AMPA receptors necessary for trafficking of or modulation by stargazin are separable.

4. The cytoplasmic tail of AMPA receptors does not contain a specific stargazin-binding site.

Stargazin did not traffic $R1_{15}$YFP to the surface. To determine if this was due to steric hindrance when the fluorophore was attached immediately after residue 15, we inserted a 38 amino acid linker between the last AMPA receptor residue of $R1i_{15}$YFP and the fluorophore ($R1i_{15+38}$YFP). Co-transfection of $R1i_{15+38}$YFP with stargazin permitted ring formation, demonstrating that no more than 15 amino acids of the cytoplasmic tail of AMPA receptors were necessary for stargazin mediated trafficking. To determine if there is a specific interaction between stargazin and any of the residues within the conserved proximal 14 amino acids in the tail of AMPA receptors, a series of point mutations was constructed. These mutations either disrupt a known protein-interacting site (**Figure S1**) or replace critical differences in the proximal cytoplasmic tail between AMPA receptors and GluR6 (**Figure 3a**), which does not associate with stargazin (18). All point mutants were constructed within $R1i_{81}$YFP or $R1i_{36}$YFP. Each of these mutant receptors permitted stargazin-mediated surface expression rings (**Figure 3a**) suggesting that specific C-terminal residues are not necessary for stargazin trafficking. Because previous

absence of stargazin. However, these receptors could form fluorescent membrane surface rings when co-expressed with stargazin. No decrease in the frequency of surface rings or differences in the ratio of membrane to cytosolic intensity were found for these truncated proteins compared with the wild type C-terminus. However, a third fusion protein that deleted all but the first 15 amino acids of the C-terminus, $R1i_{15}$YFP, resulted in a receptor that never formed surface rings (10 independent transfections with >1000 counted fluorescent cells). Rings also did not form when $R1i_{15}$YFP was co-expressed with stgCFP (**Figure 2b**). Rings were not seen even at a 1:8 stargazin ratio.

The homologous deletion made in GluR2 ($R2i_{16}$) tagged with CFP or YFP was also tested for stargazin-mediated trafficking. Similar to $R1i_{15}$YFP, the expression of this protein was cytosolic in either the absence or presence of stargazin. In contrast, the C-terminal deletion mutation $R2i_{46}$YFP also formed surface expression rings (**Figure 4a**). Thus, the cytoplasmic requirements for trafficking of GluR1 or GluR2 by stargazin appear to be similar. All flop isoforms tested followed the same trend.

3. The intracellular interaction necessary for effective stargazin-mediated trafficking is not necessary for stargazin-mediated modulation of desensitization.

The inability of stargazin to traffic $R1_{15}$YFP or $R2_{16}$YFP to the surface membrane suggests that stargazin cannot interact with these proteins. To determine whether trunctions that impair trafficking also impair modulation of AMPA receptor function, we examined the electrophysiological properties of the mutated receptors. Outside-out patches of cells transfected with the C-terminal trunctions, $R1i_{15}$YFP or $R1i_{36}$YFP, demonstrated no significant difference in stargazin-mediated slowing of desensitization compared to the non-truncated $R1i_{81}$YFP (**Figure 2c, 2e**). Stargazin slowed the kinetics of $R1i_{81}$YFP from 3.2±0.1 to 5.8±0.7 ms, $R1i_{36}$YFP from 3.4±0.5 to 4.8±0.3 ms, and $R1i_{15}$YFP from 2.9±0.1 to 5.8±0.3 ms. It is important to note that cells with surface expression rings were not selected for in these experiments and are not paired with the data used for **Figure 1**.

As expected if the formation of surface expression (and reduced ER retention) is related to overall current density, $R1i_{15}$YFP showed only a two-fold increase in current amplitude when co-expressed with stargazin (370±113 vs. 733±175 pA), whereas both $R1i_{81}$YFP (198±69 vs, 694±301 pA) and $R1i_{36}$YFP (172±82 vs, 630±140 pA) showed a ~3.5-fold increase in current amplitude (**Figure 2d**). $R1i_{14}$, which lacked a fluorophore and had one less amino acid than $R1i_{15}$YFP, produced currents that were significantly smaller 30±3 pA, but when co-transfected with stargazin the mean current increased ~11–fold to 364±118 pA. Together, the data presented in Figures 1 and 2 suggest that the domains of AMPA receptors necessary for trafficking of or modulation by stargazin are separable.

4. The cytoplasmic tail of AMPA receptors does not contain a specific stargazin-binding site.

Stargazin did not traffic $R1_{15}$YFP to the surface. To determine if this was due to steric hindrance when the fluorophore was attached immediately after residue 15, we inserted a 38 amino acid linker between the last AMPA receptor residue of $R1i_{15}$YFP and the fluorophore ($R1i_{15+38}$YFP). Co-transfection of $R1i_{15+38}$YFP with stargazin permitted ring formation, demonstrating that no more than 15 amino acids of the cytoplasmic tail of AMPA receptors were necessary for stargazin mediated trafficking. To determine if there is a specific interaction between stargazin and any of the residues within the conserved proximal 14 amino acids in the tail of AMPA receptors, a series of point mutations was constructed. These mutations either disrupt a known protein-interacting site (**Figure S1**) or replace critical differences in the proximal cytoplasmic tail between AMPA receptors and GluR6 (**Figure 3a**), which does not associate with stargazin (18). All point mutants were constructed within $R1i_{81}$YFP or $R1i_{36}$YFP. Each of these mutant receptors permitted stargazin-mediated surface expression rings (**Figure 3a**) suggesting that specific C-terminal residues are not necessary for stargazin trafficking. Because previous

studies have shown that an AMPA receptor without a C-terminus has virtually no surface expression (32), we constructed an extreme C-terminal truncation, $R1i_2$YFP as a negative control. As expected, $R1i_2$YFP did not form surface expression rings either in the absence or presence of stargazin. However, when the same 38 amino acid linker was added between the receptor and the fluorophore ($R1i_{2+38}$YFP), surface expression rings formed for a small number of cells (<1%) co-transfected with stargazin (**Table 1**). The failure to see more surface expression rings may be due to the already diminished surface expression that results from this impaired receptor.

The experiments with fluorophore-tagged receptor mutants led us to question whether the cytoplasmic tail of AMPA receptors contains a specific stargazin-binding site or whether the tail can in some cases interfere with another stargazin-binding site present at the cytoplasmic face of the receptor. To demonstrate that stargazin does not require specific determinants on the cytoplasmic tail, we used another assay for surface expression, namely immunofluorescence of unpermeabilized cells transfected with an extracellularly FLAG-tagged receptor. FLAG-$R4i_2$ (with only the first 2 amino acids of the cytoplasmic tail of GluR4i (32)) was co-transfected with stargazin. Although surface expression levels of this construct without stargazin were almost undetectable, stargazin did increase the surface expression (**Figure 3b**) but not to the levels of full-length FLAG-R4i (with or without stargazin). This experiment verified through an independent method that nearly all of the C-terminus is dispensable for stargazin-mediated trafficking of AMPA receptors, as long as there is no fluorophore attached.

5. Mutations of ER retention signal residues enhance trafficking without and with stargazin.

Stargazin may enhance AMPA receptor trafficking by masking an ER retention signal (10). Although we found that stargazin could enhance the surface expression of both the $R4i_2$ and $R1i_{2+38}$YFP constructs, the fact that stargazin did not fully rescue surface expression is likely due to the importance of the proximal cytoplasmic tail residues for AMPA receptor expression. To rule out that this lack of complete rescue was not due to an impaired ability of stargazin association with specific residues of the cytoplasmic tail, we tested $R1i_{7+38}$YFP (with the third of seven amino acids being Leu instead of Cys, so all seven residues would be identical to the first seven amino acids of the untraffickable GluR6 tail) (**Figure 3a**). This construct has the 38 amino acid linker between the seventh amino acid and the fluorophore. Although this receptor should not interact with protein 4.1, shown to be important for AMPA receptor surface expression (32,33), in one experiment we found that 28% of all fluorescent cells had pronounced stargazin-mediated surface expression rings, comparable to "wild type" $R1i_{81}$YFP. In addition, residues 4-6 of the cytoplasmic tail (implicated in ER retention (34)) were mutated from YKS to FQA (**Figure 3a**), using $R1i_{81}$YFP as a template. Even without stargazin, surface expression rings were formed in ~2% of the cells, something we had never observed for $R1i_{81}$YFP. Additionally, 36% of fluorescent cells formed stargazin-mediated surface expression rings (**Table 1**).

Since stargazin may increase surface expression by blocking an intracellular ER retention signal in the pore, we tested $R2_{46}$YFP (R_{607}). Wild type GluR2 contains a residue that undergoes RNA editing, converting the glutamine for an arginine in the pore region (35). This channel would be expected to be retained largely in the ER (34), have difficulty forming tetramers (36), and presumably not get to the surface membrane even with stargazin unless stargazin could somehow block the ER retention signal. The number of cells co-transfected with stargazin and $R2_{46}$YFP that had rings was about the same regardless of whether residue 607 was an R or a Q (**Table 1**). Together, these data suggest that stargazin occludes one or more ER retention signals at the cytoplasmic face of the receptor.

6. Stargazin mediates trafficking of AMPA receptor N-terminal deletions with isoform *differences related to differential protein* stability.

The amino-terminal domain (ATD) of glutamate receptors has been implicated in assembly, trafficking and allosteric modulation (37-39). To test whether or not the ATD plays a role in stargazin-mediated trafficking or modulation of the biophysical properties of AMPA receptors, the flip and flop isoforms of GluR2 (R2i and R2o) lacking the ATD, similar to R4i $_{ATD}$ (27), were made.

R2o $_{ATD}$ and R2i $_{ATD}$ were tagged with YFP at the C-terminus, after amino acid 46 of the cytoplasmic tail (R2o $_{ATD46}$YFP, R2i $_{ATD46}$YFP). Without stargazin, these proteins demonstrated a cytosolic expression pattern, and with stargazin, R2o $_{ATD46}$YFP formed pronounced surface expression rings (**Figure 4b**). In contrast to R2o $_{ATD46}$YFP, R2i $_{ATD46}$YFP did not form surface expression rings. A large number of cells expressing R2o $_{ATD46}$YFP or R2i $_{ATD46}$YFP formed aggresomes (40) with or without stargazin (**Table 2**), but this was most pronounced for R2i $_{ATD46}$YFP with stargazin (**Figure 4b and 4d**). All R1 and R2 fluorescently tagged, C-terminal deletions with an intact ATD, however, were virtually free of aggresomes regardless of the length of the C-terminal tail (with the exception of GluR2 R_{607}, but not $R_{607}Q$). Differential aggresomal accumulation in the flip isoform may account for the inability of R2i $_{ATD46}$YFP to permit efficient stargazin-mediated surface expression. Aggresome formation may also explain the reduction in current amplitude seen for R2i $_{ATD}$ (382±129 vs. 166±67 pA with stargazin) as well as R4i $_{ATD}$ (166±43 vs. 23±4 pA with stargazin, $p<.01$). Consistent with this interpretation, stargazin increased the current amplitude of R2o $_{ATD46}$YFP (41±17 vs. 597±146 pA with stargazin).

7. The ATD is not necessary for stargazin modulation of AMPA receptor kinetics.

Whereas previous studies using R4i $_{ATD}$ showed only a modest change in desensitization from wild type R4i (32), R2i $_{ATD}$ desensitization kinetics ($_{des}$=13.7±0.6 ms) were much slower than wild type R2i ($_{des}$=6.9±0.5 ms). $_{des}$ for R2o $_{ATD46}$YFP was 2.9±0.3 vs. 1.4±0.1 ms for wild type R2o. Stargazin also modulated desensitization of R4i $_{ATD}$ ($_{des}$=5.6±0.4 vs. 8.4±0.7 ms with stargazin) and R2i $_{ATD}$ ($_{des}$=13.7±0.6 vs. 32.3±4.1 ms with stargazin) (**Figure 4c**). In contrast, the effects of stargazin on modulation of R2o $_{ATD46}$YFP were more modest ($_{des}$=2.9±0.3 vs. 4.1±0.9 ms with stargazin). This flip/flop difference has been previously reported for full length GluR2 (21) and suggests that the ATD does not play a significant role in stargazin-mediated modulation of desensitization.

We next looked at deactivation kinetics and found no detectable slowing of deactivation for R2i $_{ATD}$ ($_{deact}$=1.9±0.6 vs. 1.4±0.3 ms with stargazin), or for R2o $_{ATD46}$YFP (1.8±0.3 vs. 2.4±0.8 ms with stargazin). The rate of deactivation, however, was slower without an ATD for both R2i $_{ATD}$ ($_{deact}$=1.9±0.6 ms compared to wt R2i = 0.9±0.1 ms (41) and R2o $_{ATD46}$YFP ($_{deact}$ = 1.8±0.3 vs. 0.7±0.1 ms for wild type R2o).

8. Fluorescence resonance energy transfer (FRET) suggests stargazin self-assembly.

Our results from the amino- and carboxyl-termini deletions strongly suggest that stargazin acts upon an AMPA receptor intracellular site to direct trafficking to the surface. Whereas biochemical methods such as "pull-down assays" would not distinguish between a direct protein-protein interaction or participation in a protein complex, FRET between fluorophores on two proteins is strong evidence for a tight (100 Å) intermolecular interaction. Therefore, we studied the interaction using FRET between the fluorophore-tagged GluR1 and stargazin proteins. Initially, we measured the ability of stargazin molecules to undergo FRET in the absence of receptor. Varying ratios and total concentrations of stgCFP and stgYFP were transfected, and FRET in the membrane was measured using a photobleaching protocol (**Figure 5a and 5c**). At all DNA concentrations and ratios tested, FRET between two stargazin molecules (7.8-16.2% efficiency) was significantly greater than a membrane control, Kv2.1CFP: $R1i_{81}$YFP: stargazin at a 1:2:2 ratio (0.2±0.1% FRET

efficiency, p<.005). Due to the profound stargazin-stargazin membrane fluorescence compared to that of cells co-transfected with fluorescent AMPA receptors and stargazin (see below), it was necessary to rule out that FRET occurred from overcrowding of the plasma membrane.

Yellow-green fluorescent beads were used to estimate how much stargazin protein was in the membrane (31). A confocal image of stgGFP-transfected cells is shown in **Figure 5b**, with a fluorescent bead in a different dish taken at an identical setting. Analysis of the comparative intensity of the bead and the cell (see figure legend) suggests that the membrane density of stargazin was ~820 molecules per m^2, and therefore overcrowding by fluorophore-tagged stargazin could not explain the FRET data shown in **Figure 5c**, unless certain regions of the membrane have greatly increased protein density. These data are consistent with an interpretation that stargazin:stargazin FRET arises from specific homo-oligomerization rather than nonspecific membrane crowding.

9. FRET occurs between stargazin and GluR1.

To determine whether stargazin and AMPA receptors interact closely enough to permit energy transfer that can be measured by FRET, we used a competition assay. The first goal was to determine whether the stargazin complex known to FRET (stgCFP:stgYFP) could be disrupted by co-expression with a non-fluorescent AMPA receptor. The FRET efficiency of a 1:1 ratio of stgCFP and stgYFP (0.2 g total cDNA) was 10.6±1.4%, which was competed by over-expressing R1i (2 g of cDNA), reducing the FRET efficiency to 3.9±1.1%, p=.003 (**Figure 6a** and **6c**). However, neither 2.0 g of cDNA encoding CD8 (11.8±2.6%), Kv2.1 (8.0±0.9%) nor R6 (8.5±1.6%) significantly decreased membrane FRET (**Figure 6a**). A dose-dependency of R1i competition was determined, in that concentrations of 0.5, 1.0 and 2.0 g cDNA significantly reduced membrane FRET efficiency from the basal level of 16.2±2.8% to 7.7±1.4, 9.1±1.6, and 5.8±1.1%, respectively (**Figure 6b** and **6d**). The reduction of FRET between stargazin molecules suggests that when there is an excess amount of R1i, but not other membrane proteins, the stargazin homo-oligomer population declines.

Based upon the mutational analysis of the C-terminus of GluR1, one would predict that co-expression of $R1i_{81}$CFP with stgYFP would permit FRET, whereas co-expression of $R1i_{15}$CFP with stgYFP would not. Indeed, $R1i_{81}$CFP:stgYFP produced robust FRET (20.2±2.1%) in the plasma membrane, but also produced FRET (7.6±1.0%) in the cytosolic, reticular network of cells with AMPA receptor rings (**Figure 6e**, left). However, cells that did not contain $R1i_{81}$CFP rings had a cytosolic FRET efficiency (3.4±1.0%) that was significantly lower and not significantly different than the negative soluble CFP and YFP control (2.4±0.5%). As predicted, co-expression of $R1i_{15}$CFP with stgYFP showed no membrane fluorescence (**Figure 6e**, right) and no significant FRET efficiency in the cytosol (4.1±1.0%).

As a putative negative control for membrane FRET, the T cell receptor CD3CFP (29) was co-expressed with stgYFP (0.3 g: 1 g stgYFP), but also showed robust membrane FRET efficiency (30.4±2.1%) that was competed to 15.4±2.0% by stargazin. Thus, we cannot rule out that the high expression levels of stargazin may contribute to some background FRET from overcrowding. The FRET between stargazin and both negative controls, CD3 and Kv2.1CFP (~20%), was much higher than would be expected of a negative control. Nevertheless, a control FRET experiment using Kv2.1CFP with excess $R1_{81}$YFP and non-fluorescent stargazin (to get $R1_{81}$YFP to the membrane) demonstrated ~0% membrane FRET efficiency.

10. AMPA receptor hetero-oligomerization can rescue C-terminal deletions with trafficking defects.

The previous experiments focused on AMPA receptor homo-oligomer trafficking by stargazin. Because our data support the idea that stargazin and AMPA receptors associate in the ER where subunit assembly is also occurring, we tested whether stargazin-mediated trafficking

requires access to each of the subunits in the tetrad. $R1_{15}$- and $R2_{16}$-tagged channels ("shorter" C-termini) that did not form surface expression rings with stargazin were co-transfected with both stargazin and an R1 or R2 channel that did form surface expression rings when co-transfected with stargazin ("medium" or "longer" C-termini). $R1i_{81}$YFP, $R1i_{46}$CFP, and $R1i_{36}$YFP could rescue $R1i_{15}$CFP trafficking (**Figure 7a**). $R1i_{46}$CFP was able to rescue $R2o_{16}$YFP as well as $R2o_{ATD16}$YFP, suggesting that stargazin does not need to bind all four subunits in a tetramer.

We further analyzed the data to asses the trafficking of subunits with different C-termini within a tetramer. Two channels that could be trafficked independently by stargazin had virtually the same membrane to cytosolic fluorescence intensity ratio, $(I_{membrane}/I_{cytosol})_A/(I_{membrane}/I_{cytosol})_B$, where A=$R1i_{46}$CFP and B=$R2o_{46}$YFP (.99±.06) or A=$R1i_{46}$YFP and B=$R1i_{81}$CFP (0.94±.06). In contrast, short channels co-expressed with long channels had significantly reduced membrane to cytosolic ratios compared to the long forms, for example, where A=$R2o_{16}$YFP and B= $R1i_{46}$CFP (0.78±.06); where A=$R1i_{15}$YFP and B=$R1i_{46}$CFP (0.77±.04); and, where A=$R1i_{15}$CFP and B=$R1i_{36}$YFP (0.71±.08) (**Figure 7b**).

Shorter forms are rescued to the point that they are only ~25% less effectively trafficked than the longer forms. This suggests that perhaps only 1 long form per tetramer is needed for stargazin mediated trafficking. We therefore compared the membrane FRET, in the presence of stargazin, between tetramers composed of short and medium length subunits, $R1i_{15}$ and $R1i_{46}$, at different ratios of co-expression (**Figure 7c**). As a control for differences in expression levels we compared the FRET between $R1i_{15}$CFP and $R1i_{46}$YFP (1:1; 0.5 CFP: 0.5 YFP: 2 stg) or (1:4; 0.2 CFP:0.8 YFP: 2 stg) and $R1i_{46}$CFP and $R1i_{15}$YFP (1:1) or (1:4) in the cytosol. We found equal FRET between both combinations of subunits at 1:1 (~7%) and 1:4 (~11%). As expected the FRET efficiency was greater at the 1CFP:4YFP ratio because more tetramers would be composed of excess YFP subunits. We next measured the FRET efficiency at the membrane for $R1i_{15}$CFP and $R1i_{46}$YFP at 1:4 (18.5±2.9%) to determine the maximum FRET efficiency and what value we could expect if stargazin was trafficking tetramers predominantly in a $1R1i_{15}$:$3R1i_{46}$ ratio. The membrane FRET efficiency of the 1:1 ratio (16.5±2.8%) was significantly greater than the 1:1 cytosolic ratio, but not different from the 1:4 cytosolic or membrane FRET. This suggests that the preferred heteromeric stoichiometry for stargazin mediated trafficking was $1R1i_{15}$: $3R1i_{46}$. In support of this conclusion, membrane FRET efficiency between $R1i_{46}$CFP and $R1i_{15}$YFP at 1:1 was significantly less (6.5±1.8%), and no greater than the cytosolic 1:1 ratio, suggesting that tetramers composed of fewer $R1i_{15}$YFP and more $R1i_{46}$CFP were preferentially trafficked.

As an attempt to rule out that other combinations of heteromeric receptors besides $1R1i_{15}$:$3R1i_{46}$ could not be trafficked by stargazin we looked at membrane FRET using a $1R1i_{46}$CFP:$4R1i_{15}$YFP ratio, to force the majority of tetramers with a CFP subunit into a $3R1i_{15}$:$1R1i_{46}$ ratio. The membrane FRET efficiency (13.3±1.6%) was significantly greater than the 1:1 membrane FRET efficiency ($p<.03$). This suggests that stargazin can traffic hetero-oligomers containing two short subunits, and does not rule out the possibility that stargazin may traffic tetramers containing a single long subunit.

DISCUSSION

In this study, we found that stargazin-mediated trafficking of GluR1 and GluR2 is hindered when CFP or YFP is inserted at the proximal cytoplasmic tail. We also determined that the first 380 amino acids of AMPA receptors (the ATD) are not necessary for stargazin trafficking but this domain has an important role in tetrameric stability of AMPA receptors. FRET analysis demonstrated that a homo-oligomeric population of stargazin exists in the plasma membrane, which could be specifically out-competed by GluR1 protein, but not by high concentrations of CD8, GluR6 or Kv2.1. AMPA receptors with traffickable C-termini interact with stargazin in a close association that permits FRET in both the plasma membrane and the ER network of

transfected cells.

The AMPA receptor-stargazin binding site. We propose that stargazin interacts with AMPA receptors via a binding site that is comprised of the AMPA receptor "domain 2" of the ligand-binding core (including the flip/flop region), the transmembrane domains, and the cytoplasmic face including access to the pore. An extracellular interaction with the flip/flop domain is consistent with single-particle electron microscopy experiments that show the primary interaction being near the transmembrane domains (23,24). Swapping experiments using -5 (an inactive, structurally similar protein to stargazin) suggest that only the second stargazin transmembrane domain is an important AMPA receptor contact, and was necessary for maintaining kainate responses (20). Consistent with our results, it was not a required domain for trafficking. Since our experiments suggest that the primary, specific, intracellular site of interaction with stargazin is not the C-terminus of AMPA receptors, other intracellular sites are implicated. The part of the cytoplasmic tail of stargazin that was found to be essential for AMPA receptor trafficking (up to residue 269, (26)) contains 16 basic residues (and 4 negative residues). Interestingly, the 26 amino acid intracellular domain after M1 of GluR1 contains 8 acidic residues (and 3 positive residues). This cytoplasmic region between M1 and the pore loop may contribute to the stargazin-AMPA receptor interaction necessary for trafficking receptors to the surface. A stargazin interaction with this site may explain how GluR2 R_{607} homo-oligomers, typically retained in the ER (34), can form surface expression rings when co-transfected with stargazin.

Our results are consistent with previous studies suggesting that the first extracellular domain of stargazin plays a role in AMPA receptor trafficking (21,26). The swap of -5 in this region still results in a stargazin hybrid that enhances AMPA receptor surface expression, though not as robustly (26). If there are at least two distinct sites of interaction between stargazin and AMPA receptors (one extracellular, and one intracellular) the removal of an extracellular interaction, though not intrinsically necessary for trafficking, would reduce association between the two proteins.

Stargazin enhances trafficking by blocking ER retention. Our data suggest that in order for GluR1 and GluR2 to be trafficked by stargazin, it must have intracellular access to the cytoplasmic face of AMPA receptors (**Figure 8**). In contrast, no such cytoplasmic interaction is necessary for subsequent stargazin-mediated modulation of desensitization. The intracellular interaction responsible for stargazin-mediated trafficking may block one or multiple ER retention signals; multiple ER retention signals are consistent with the graded response in current density seen with progressive C-terminal deletions of stargazin (21). The receptor mutant that exemplifies the different moieties of the stargazin-receptor interaction is $R1i_{15}$CFP. Although the kinetics of this channel were modulated by stargazin as well as the kinetics of $R1i_{81}$CFP, stargazin was unable to force the channel to form surface rings. This difference could be explained if $R1i_{81}$CFP interacts with stargazin in the ER while $R1i_{15}$CFP does not (or has a reduced affinity of interaction), or if association of stargazin in the ER with $R1i_{15}$CFP homo-oligomers does occur, but fails to block any ER retention signals.

Support for the hypothesis that there is an initial interaction between AMPA receptors and stargazin in the ER is lent not only by measuring FRET between stargazin and AMPA receptors in the cytosol but also by experiments in which different glutamate receptor constructs were over-expressed in the presence of stargazin. If there were an initial protein-protein interaction in the ER, we should be able to sequester stargazin in the ER and prevent it from forming surface expression rings. An interpretation of results of this experiment (**Table 3**) is that stargazin can be sequestered in the ER by over-expression of $R1_{81}$CFP but not $R1_{15}$CFP, suggesting not only that association between stargazin and $R1_{15}$CFP occurs preferentially at the surface membrane, but also that multiple stargazin molecules per tetramer traffic AMPA receptors more efficiently.

Stargazin is found primarily in the surface membrane and could forego its interaction with AMPA receptors until both

proteins reached the plasma membrane. The lower-affinity association may be similar to stargazin's association with calcium channels, which alters the biophysical properties of this voltage-gated channel without influencing its trafficking (42). Our hypothesis would predict that stargazin over-expression would result in more association with $R1_{15}$YFP in the ER. The failure of $R1_{15}$YFP to form surface expression rings even when co-expressed with a 1:8 stg ratio is consistent with there being a transmembrane/extracellular association between the two proteins in the ER that does not associate intracellulary to block any retention sites.

Stargazin modulation demonstrates flip/flop isoform differences in channels without the ATD. Although this study did not focus on splice-isoform differences in stargazin trafficking and/or modulation of AMPA receptors, there is evidence that stargazin affects AMPA receptors in an isoform-selective manner (21). Flip and flop isoforms differ in their kinetic properties and allosteric modulation (43-45), so if stargazin is modulating deactivation and/or desensitization through the ligand-binding core, one might predict that there could be splice isoform differences. Isoform differences may also explain the discrepancy between our data and those of Arai and co-workers, who found that C-terminal deletions of GluR1o resulted in increased rates of deactivation and desensitization (46). The desensitization kinetics of the GluR1i C-terminal deletions we studied were not significantly different from wild type. Additionally, deletion of 52 amino acids of the C-terminus (equivalent to $R1_{29}$) for GluR1o was shown to prevent stargazin-mediated effects on desensitization and deactivation (47), which is significantly different than what we found with GluR1i.

Our results indicate that the ATD is not necessary for stargazin modulation of desensitization for either the flip or flop isoform. However, stargazin association may alter the stability of the both GluR2i $_{ATD}$ and GluR4i $_{ATD}$ homo-tetramers. GluR2o $_{ATD}$ was not only trafficked effectively to the surface membrane by stargazin, aggresome frequency was decreased with stargazin (**Table 2**). In contrast, the aggresomes increased in size for GluR2i $_{ATD}$ co-transfected with stargazin (**Fig 4d**) without changing significantly in frequency. Since GluR2 modulation of desensitization by stargazin is strongly influenced by the flip-flop isoform, this suggests that there could be an interaction between stargazin and the flip/flop region.

Aggresome formation and density may be related to the amount of monomeric and dimeric subunits in the ER. This correlation is in agreement with the aggresome formation observed when we expressed wt GluR2 R_{607} homomers but not $R_{607}Q$ homomers (**Table 2**). R_{607} homomers are mostly in the monomeric or dimeric state in the ER while $R_{607}Q$ homomers have an enhanced proclivity to form tetramers (36). It is interesting that stargazin did not alter the number of aggresomes for R_{607}. This result is in agreement with previous work that provides evidence that stargazin binds only to tetramers in the ER and would not affect the dimer-dimer interaction.

Insight into the stoichiometry of the stargazin-AMPA receptor interaction. The finding that GluR1 subunits with differing C-termini could form hetero-oligomers but were different in their ability to be trafficked by stargazin enabled us to rule out that four stargazin binding sites (1 per subunit) were necessary for stargazin-mediated trafficking. The ability of multiple stargazin molecules to associate with a receptor was confirmed by different stoichiometry-dependent FRET efficiencies (**Figure S2**). Our study of hetero-oligomers leaves open the possibility that stargazin binds to a dimer interface composed of two "sufficient" subunits (2 short: 2 long) or binds to a single "sufficient" subunit (3 short: 1 long). We hypothesize that only one stargazin per tetramer needs to bind to enhance trafficking of the AMPA receptor although more than one association leads to the blockade of more ER retention signals and thus more effective trafficking. The question still remains as to whether there are two stargazin binding sites per tetramer or one for each subunit.

Summary. Our studies bring a new level of resolution to investigate the nature of the interaction between AMPA receptors and

stargazin. However, stargazin's contribution to the synapse is complex, in part because of the many unpredicted activities of this protein (see for example, (48)), and the fact that its actions are activity-dependent (49). An intriguing property of stargazin is that it interacts with both calcium channels and AMPA receptors at the plasma membrane (50). It is unclear whether stargazin's trafficking of AMPA receptors from the ER, modulation of AMPA receptor biophysical properties in the plasma membrane, complex-formation with AMPA receptors and calcium channels, or ability to mediate cell-cell adhesion are all regulated by activity and contribute to synaptic plasticity. Additional experiments will be needed to address these important issues.

REFERENCES

1. Palmer, C. L., Cotton, L., and Henley, J. M. (2005) *Pharmacol Rev* **57**, 253-277
2. Mayer, M. L. (2005) *Current Opinions in Neurobiology* **15**, 282-288
3. Dingledine, R., Borges, K., Bowie, D., and Traynelis, S. F. (1999) *Pharmacology Reviews* **51**, 7-61
4. Gouaux, E. (2003) *Journal of Physiology (London)* **554.2**, 249-253
5. Sommer, B., Köhler, M., Sprengel, R., and Seeburg, P. H. (1991) *Cell* **67**, 11-19
6. Kim, E., and Sheng, M. (2004) *Nature Reviews Neuroscience* **5**, 771-781
7. Malinow, R. (2003) *Philos Trans R Soc Lond B Biol Sci* **358**, 707-714
8. Malenka, R. C. (2003) *Ann NY Acad Sci* **1003**, 1-11
9. Barry, M. F., and Ziff, E. B. (2002) *Current Opinions in Neurobiology* **12**, 279-286
10. Vandenberghe, W., Nicoll, R. A., and Bredt, D. S. (2005) *Proc Natl Acad Sci U S A* **102**, 485-490
11. Tomita, S., Chen, L., Kawasaki, Y., Petralia, R. S., Wenthold, R. J., Nicoll, R. A., and Bredt, D. S. (2003) *J Cell Biol* **161**, 805-816
12. Letts, V. A. (2005) *Epilepsy Currents* **5**, 161-165
13. Bredt, D. S., and Nicoll, R. A. (2003) *Neuron* **40**, 361-379
14. Nicoll, R. A., Tomita, S., and Bredt, D. S. (2006) *Science* **311**, 1253-1256
15. Letts, V. A., Felix, R., Biddlecome, G. H., Arikkath, J., Mahaffey, C. L., Valenzuela, A., Bartlett, F. S., Mori, Y., Campbell, K. P., and Frankel, W. N. (1998) *Nature Genetics* **19**, 340-347
16. Chen, L., Chetkovich, D. M., Petralia, R. S., Sweeney, N. T., Kawasaki, Y., Wenthold, R. J., Bredt, D. S., and Nicoll, R. A. (2000) *Nature* **408**, 936-943
17. Yamazaki, M., Ohno-Shosaku, T., Fukaya, M., Kano, M., Watanabe, M., and Sakimura, K. (2004) *Neuroscience Research* **50**, 369-374
18. Chen, L., El-Husseini, A., Tomita, S., Bredt, D. S., and Nicoll, R. A. (2003) *Mol Pharmacol* **64**, 703-706
19. Priel, A., Kolleker, A., Ayalon, G., Gillor, M., Osten, P., and Stern-Bach, Y. (2005) *J Neurosci* **25**, 2682-2686
20. Tomita, S., Adesnik, H., Sekiguchi, M., Zhang, W., Wada, K., Howe, J. R., Nicoll, R. A., and Bredt, D. S. (2005) *Nature* **435**, 1052-1058
21. Turetsky, D., Garringer, E., and Patneau, D. K. (2005) *J Neurosci* **25**, 7438-7448
22. Hall, R. A., Hansen, A., Andersen, P. H., and Soderling, T. R. (1997) *Journal of Neurochemistry* **89**, 625-630
23. Nakagawa, T., Cheng, Y., Ramm, E., Sheng, M., and Walz, T. (2005) *Nature* **433**, 545-549
24. Nakagawa, T., Cheng, Y., Sheng, M., and Walz, T. (2006) *Biol Chem* **387**, 179-187
25. Leever, D. L., Clark, S. Z., Weeks, A. M., and Partin, K. M. (2003) *Molecular Pharmacology* **64**, 5-10
26. Tomita, S., Fukata, M., Nicoll, R. A., and Bredt, D. S. (2004) *Science* **303**, 1508-1511
27. Pasternack, A., Coleman, S. K., Jouppila, A. K., Mottershead, D. G., Lindfors, M., Pasternack, M., and Keinanen, K. (2002) *Journal of Biological Chemistry* **277**, 49662-49667

28. O'Connell, K. M., and Tamkun, M. M. (2005) *Journal of Cell Science* **118**, 2155-2166
29. Yachi, P. P., Ampudia, J., Gascoigne, N. R., and Zal, T. (2005) *Nat Immunol* **6**, 785-792
30. Leuranguer, V., Papadopoulos, S., and Beam, K. G. (2006) *J Biol Chem* **281**, 3521-3527
31. Sugiyama, Y., Kawabata, I., Sobue, K., and Okabe, S. (2005) *Nature Methods* **2**, 677-684
32. Coleman, S. K., Cai, C., Mottershead, D. G., Haapalahti, J. P., and Keinanen, K. (2003) *J Neurosci* **23**, 798-806
33. Shen, L., Liang, F., Walensky, L. D., and Huganir, R. L. (2000) *J Neurosci* **20**, 7932-7940
34. Greger, I. H., Khatri, L., and Ziff, E. B. (2002) *Neuron* **34**, 759-772
35. Higuchi, M., Single, F. N., Köhler, M., Sommer, B., Sprengel, R., and Seeburg, P. H. (1993) *Cell* **75**, 1361-1370
36. Greger, I. H., Khatri, L., Kong, X., and Ziff, E. B. (2003) *Neuron* **40**, 763-774
37. Ayalon, G., and Stern-Bach, Y. (2001) *Neuron* **31**, 103-113
38. Zheng, F., Erreger, K., Low, C. M., Banke, T., Lee, C. J., Conn, P. J., and Traynelis, S. F. (2001) *Nature Neuroscience* **4**, 894-901
39. Xu, D., Hopf, C., Reddy, R., Cho, R. W., Guo, L., Lanahan, A., Petralia, R. S., Wenthold, R. J., O'Brien, R. J., and Worley, P. (2003) *Neuron* **39**, 513-528
40. Corboy, M. J., Thomas, P. J., and Wigley, W. C. (2005) *Methods in Molecular Biology* **301**, 305-327
41. Jin, R., Clark, S., Weeks, A. M., Judman, J. T., Gouaux, E., and Partin, K. M. (2005) *J Neurosci* **25**, 9027-9036
42. Black, J. L., 3rd. (2003) *J Bioenerg Biomembr* **35**, 649-660
43. Mosbacher, J., Schoepfer, R., Monyer, H., Burnashev, N., Seeburg, P., and Ruppersberg, J. P. (1994) *Science* **266**, 1059-1062
44. Koike, M., Tsukada, S., Tsuzuki, K., Kijima, H., and Ozawa, S. (2000) *J Neurosci* **20**, 2166-2174
45. Partin, K. M., Fleck, M. F., and Mayer, M. L. (1996) *Journal of Neuroscience* **16**, 6634-6647
46. Suzuki, E., Kessler, M., and Arai, A. C. (2005) *Mol Cell Neurosci* **29**, 1-10
47. Arai, A. C., and Suzuki, E. (2005) *Abstract Viewer/Itinerary Planner. Washington, DC: Society for Neuroscience, 2005. Online.* **Program No. 949.8**
48. Price, M. G., Davis, C. F., Deng, F., and Burgess, D. L. (2005) *Journal of Biological Chemistry* **280**, 19711-19720
49. Rouch, N., Byrd, K., Petralia, R. S., Elias, G. M., Adesnik, H., Tomita, S., Karimzadegan, S., Kealey, C., Bredt, D. S., and Nicoll, R. A. (2005) *Nature Neuroscience* **8**, 1525-1533
50. Kang, M.-G., Chen, C.-C., Wakamri, M., Hara, Y., Mori, Y., and Campbell, K. P. (2006) *Proc Natl Acad Sci U S A* **103**, 5661-5666
51. Malinow, R., and Malenka, R. C. (2002) *Annu Rev Neurosci* **25**, 103-126
52. Hayashi, T., Rumbaugh, G., and Huganir, R. L. (2005) *Neuron* **47**, 709-723

FOOTNOTES

Abbreviations used: AMPA, -amino-3-hydroxy-5-methylisoxazole-4-propionate; cMEM complete minimal essential medium; FRET, fluorescence resonance energy transfer; ECFP, enhanced cyan fluorescent protein; EYFP, enhanced yellow fluorescent protein; EGFP, enhanced green fluorescent protein; PCR, polymerase chain reaction; GluR, glutamate receptor; HEK, human embryonic kidney; ATD, amino terminal domain; stg, stargazin; i, flip; o, flop; R1, GluR1; R2, GluR2.

Acknowledgements: This work was supported by an NIH predoctoral training grant to MAB (NS43115-02) and by R01MH64700 (KMP). The authors thank John Gieser for his help in the production of this manuscript. We thank Drs. Kurt Beam, Nancy Lorenzon and Michael Tamkun for useful discussions and their critique of an earlier version of the paper.

FIGURE LEGENDS

Fig 1. Stargazin traffics fluorophore-tagged GluR1 to the plasma membrane. (a) Topology of the AMPA receptor and stargazin (stg) proteins showing the site of fluorophore insertions at the carboxyl termini. Dashed line indicates C-terminal truncation of fluorophore-tagged stargazin. (b) Confocal images of yellow fluorescence in HEK293 cells expressing ($R1i_{81}$YFP, *left*), (stgYFP, *center*) and $R1i_{81}$YFP co-expressed with stg, *right*. Profile intensities (in arbitrary units) along the red line demonstrate that surface expression of GluR1 is markedly enhanced by stargazin. (c) Time constants of desensitization (black bars) measured as the decay in response to a 500 ms pulse of 10 mM glutamate, or deactivation (gray bars) measured as the decay in response to a 1 ms pulse of 10 mM glutamate, for $R1i_{81}$YFP in the absence or presence of stargazin, *left*. Cells co-expressing $R1i_{81}$YFP and stargazin were visually scored as either not having pronounced surface expression (- rings) or having pronounced surface expression (+ rings). Mean current amplitude measured in response to a 500 ms pulse of 10 mM glutamate in the absence or presence of stargazin, with and without surface expression rings, *right*. (*, $p<.05$;**, $p<.01$ comparing stargazin + or – rings to without stargazin; ##, $p<.02$ comparing $R1i_{81}$YFP deactivation with stargazin + or – visible surface expression rings). Inset shows ring formation as a function of increasing concentrations of stargazin cDNA (filled circles), co-transfected with a constant amount (0.2 g) of $R1i_{81}$YFP. The solid line represents a curve fit with to a logarithmic function extrapolated to 0, $R^2 = .91$.

Fig 2. A cytoplasmic interaction between stargazin and GluR1 promotes stargazin modulation of trafficking but is not essential for stargazin modulation of desensitization. (a) Fluorophore-tagged C-terminal deletions of GluR1 (*left*); + or – indicate whether co-expression with stargazin increased surface expression (*right*). Two constructs ($R1i_{2+38}$YFP and $R1i_{15+38}$YFP) have an insertion of a 38 amino acid linker between the receptor and the fluorophore (*thin line*). Note that $R1i_{14}$ does not contain a fluorophore tag. (b) Confocal images and corresponding profile intensities of yellow fluorescence from R1i truncations co-expressed with stgCFP. (c) Electrophysiological response of R1i truncations to a 500 ms pulse of 10 mM glutamate (black line is response without stargazin, gray line is response with stargazin. Mean current amplitudes plotted on a log scale (d) and desensitization rates (e) of tagged $R1i_{81}$YFP, $R1i_{36}$YFP and $R1i_{15}$YFP, and $R1i_{14}$ expressed with (gray bars) and without (black bars) stargazin. (*, $p<.05$; **, $p<.01$; ***, $p<.005$)

Fig 3. The GluR1 cytoplasmic tail does not contain a specific stargazin-binding site. (a) Alignment of the first 14 amino acids of the cytoplasmic tails of the AMPA receptors GluR1-4, and the kainate receptor GluR6, *top*. Shaded areas show identity to GluR1. Below are a series of mutant $R1i_{81}$YFP constructs with the mutations as indicated by the unshaded residues. All constructs formed stargazin-mediated surface expression rings, as indicated with by the +. (b) Confocal images of fixed, unpermeabilized HEK293 cells expressing FLAG-R4i or FLAG-R4i $_{CTD}$ without or with stargazin. Cells were labeled with a FLAG antibody and visualized with Alexa Fluor 568. All fluorescent images were acquired at the same gain; red pseudo-color represents intensity saturation. A smaller DIC image is shown for each field of cells.

Fig 4. The amino-terminal domain (ATD) is not essential for stargazin modulation of trafficking or desensitization. (a) Fluorophore-tagged N- and/or C-terminal deletions of GluR2 (*left*); + or – indicate whether co-expression with stargazin increased surface expression as determined by confocal microscopy (*right*). (b) Confocal images of R2i $_{ATD46}$YFP/stg (*left*) and R2o $_{ATD46}$YFP/stg (*right*) demonstrating the formation of surface rings and aggresomes (arrows). (c) Bar graphs show mean time constant of desensitization (*left*) and mean current amplitudes on a log scale (*right*) of R2o $_{ATD46}$YFP and R2i $_{ATD}$ without (black) or with (gray) stargazin. Inset showing glutamate-evoked currents; red line is without stargazin and black line is with, vertical scale bar is 200 pA, horizontal scale bar is 60 ms. (***, $p<.001$) (d) Representative images of cells co-transfected with ATD-deleted receptors and stargazin. Panels 1, 3, and 5 are confocal images acquired at a 652 amplifier gain setting and 2, 4, and 6 are the same field acquired at a 237 amplifier gain setting to permit visualization of only the aggresomes. Images 1 and 2 are

cells transfected with GluR2i $_{ATD46}$YFP (no aggresomes), images 3 and 4 are cells co-transfected with R2i $_{ATD46}$YFP/stg (large aggresomes), and images 5 and 6 are cells co-transfected R2o $_{ATD46}$YFP/stg (no aggresomes). Red pseudo-color represents intensity saturation.

Fig 5. Fluorescence resonance energy transfer (FRET) suggests stargazin self-assembly. (a) Photobleaching of stgCFP and stgYFP co-transfected into HEK293 cells (1CFP:4YFP). Upper two panels demonstrate CFP and YFP emission prior to photobleaching; lower two panels show that after selective YFP photobleaching, stgCFP emission is enhanced. (b) Confocal images of green fluorescence from 1 g stgGFP transfected into HEK293 cells (*left*) and green fluorescence arising from a 0.4 m fluorescent bead (*right*) measured by the same settings as the cells (the image of the bead was then digitally magnified for clarity). CFP and YFP have a Forster radius of about 50 Å, so the maximum distance these fluorophores could be apart and still transfer energy is 100 Å. By this reasoning, 10^4 molecules/ m^2 would be necessary to get FRET from overcrowding of the membrane. Imaging the beads at the lowest setting possible yielded a maximum detection limit before saturation of 820 stargazin molecules per m^2. Approximately 50% of the imaged cells were not saturated. If the brightest cells were even twice the detection limit at 1640/ m^2, this would still fall short of the 10,000/ m^2 needed. (c) Mean membrane FRET efficiencies ($E=1-(I_{CFPpre}/I_{CFPpost})$) arising from stargazin self-assembly in HEK293 cells with varying input ratios and total DNA concentrations (0.1 -1.0 g); in all cases, the FRET interaction between stargazin molecules is significantly greater than control ($p<.03$).

Fig 6. Stargazin assembly with GluR1i is a specific interaction. (a) The FRET efficiency of self-assembled stargazin molecules at the membrane (1 stgCFP:1 stgYFP) is competed when co-transfected with excess R1i in HEK293 cells (1:1:20 or 0.1:0.1:2 in g), but not by CD8, Kv2.1 or GluR6 (1:1:20 or 0.1:0.1:2). (b) Membrane FRET efficiency between stargazin molecules (.07 g stgCFP:0.13 g stgYFP) co-transfected with 0.5, 1.0, or 2.0 g of R1i. (c) Confocal images of (.07 g stgCFP:0.13 g stgYFP) before (red) and after stgYFP photobleach (blue) with corresponding profile intensities. (d) Same interaction as (c) but competed with 2 g of R1i. (*, $p< .05$; **, $p<.005$; ***, $p <.001$). (e) Confocal images of a HEK293 cell co-transfected with R1i$_{81}$CFP and stgYFP, pre and post photobleaching of YFP (*left*). Confocal images of HEK293 cells co-transfected with R1i$_{15}$CFP and stgYFP pre and post photobleaching of YFP (*right*).

Fig 7. Hetero-oligomerization can rescue C-terminal deletions with trafficking defects. (a) Confocal images of cyan and yellow fluorescence from HEK293 cells expressing R1i$_{15}$ or R2o$_{16}$, with either longer form of R1i or R2o (1 shorter:1 longer:2 stg). In all cases, R1$_{15}$ and R2$_{16}$ co-transfected with stargazin without a longer form had failed to form surface expression rings (Figure 2 and data not shown). (b) The ratio of mean membrane fluorescence intensity/ mean cytosol fluorescence intensity was compared between two different constructs ("A", constructs in the left column; or "B", constructs in the right column) that could either be independently trafficked by stargazin or required co-expression of a longer form to form rings. Two constructs that could independently form surface expression rings with stargazin had approximately equal amounts of membrane:cytosolic intensity, whereas short forms co-expressed with long forms were significantly less and were trafficked ~75% as well as the long forms. (*, $p< .05$ for both controls; , $p< .05$ compared to R1i$_{46}$C + R2o$_{46}$Y). (c) Membrane FRET efficiency between R1i$_{15}$ and R1i$_{46}$ was compared to cytosolic FRET efficiency using a 1CFP:1YFP:2stg or 0.2CFP:0.8YFP:2stg ratio between tagged R1i$_{15}$ and R1i$_{46}$.

Fig 8. Model of stargazin modulation of trafficking versus desensitization of R1i$_{15}$YFP and R1i$_{81}$YFP. Shown is a model that assumes that stargazin binding occurs at both dimer interfaces of the tetrameric channel; our data would also be consistent with a model in which stargazin binds individual subunits within the tetramer. In the ER stargazin (red) associates with higher affinity to the dimer interface of the R1i$_{81}$YFP AMPA receptor tetramer (magenta, with an extended tail showing the yellow YFP attachment) than to the dimer interface of the R1i$_{15}$YFP AMPA receptor (magenta, with a minimal

tail showing the yellow YFP). The thickness of the magenta arrows correlates with the hypothesized relative affinities; the lower affinity arises due to some steric hindrance by the fluorophore. Known ER retention signals are shown in black; one is located in the proximal cytoplasmic tail and the other within the pore loop. Association between stargazin and $R1i_{81}$YFP in the ER blocks at least one retention signal, hypothesized to be the pore loop. When more than one stargazin associates with AMPA receptors in the ER more retention signals are blocked, permitting greater exodus from the ER to the surface membrane (blue). This pathway represents stargazin modulation of trafficking, which is sensitive to the C-terminus. The few $R1i_{15}$YFP channels that reach the surface membrane without the aid of stargazin can associate with stargazin (red arrow) despite the lowered affinity because of the excess amount of stargazin in the surface membrane. This pathway represents stargazin modulation of desensitization and deactivation, which is relatively independent of the nature of the C-terminus.

SUPPLEMENTAL FIGURE LEGENDS

Fig S1. Similarity of the C-termini of AMPA receptors and the kainate receptor GluR6. Alignment of amino acid sequences between the M4 domain and the C-terminus are shown. Sites of deletions are indicated with arrows ($R1_{15}$, $R1_{36}$, $R1_{46}$, $R2_{16}$, and $R2_{46}$). Known protein-interacting sites (4.1, SAP97/RIL, NSF, GRIP, ABP and PICK1) are boxed and shown in blue (7,8). An ER retention sequence is shown in green (34). Serine residues phosphorylated by PKC or PKA are shown in red (51). A palmitoylated cysteine is shown in orange (52).

Fig S2. Multiple stargazin molecules can bind to GluR1i in the plasma membrane. (a) FRET between stargazin molecules bound to GluR1i increases significantly (from 3.9±1.1% to 9.1±2.0%, p=.01) as the relative concentration of acceptor (stgYFP) is increased from 1:1 to 1:4 respectively while keeping the total stargazin concentration the same. Ratios used in g for 1:1 and excess channel (0.1 stgCFP: 0.1 stgYFP: 2 R1i) and 1:4 and excess channel (0.04 stgCFP: 0.16 stgYFP: 2 R1i). The ratio of 1:2 had an intermediate value of 5.8±1.1%. This is consistent with the interpretation that multiple stargazin molecules can bind to each GluR1i receptor complex, and there are at least two stargazin binding sites per tetrameric complex. Although there was a trend, no significant differences were seen between FRET efficiencies with stargazin alone at 1:1 (10.6±1.4%), 1:2 (16.2±2.8%), 1:4 (14.3±2.3%) or with GluR6 at 1:1 (8.5±1.6%), or 1:4 (12.0±3.0%). (b) A model of different stgCFP and stgYFP ratios with or without excess AMPA receptor. At a 1:1 stgCFP/stgYFP ratio with no channel (*top*) it is expected that if stargazin (red) can form a dimer, some dimers will be composed of 1 CFP and 1 YFP stargazin and thus FRET (an interaction denoted by a black arrow from CFP to YFP), but some dimers will consist of 1 CFP and 1 YFP stargazin which would not FRET. We also suggest that there are some CFP and YFP stargazin monomers in the membrane. If the ratio is changed to 1:4 stgCFP to stgYFP almost all CFP molecules bound in a dimer or multimer would be in a complex with at least another YFP and thus the FRET efficiency measurement would increase. Our interpretation of the data is that a hetero-oligomeric population of 1 and 2 stargazin molecules per AMPA receptor tetramer (green), as well as stargazin monomers that did not bind to R1i on their way to the plasma membrane, may be found (*middle, bottom*). Changing the ratio of stgCFP: stgYFP to 1:4 while keeping the total stargazin concentration the same should drive the majority of channels that have 2 stargazin molecules bound to be either CFP and YFP or YFP and YFP; the latter would not affect FRET measurements.

TABLES

Table 1. C-terminal mutations of GluR1 and GluR2 alter stargazin-mediated trafficking. The constructs imaged with confocal microscopy after co-expression with excess stargazin are shown in the left column, the corresponding percentage of cells forming stargazin-mediated rings is shown in the right column. The raw data (actual number of cells with rings/total cells counted) for each construct is shown in parentheses.

C-terminal truncation	*Cells with surface expression (%)*
GluR1	
$R1i_{81}$YFP	12 (26/218)
$R1o_{81}$YFP	4 (7/178)
$R1i_{36}$YFP	9 (22/241)
$R1i_{15}$YFP	0 (0/1000)
$R1i_{15+38}$YFP	2 (3/129)
$R1i_{2}$YFP	0 (0/200)
$R1i_{2+38}$YFP	<1 (2/243)
$R1i_{7}$(C to L)	0 (0/200)
$R1i_{7+38}$(C to L)	28 (36/130)
$R1i_{81}$(YKS to FQA)YFP	36 (48/133)
GluR2	
$R2i_{46}$YFP (R607Q)	7 (6/90)
$R2i_{46}$YFP (R607)	9 (9/101)
$R2i_{16}$YFP (R607Q)	0 (0/200)
$R2o_{16}$YFP (R607Q)	0 (0/200)

Table 2. ATD deletions promote aggresome formation in the absence or presence of stargazin. The constructs tested are indicated in the left column, and the percentage of cells forming aggresomes in the right column. The raw data (actual number of cells with aggresomes/total cells counted) for each condition is shown in parentheses. Stargazin was co-expressed in a 1:2 stg ratio (in g) and the total concentration of AMPA receptor DNA was not changed.

Receptor Constructs	*Cells with aggresomes (%)*
$R2i_{46}$YFP (R607Q)	~0
$R2i_{46}$YFP (R607Q)+stg	~0
$R2i_{46}$YFP (R607)	17 *(25/148)*
$R2i_{46}$YFP (R607)+stg	15 *(15/101)*
$R2i_{46\ ATD}$YFP (R607Q)	70 *(97/139)*
$R2i_{46\ ATD}$YFP (R607Q)+stg	74 *(105/142)*
R2o ATD $_{46}$YFP (R607Q)	62 *(110/178)*
R2o ATD $_{46}$YFP (R607Q)+stg	40 *(51/126)*
$R1i_{2+38}$YFP+stg	2 *(6/243)*

Table 3. Stargazin surface expression is reduced by $R1i_{81}CFP$. Quantification of the cells forming stgYFP expression rings when stgYFP was expressed alone or in the presence of channel (0.15 stg: 2 g channel). Channel combinations are indicated in the left column, with the percentage of cells with pronounced stgYFP rings in the right column. The raw data (actual number of cells with rings/total cells counted) for each condition is shown in parentheses.

Co-expressed proteins	*Cells with stgYFP surface expression (%)*
stgYFP	82 *(97/119)*
+ GluR6	76 *(41/54)*
+ $R1i_{15}CFP$	73 *(24/33)*
+ $R1i_{81}CFP$	44 *(25/57)*

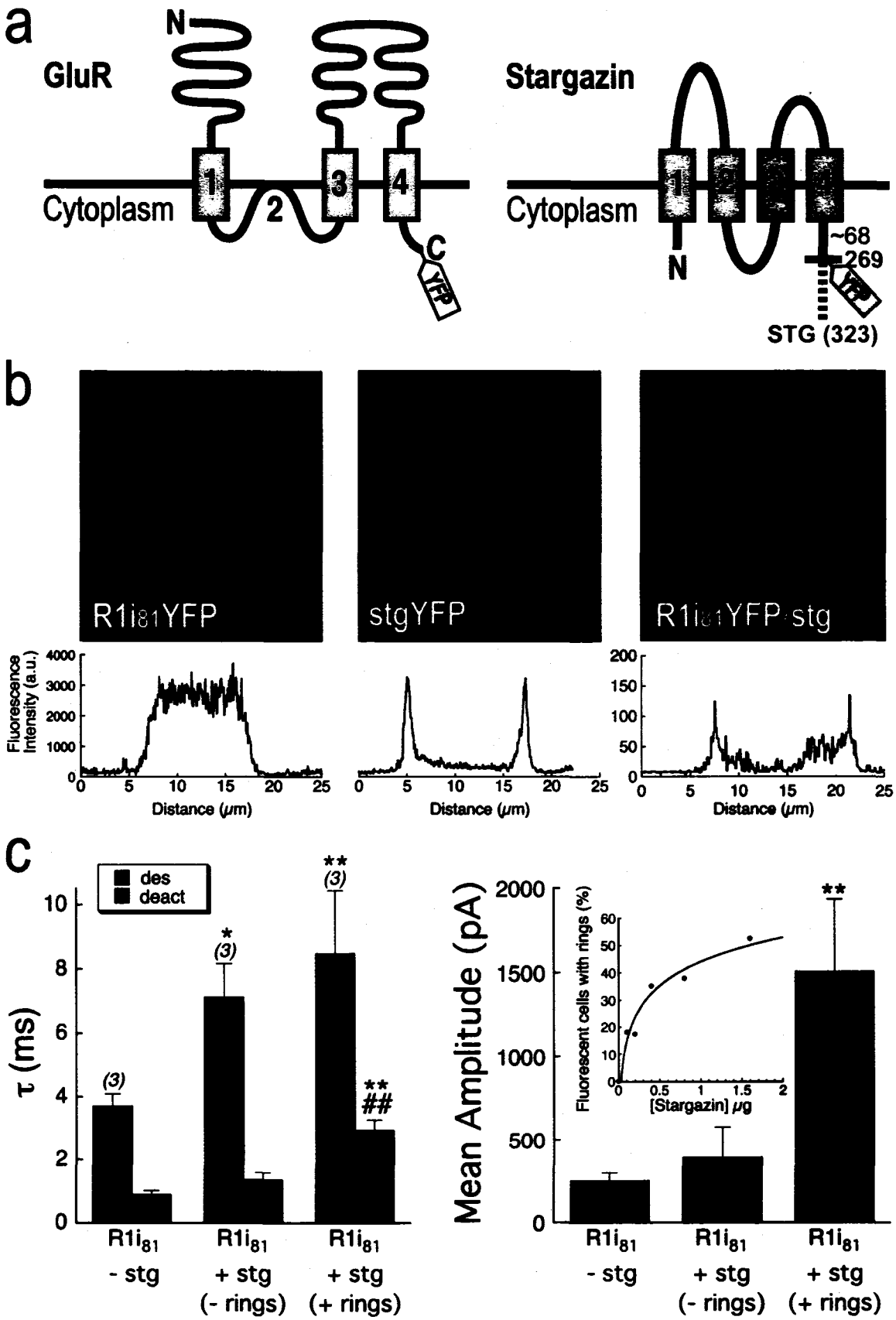

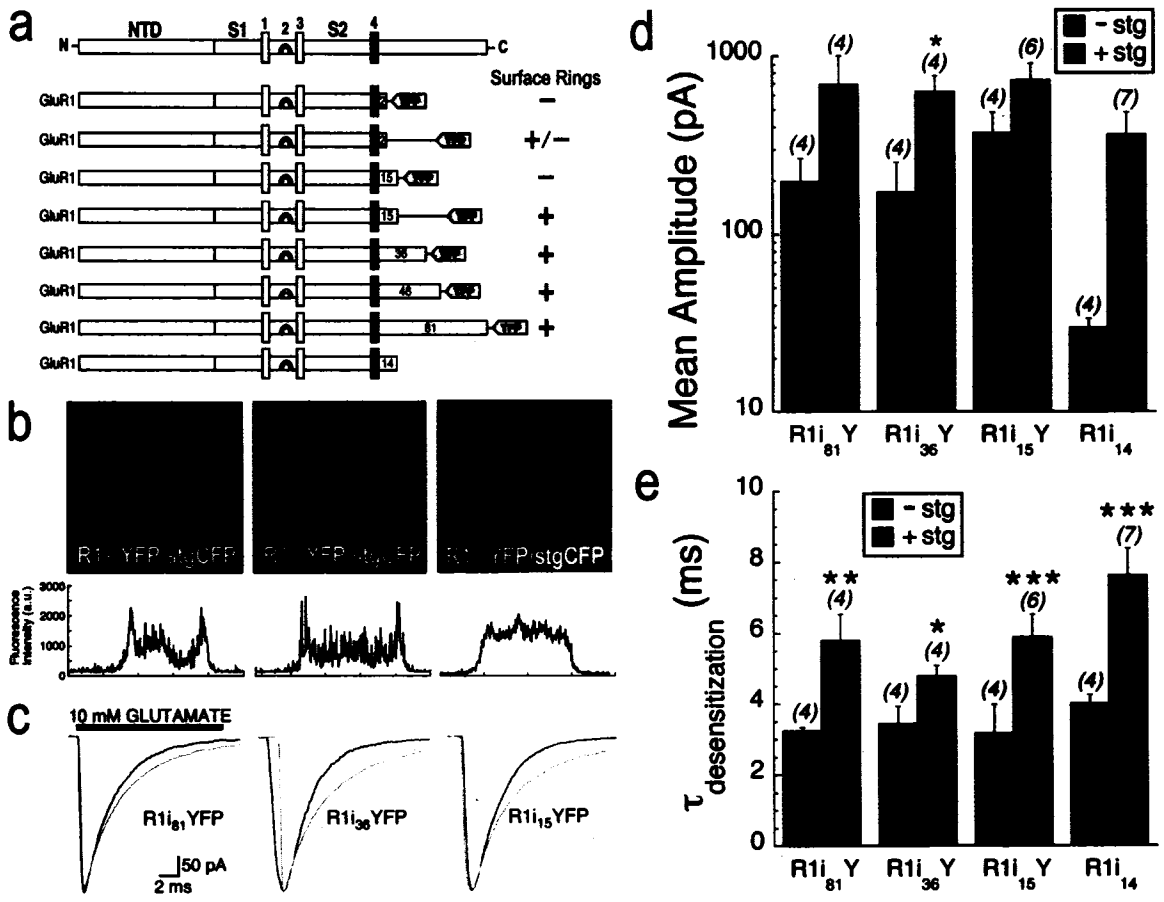

a

														Surface Rings
GluR1	E	F	C	Y	K	S	R	S	E	S	K	R	M	K	
GluR2	E	F	C	Y	K	S	R	A	E	A	K	R	M	K	
GluR3	E	F	C	Y	K	S	R	A	E	S	K	R	M	K	
GluR4	E	F	C	Y	K	S	R	A	E	A	K	R	M	K	
GluR6	E	F	L	Y	K	S	R	K	N	N	D	V	E	Q	
$R1i_{364.1}$ mut	E	F	C	Y	K	S	S	S	E	S	S	S	M	K	+
$R1i_{813C \rightarrow L}$	E	F	L	Y	K	S	R	S	E	S	K	R	M	K	+
$R1i_{819E \rightarrow A}$	E	F	C	Y	K	S	R	S	A	S	K	R	M	K	+
$R1i_{8113M \rightarrow A}$	E	F	C	Y	K	S	R	S	E	S	K	R	A	K	+
$R1i_{8114K \rightarrow A}$	E	F	C	Y	K	S	R	S	E	S	K	R	M	A	+
$R1i_{7Linker3C \rightarrow L}$	E	F	L	Y	K	S	R								+
$R1i_{81}$FQA mut	E	F	C	F	Q	A	R	S	E	S	K	R	M	K	+

b

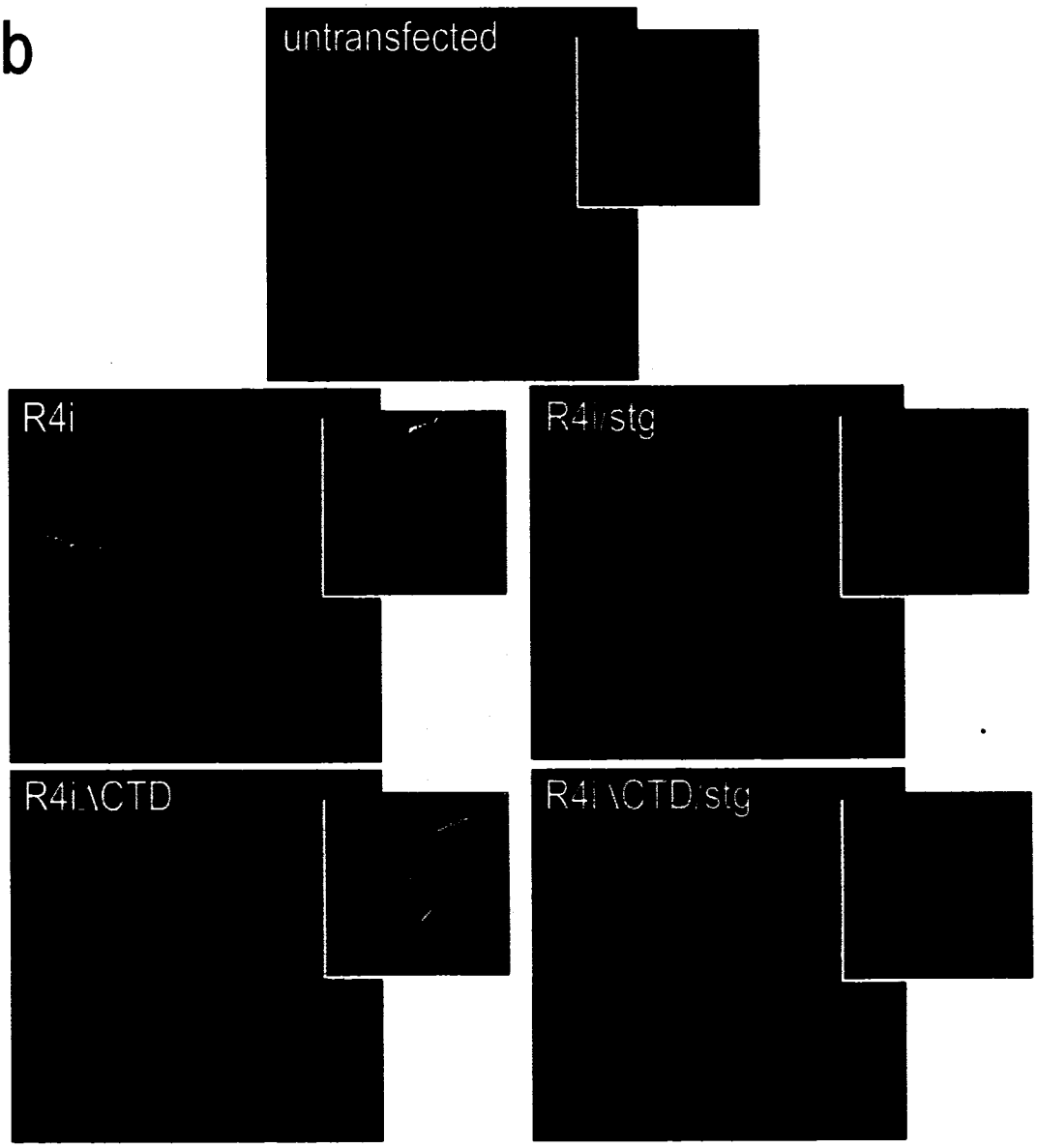

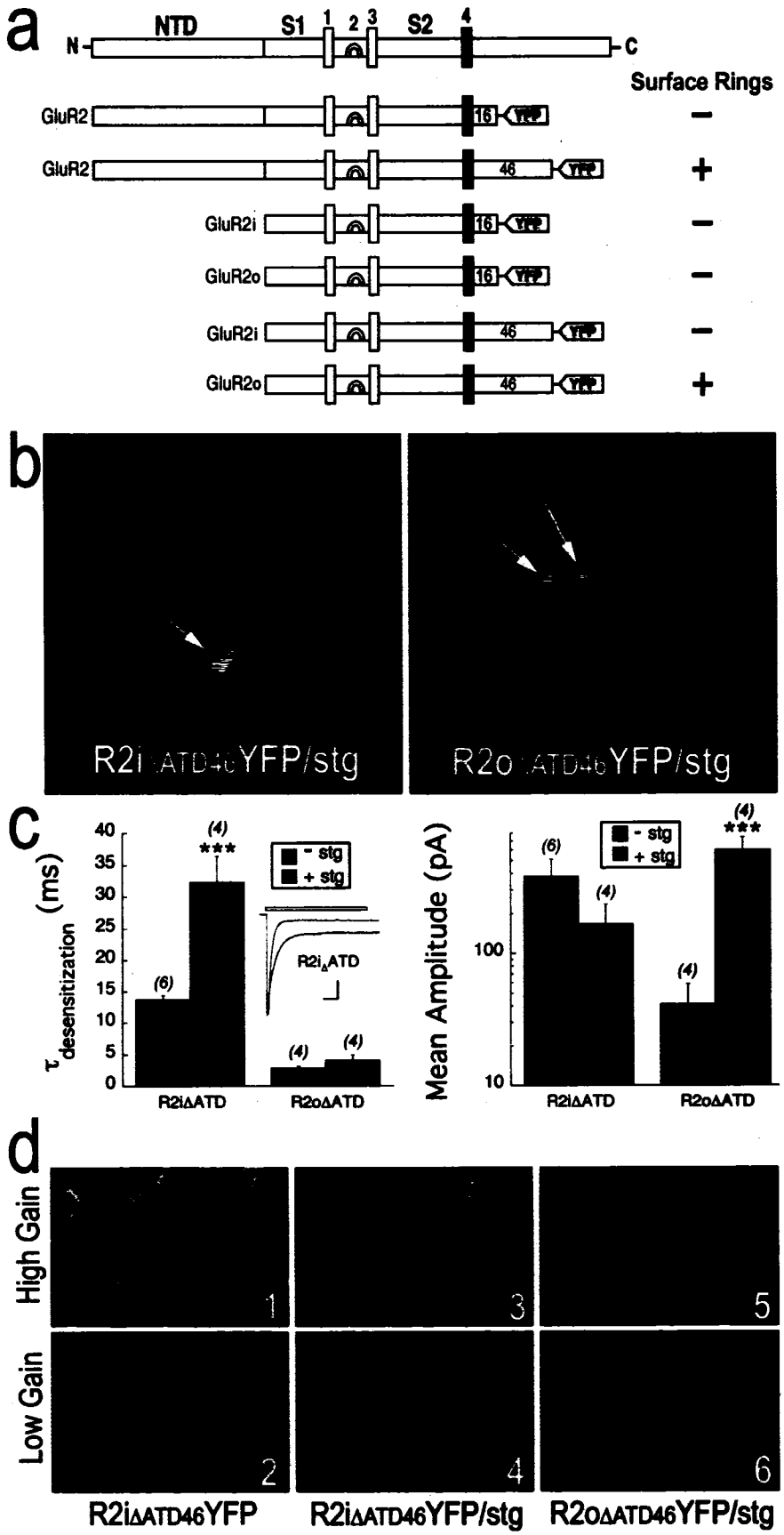

A1.4.24

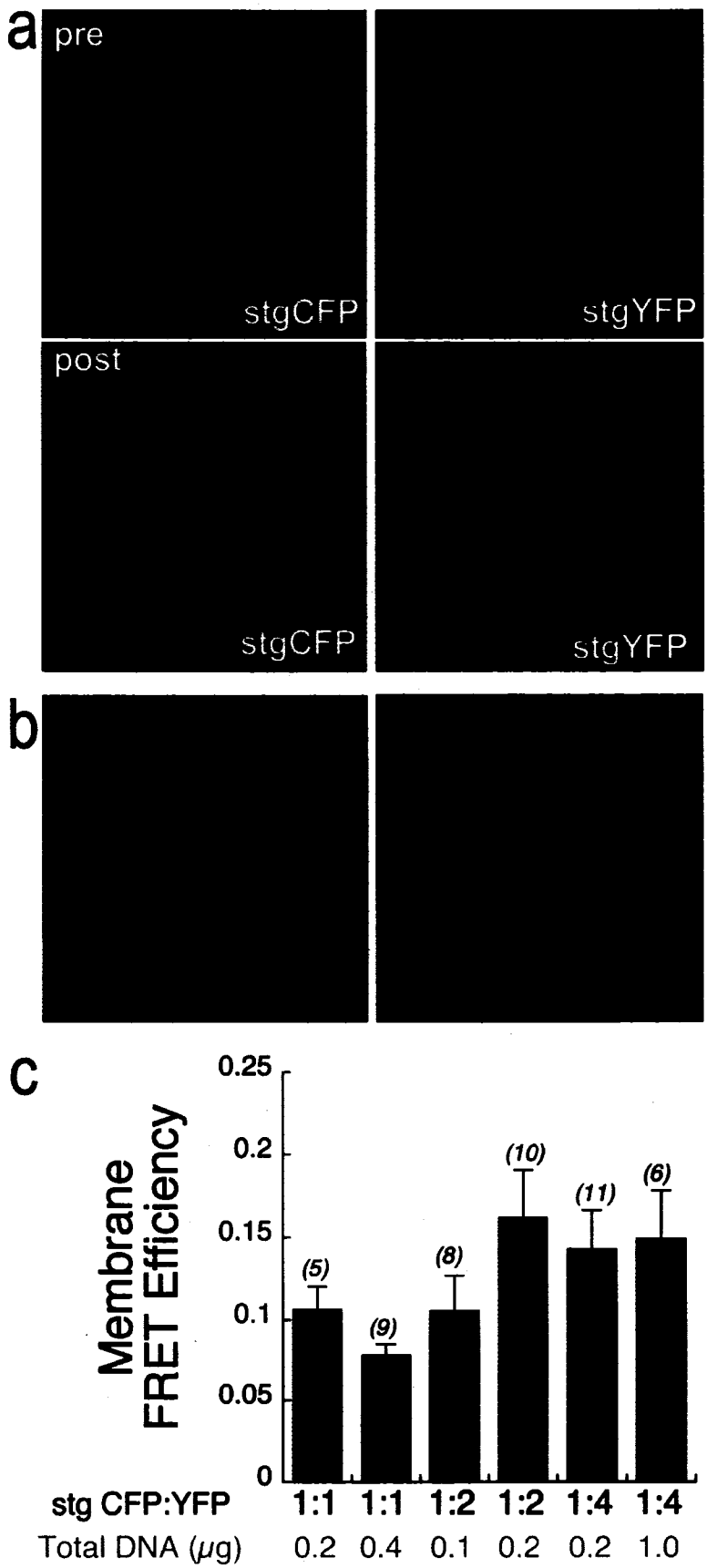

A1.4.25